IMMOBILIZED IONIC LIQUIDS FOR HIGH TEMPERATURE POLYMER ELECTROLYTE FUEL CELL APPLICATIONS

Dissertation
zur Erlangung des Grades
des Doktors der Naturwissenschaften
der Naturwissenschaftlich-Technischen Facultät
der Universität des Saarlandes

von
Galina Skorikova

Saarbrücken
2021

Tag des Kolloquium :	1 April 2022
Dekan :	Prof. Dr. Jörn Eric Walter
Berichterstatter:	Prof. Dr. Dr. h.c. Rolf Hempelmann; PD Dr.-Ing Guido Falk
Vorsitz :	Prof. Dr.-Ing Markus Gallei
Akad. Mitarbeiter:	Dr. Carsten Präsang

ABSTRACT

Polymer electrolyte membrane hydrogen fuel cells (PEMFC) is a mature technology able to convert the chemical energy of hydrogen and oxygen into electricity and a clean product – water. The high-temperature operation has the potential to increase catalytic activity and tolerance towards carbon monoxide which would reduce the cost of catalysts and allow the system integration with combined heat and power generation and a reformer unit. The major drawback lies in the conductivity loss of the membrane operated above 100 ºC and in highly dry conditions. In this work immobilized ionic liquids (IL) have been explored as a sustainable alternative conducting phase in polymers and catalysts. In this work, two types of composite membranes based on protic IL were fabricated. All the samples demonstrated good thermal stability and various ionic conductivity. Additionally, IL were impregnated in the catalytic layer of the gas-diffusion electrodes (GDE) using several approaches. The combination of the ionic liquids with conventional phosphoric acid was studied and described. Quasi-solidified ionic liquid membranes type doped with phosphoric acid (PA) exhibited high ion conductivities and good mechanical properties. Finally, H_2/air single-cell fuel cell tests and durability tests of the MEA based on self-fabricated QSILM and GDE showed performances comparable to state-of-the-art membranes operated at dry conditions and temperature ranges of 120-220 ºC.

ABSTRAKT

Polymeerelektrolytmembraan waterstofbrandstofcellen (PEMFC) is een volwassen technologie die de chemische energie van waterstof en zuurstof kan omzetten in elektriciteit en een schoon product: water. De werking bij hoge temperatuur heeft het potentieel om de katalytische activiteit en tolerantie ten opzichte van koolmonoxide te verhogen, wat de kosten van katalysatoren zou verlagen en de systeemintegratie met gecombineerde warmte- en krachtopwekking en een reformereenheid mogelijk zou maken. Het grootste nadeel ligt in het geleidbaarheidsverlies van het membraan dat boven 100 ºC en in zeer droge omstandigheden wordt gebruikt. In dit werk zijn geïmmobiliseerde ionische vloeistoffen (IL) onderzocht als een duurzame alternatieve geleidende fase in polymeren en katalysatoren. In dit werk werden twee soorten composietmembranen op basis van protische IL gefabriceerd. Alle monsters vertoonden een goede thermische stabiliteit en verschillende ionische geleidbaarheid. Bovendien werden IL geïmpregneerd in de katalytische laag van de gasdiffusie-elektroden (GDE) met behulp van verschillende benaderingen. De combinatie van de ionische vloeistoffen met conventioneel fosforzuur werd bestudeerd en beschreven. Quasi-gestolde ionische vloeibare membranen van het type gedoteerd met fosforzuur (PA) vertoonden hoge ionengeleidingen en goede mechanische eigenschappen. Ten slotte lieten H_2/lucht eencellige brandstofceltesten en duurzaamheidstests van de MEA op basis van zelfgefabriceerde QSILM en GDE prestaties zien die vergelijkbaar zijn met state-of-the-art membranen die worden gebruikt bij droge omstandigheden en temperatuurbereiken van 120-220 ºC.

PUBLICATIONS

G. Skorikova et al. Protic ionic liquids immobilized in phosphoric acid-doped polybenzimidazole matrix enable polymer electrolyte fuel cell operation at 200 °C, Journal of Membrane Science, 608, (2020)

POSTERS

G. Skorikova , R. Hempelmann Impregnated protic ionic liquids as electrolytes for HT-PEM fuel cell operation, EMEA 2017 (Bad Zwischenahn, Germany)

G. Skorikova , R. Hempelmann The synergy effect of ionic liquids impregnated into PBI matrices with a phosphoric acid post treatment, Euromembrane 2018 (Valencia, Spain)

INTERNSHIPS

Korea Institute of Science and Technology, Fuel Cell Center 2017 (Seoul, South Korea)

Technical University of Denmark, Department of Energy Conversion and Storage 2018 (Lyngby, Denmark)

ACKNOWLEDGEMENTS

This chapter is meant to thank everyone who contributed to my scientific work and experience as a Ph.D. student. The order does not express the level of my gratitude - you all have helped me a lot and made this time unforgettable.

Firstly, I would like to express my great gratitude to my supervisor - Prof. Rolf Hempelmann. He kindly received me for the internship opening a door to the European research community to me. Afterward, he believed in my potential and offered me a Ph.D. position on an exciting and yet challenging topic. Thank you Prof. Hempelmann that you gave me many opportunities in terms of learning new scientific matters, learning new cultures, learning how to write and present, and learning how to be an independent researcher eventually. Thank you for giving me a certain level of freedom to explore possible routes and think critically. Thank you that you supported my internships in Seoul and Copenhagen and trips to different other locations where I presented our work. And the last but not least, thank you deeply for motivating me to finish in a professional way the journey I have started. It was a great pleasure to spend time with you discussing both work and hobbies, learn from your experience and enthusiasm. I am always open to any collaborations you might envision and to be of any help you need.

I would like to extend my gratitude to the person who had a great impact on my project - Daniel Rauber. Thank you Daniel that you were always there for me ready to have a fruitful discussion with a cup of coffee, answer the questions that I often had on chemistry or lab equipment. You synthesized the ionic liquids that I used for my experiments, hence you directly supported my work. I am convinced that you are a gifted scientist and a teacher, as well you as a very kind person. I wish you a big pool of opportunities and never-ending enthusiasm to explore them.

Another big gratitude I would like to express to another bright researcher Dan Durneata. Thank you for explaining to me all the fundamentals of PEM fuel cells and the in-house equipment that you developed. Thank you for your patience to answer millions of my questions and for encouraging me to always do more. You have always been a person on whom I could rely if I faced technical challenges. Thank you for the nice conversations with had at lunch and that you helped me not to sneak away from writing this thesis. I know you as a determined person with a solid scientific and technical background, thinking critically, having a broad overview, and being brave to start something up. I wish you great success in your development way and wealth to your beloved family.

Thank you Rudi for designing critical equipment for me. Thank you, Silvia, Petra, Konstantin, Stefan, and others from the group of Prof. Hempelmann. It was a please to eat cakes with you and learn about German culture.

Nuriye, you have always been there by my side when I needed a piece of good advice or a different perspective. We had lots of fun together. Our tea pauses were very insightful and gave me a sense of family far away from my hometown. Thank you for your wisdom and for supporting me in challenging times. Thank you that always found a moment when I asked you to explain something or to review something. Thank you that you made me

believe that my work was worth something and I did it well. You are a curious and courageous scientist and else, you are a wonderful person and friend. I believe that you are the leader who can guide to the light, Jasmin has a very good example.
Ruth, thank you for teaming up with us - it was nice to have an oasis. Thank you that we could share our struggles with Ph.D. work and later with a job search. I hope you found what you were looking for and are content with the current environment. Thank you Daniela for your kindness and always warm hugs. You have a big heart and let it beat long.
Jonathan, I am happy we could spend quite some time together talking about science and life. I enjoyed visiting your creative space in the lab and watching you being busy with inventions or just fixing the bugs. Your memory capacity is insane and your ideas are innovative. I congratulate you on the first book and wish you much more to come on the explorative way of science and technology. Thank you for all your support, sharp humor, and tolerance to my at times lame language skills.
My big gratitude I would like to express to Sangwon Kim who was in charge of our research activities within sustainable electrochemistry. Thank you that you helped me to navigate well in the new culture. Thank you for ensuring my visit to KIST Seoul which had a great impact on my work. Thank you for all our fruitful seminars, working in the labs, and spending time after work having bbq or celebrating birthdays and Christmas.
Thank you Yonglai and Zhifeng for working hand to hand with me. Thank you for sharing our challenges and helping each other. I admire that you did such nice publications and successfully defended your theses. Zhifeng, you brought me a wooden pen holder from China saying that it will remind me that I will defend my thesis. Thank you for your kindness and belief in me! Another wonderful lady from Egypt also gave me a symbol that would help me to successfully finish my Ph.D. I do believe that when many people wish you well, you do well.
Thank you to all the colleagues from KIST Europe and Transfercenter Sustainable Electrochemistry. Thank you Carsten for all those hours we spent together in front of SEM sipping coffee and discussing life. And samples. Thank you, Matthias, Oliver, Susanne, Sabrina, and all many others.
My special thanks are going to my beloved Dutchmen. Thank you Leon for teaching me that science can and should be fun. That there are multiple ways to look at the problem. Thank you that you asked me what was my research question and teaching me to ask it myself. Thank you for spending your time repairing my phone and arranging a great visit to TU Twente. And thank you for all the moments we shared at KIST and outside. You are a talented teacher, in my opinion, therefore I wish you to have my students who are keen to try something absolutely new or even absurd at first, learn from you and take a step further. For instance, now I confidently know that the answer is 42.
Thank you Tijmen for helping me out with work and sometimes distracting me from work when it was needed. Thank you for the time we spent together playing board games, traveling, cooking, and discussing whether robots would replace most of our jobs. My gratitude would never fit in this text. The same holds to you, Dave. Thank you for your

sharp mind, your extraordinary sense of humor, and for always being there for me. It means a lot to me.
Thank you, Eva, Maja, and all other great students from HIPS. Stay cool, keep on experimenting and have fun. Good luck with your theses! My other friends from Saarbrucken – thank you Ivan, Fabrizio, Antonio, Charlotte and others for making my free time so bright!
I would also like to thank my colleagues from KIST Seoul: Prof. Henkensmeier and Anastasia for helping me in the new environment and overcome scientific challenges. Additionally, my big thank you are going to another part of the world - to Denmark and specifically to Danish Technical University. Thank you David for making my internship possible. you cannot even imagine how big was the impact of that experience for me. Thank you for helping me to publish the results of our work. Santiago, thank you for your unbelievable sense of humor and perfectionism at work. Thank you for your guidance in experimental work and in life. I hope you moved back to Madrid and found an interesting job with a salary that deserves your deep knowledge. You both are examples of excellent scientists to me. I have learned from you a lot and hope that our research pathways will cross again.
Finally, special gratitude is traveling to Russia, Netherlands, and all the world to my family members. I can hardly imagine that I would have started Ph.D. studies and especially finished them without your support. Thank you mum and dad for being so smart and passing me the genes - haha. You two are some of the most intelligent, honest, and brave people that I have ever known. I love the fact that I grew up surrounded by your love and care. My beloved brother, we grew up together and shared life. Difficult to compress my gratitude into a single paragraph here. I am extremely grateful to you that we have stayed close since our childhood being there for each other like our father taught us. Being younger, you got your Dr. degree earlier than me leading me by example. I wish you to be surrounded only by bright-minded and kind people with who you could explore the world. Big thank you to my grandparents who spent so much time with me in my childhood and always stay tuned for my progress in life. Thank you for letting me go even though you love me and need me. Thank you for giving me all the possible resources you had. I love you all, and this thesis is for you.

LIST OF FIGURES

LIST OF TABLES

LIST OF ACRONYMS

ADL	Acid doping level
AFC	Alkaline fuel cells
BETI	Bis(perfluoroethylsulfonyl)imide
BETI	Brunauer–Emmett–Teller
CE	Counter-electrode
CHP	Combined heat and power
CV	Cyclic voltammetry
DIP	Delayed immersion precipitation
DL	Doping level
DPS	Danish Power Systems
DTU	Technical University of Denmark
EAS	Electrochemical active surface
EDX	Energy-dispersive X-ray spectroscopy
EIS	Electrochemical impedance spectra
EMF	Electromotive force
FC	Fuel cells
FT-IR	Fourier-transform spectroscopy
GC	Glassy carbon
GDE	Gas diffusion electrode
GDL	Gas diffusion layer
GHG	Greenhouse gas
HOR	Hydrogen oxydation reaction
HT-PEMFC	High-temperature polymer electrolyte fuel cells
HT-PEMFC	High temperature
IL	Ionic liquid
IT	Intermediate temperature
KIST	Korea Institute of Science and Technology
LT	Low temperature
LT-PEMFC	Low-temperature polymer electrolyte fuel cells
MCFC	Molten carbonate fuel cells
MEA	Membrane-electrode assembly
OCV	Open circuit voltage
ORR	Oxygen reduction reaction
OTf	Trifluoromethanesulfonate
PAFC	Phosphorc acid fuel cells
PAFC	Phosphoric acid
PBI	Polybenzimidazole
PEMFC	Polymer electrolyte membrane fuel cells

PFSA	Perfluorosulphonic acid
PI	Polyimide
PIL	Protic ionic liquid
pPIL	Ionic liquid supported by porous polybenzimidazole
PS	Polysulfone
PTFE	Polytetrafluoroethylene
QSILM	Quasi-solidified ionic liquid membranes
RE	Reference electrode
RH	Relative humidity
RHE	Reversible hydrogen electrode
SCILL	Solid catalyst with ionic liquid layer
SEM	Scanning electron microscopy
SILM	Supported ionic liquid membranes
SOFC	Solid oxide fuel cells
SPEEK	Sulfonated polyetheretherketone
Tf_2N	Bis(trifluoromethanesulphonyl)imide
TFA	Trifluoroacetic acid
TFSI	Bis- (trifluoromethanesulfonyl)imide
TGA	Thermogravimetric analysis
VIPS	Vapor-induced phase separation
WE	Working electrode

Introduction

According to the Paris Agreement from 12 December 2015, there was set an ambitious goal to strengthen the global response to climate change by limiting global temperature increase to well below 2°C with respect to pre-industrial level. In order to achieve this goal, parties aim to reach global peaking of greenhouse gas emissions (GHG) as soon as possible [1]. EU determined a national contribution as at least 40% GHG emissions reduction by 2030 compared to 1990 [2]. Primary anthropogenic GHGs are carbon dioxide (CO_2) and methane (CH_4) and nitrous oxide (N_2O) [3].The main contributor to CO_2 emissions is the energy sector from which 82.4% is occupied by the electricity and heat generation, transportation and other fuel combustion (Figure 1).

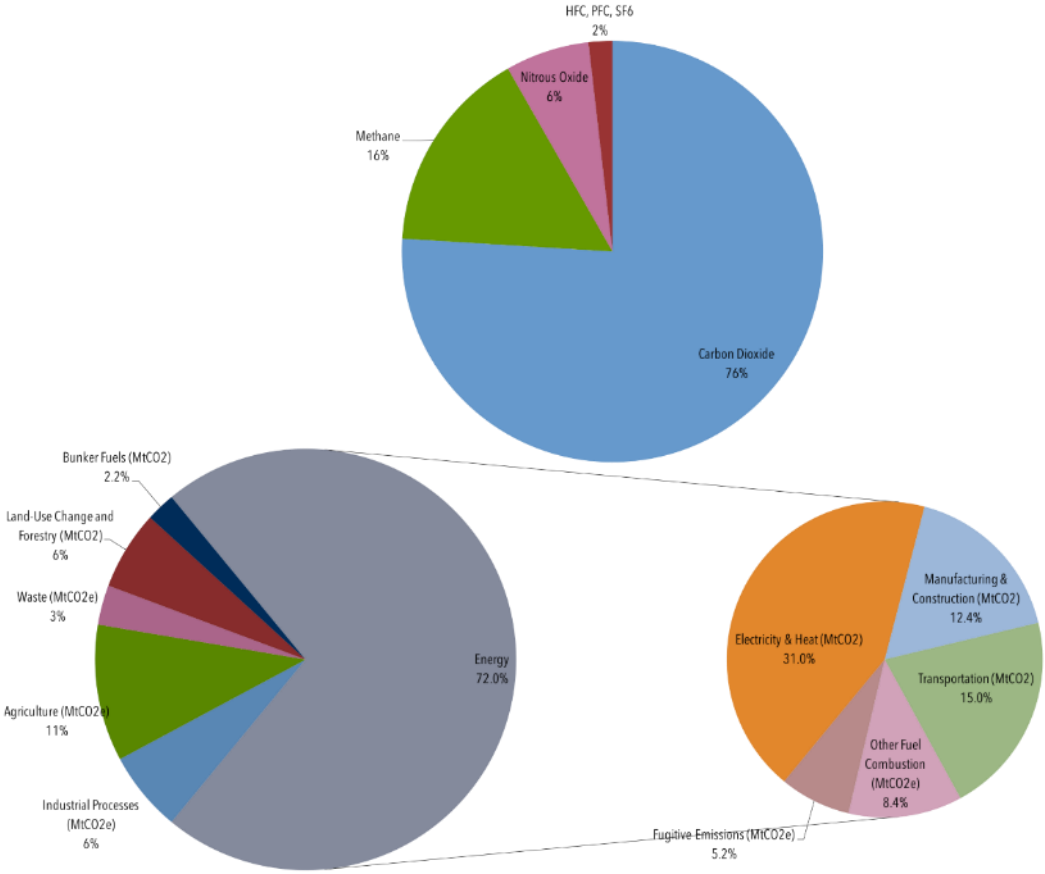

Figure 1 - Main anthropogenic greenhouse gases and the main emitting sectors (2013-2015). World Resources Institute, 2017; Climate Analysis Indicators Tool (World Resources Institute, 2017)

Figure 2 shows the history of CO_2 emissions since 1850 and a projected level of emissions till 2040 in case that no changes in technologies and policies would be made.

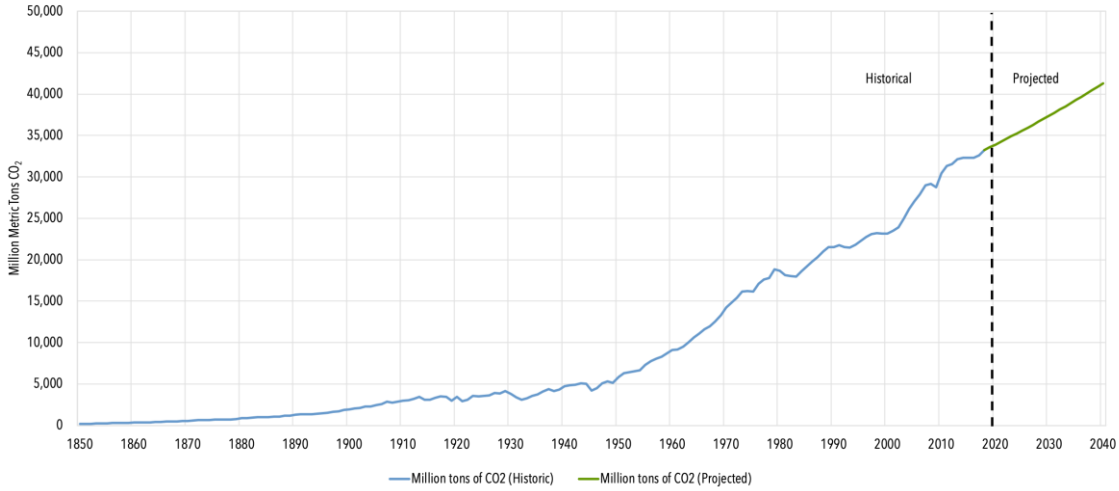

Figure 2 - Global Carbon Dioxide Emissions (1850–2040). Carbon Dioxide Information Analysis Center (Oak Ridge National Laboratory, 2017); World Energy Outlook (International Energy Agency, 2019)

In order to reduce CO_2 emissions from the energy sector, lots of initiatives on alternative to fossil fuels energy sources have been developed and implemented such as solar, nuclear and geothermal power, CO_2 capture and utilization, hydraulic, wind, tidal, wave and biomass energy, as well as natural gas, biofuels and hydrogen gas [4,5].

1. Theoretical background

1.1.Basic structure of a fuel cell

Fuel cell (FC) is a device which coverts chemical energy of a fuel into electrical energy driven by electrochemical reaction. In essence FC consist of an anode (negative electrode) and cathode (positive electrode) separated by an electrolyte layer which is schematically represented in Figure 3.

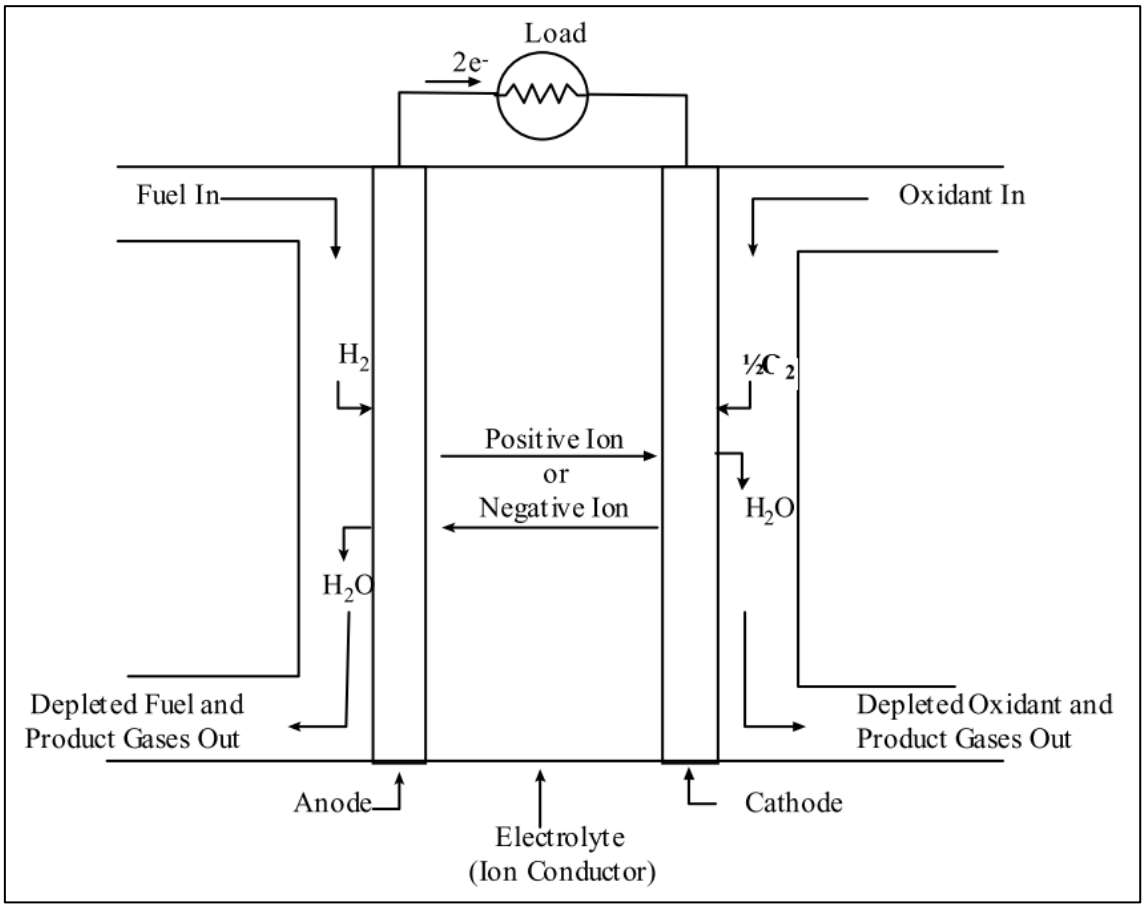

Figure 3 - Schematic of an Individual Fuel Cell. Reprinted from [6].

In a typical fuel cell, the anode compartment is continuously fed with fuel (e.g. hydrogen, methanol etc.) and the cathode compartment is fed with oxidant (e.g. oxygen, air etc.). Electrochemical half-reactions happening on both electrodes cause an ion flow across the electrolyte and a corresponding flow of electrons in the outer circuit, which forms electric current to perform work on the load. Thus, a FC keeps on producing electricity as long as fuel is supplied, and this is a key difference between a FC and a battery [7]. The key advantage of a FC over a traditional combustion engine is the ability to transform chemical energy into electricity in one step skipping an intermediate step of mechanical energy form.

FC can be classified on the basis of fuel, operating temperature, incorporated electrolyte and the nature of ions that it conducts such as *PEMFC* – polymer electrolyte FC; *PAFC* – phosphoric acid FC; *AFC* – alkaline FC; *MCFC* – molten carbonate; *SOFC* – solid oxide FC. Common types of FC and operating conditions are listed in Table 1.

Table 1 - Main fuel cell types [7]

	Electrolyte	Charge carrier	Operating temperature	Fuel/Oxidant	Catalyst	Application
PEMFC	Polymer membrane	H^+	80°C; 80-160°C; 160-200°C	H_2, methanol / air, O_2	Pt	Transport, portable power (ca. 1kW)
PAFC	H_3PO_4 (immobilized)	H^+	200°C	H_2 / air, O_2	Pt	Stationary power system (ca. 100kW)
AFC	KOH (immobilized)	OH^-	60-220°C	H_2 / pure O_2	Pt	Power supply for spacecraft (ca. 2kW)
MCFC	Molten carbonate	CO_3^{2-}	600-700°C	H_2, CH_4 /air, O_2	Ni	Stationary (ca. 100kW-3MW)
SOFC	Ceramic	O^{2-}	400-700°C; 700-1000°C	H_2, CH_4, CO / air, O_2	Perovskites (ceramic)	Vehicles, stationary (ca. 100kW-2MW)

Additionally, there are less common types of FC and related electrochemical devices such direct liquid-fueled FC (such as direct methanol, direct formic acid, and direct borohydride fuel cells), biological fuel cells, membraneless fuel cells, metal–air cells, single-chamber SOFCs, direct-flame SOFCs, liquid-tin anode SOFCs, protonic ceramic fuel cells [8]. For instance, the direct methanol fuel cell (DMFC) is a PEMFC that directly oxidizes methanol and has been under extensive investigation for the past years. The PEMFC provides an excellent resistance to gas cross-over, rapid start-up and on–off cycling characteristics. For these reasons, it is well suited for portable power and transport applications especially for prime power for fuel cell vehicles (FCVs). However, PEMFC also exhibit some disadvantages such as utilization of expensive noble metal catalysts and its poor tolerance towards CO and sulfur especially at low temperatures. Another drawback is the active water and heat management due to low temperature operating window. Additionally, polymer electrolyte and auxiliary components used in PEMFC are of high cost (Figure 4). However, PEMFC currently exhibit the highest power density of all the FC types (0.5–2.5 W/cm^2) and is of the major focus of car companies [6].

(a)

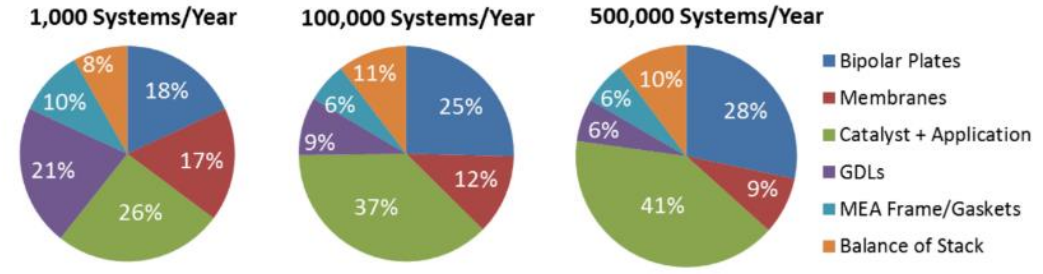

(b)

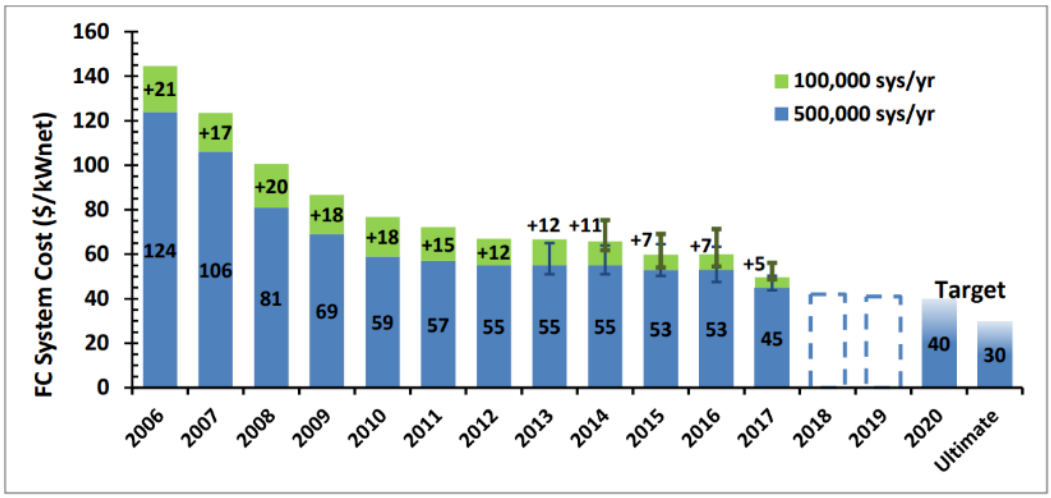

Figure 4 – (a) Fuel cell system cost breakdown of the year 2017. (b) Reduction of fuel cell system cost. Reprinted from [9].

1.2.Polymer Electrolyte Membrane Fuel Cells

This type of FC is named after a nature of the electrolyte which is a thin polymer membrane (ca. 20-200 μm). The main function of the membrane is reactants separation and ion transport. The most investigated and commercially developed PEMFC today are fueled with hydrogen and can be divided into low temperature (LT), intermediate temperature (IT) and high-temperature (HT) FC depending on operating conditions. Hydrogen can be produced from fossil fuels via reforming process or in an electrolyzer unit by electrochemical water splitting. However, in the first case hydrogen must be purified since Pt as a typical catalyst within PEMFC has a poor tolerance towards CO and sulfur especially at low temperatures.

The polymer membrane is either subsequently coated on one side with a thin layer of a catalyst and porous carbon electrode support material on another side or sandwiched with a hot press in between those layers. This sandwich structure is further referred to as a membrane electrode assembly (MEA) which is the core element of the PEMFC.

Figure 5 schematically shows the main steps within a fuel cell. *Reactant transport* plays an important role since the speed of fuel supply and distribution directly influences the harvesting of electricity especially at high current densities. Therefore, flow field plates

(typically made of carbon or stainless steel with specific coatings) with a certain pattern and porous structure of gas diffusion layers electrodes *(GDE)* are used to ensure the homogeneous distribution of a gas over the active surface area. The kinetics of the *electrochemical reactions* have a direct correlation with the FC performance: fast reactions result into high electrical output. Therefore, reactions are facilitated by catalysts, and catalyst development is one of the main research directions in the field of FC. *Ionic transport* across the electrolyte is another key limitation of the FC performance. There is a significant number of research in direction of material development and membrane technology aiming to overcome the performance deterioration associated with a resistance loss. *Product removal* from the reaction zone is the last step in the process. There is a risk of "flooding" of cathode compartment by product water when it is not efficiently removed, and hence, suppressed mass transport of the reactants.

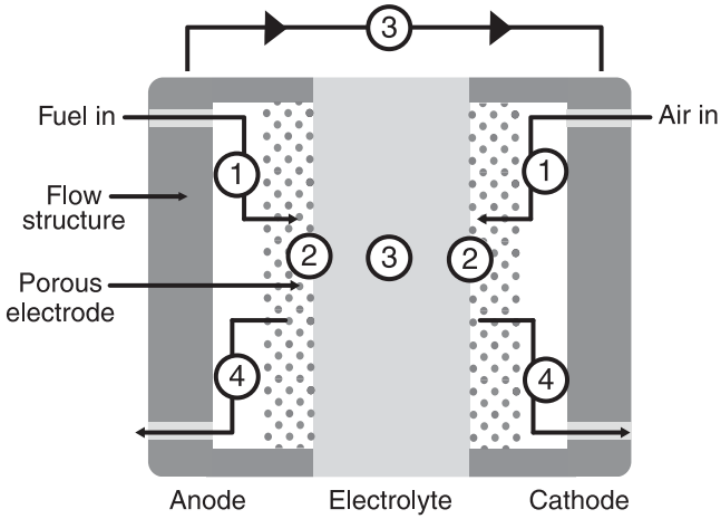

Figure 5 - Cross section of fuel cell illustrating major steps in electrochemical generation of electricity: (1) reactant transport, (2) electrochemical reaction, (3) ionic and electronic conduction, (4) product removal. Reprinted from [7]

It is known for fuel cells that anode *(An)* is a negatively charged electrode where oxidation reaction takes place, and a cathode *(Cat)* is a positively charged electrode where reduction takes places. Therefore, electrons are formed on the anode side and flow to the cathode side over an outer circuit. The main electrochemical half reactions for a hydrogen PEMFC are the following:

(An) $H_2 \rightarrow 2H^+ + 2e^-,$ E^0=0V *Equation 1*

(Cat) $\frac{1}{2}O_2 + 2H^+ + 2e^- \rightarrow H_2O,$ E^0=1.23V *Equation 2*

Thus, there is *hydrogen oxidation reaction (HOR)* happening on the anode and *oxygen reduction reaction (ORR)* happening on the cathode. These reactions are facilitated by a catalyst (typically Pt and its alloys). Overall reaction can be represented as:

$H_2 + \frac{1}{2} O_2 \rightarrow H_2O, \quad E^0 = 1.23V$ *Equation 3*

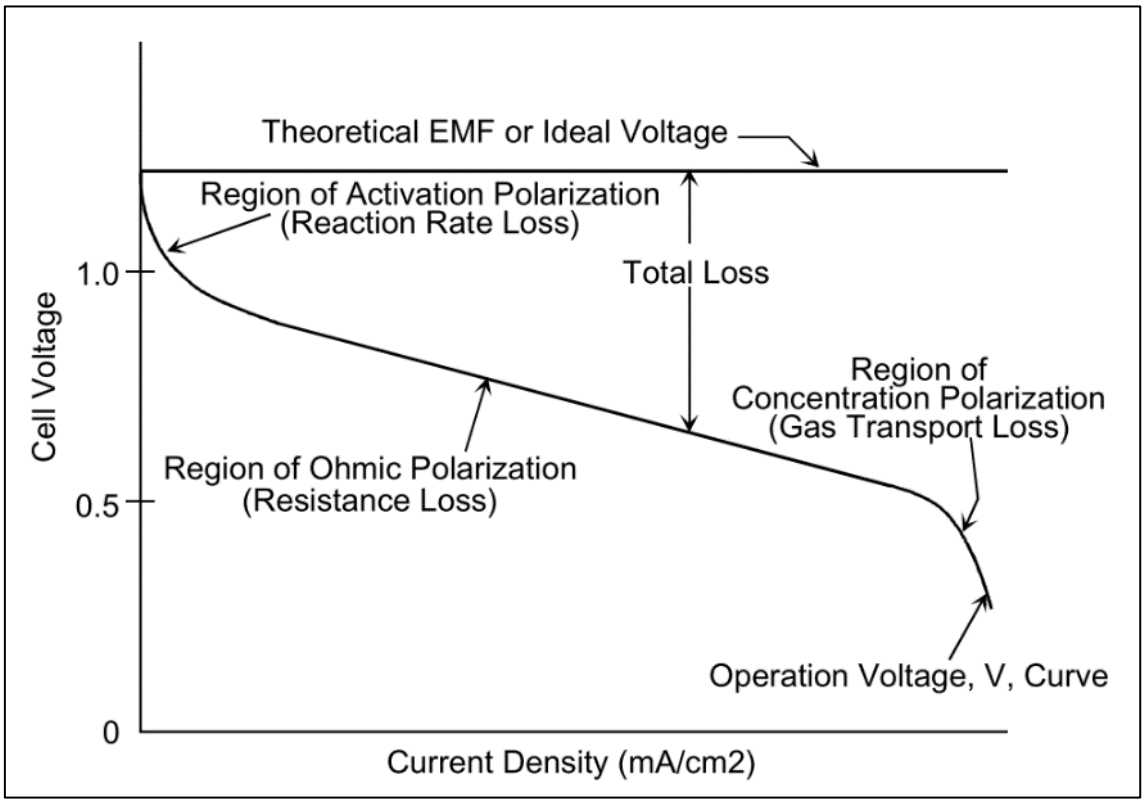

Figure 6 - Schematic of fuel cell i–V curve. In contrast to the ideal, thermodynamically predicted voltage of a fuel cell, the real voltage of a fuel cell is lower due to unavoidable losses. Reprinted from [6].

The key performance indicator of a FC is a polarization *(i-V)* curve which represents voltage output with respect to the current density output. Typical *i-V* is represented in Figure 6. Ideal hydrogen PEMFC voltage is 1.23*V* which is determined by the overall reaction in

$H_2 + \frac{1}{2} O_2 \rightarrow H_2O, \quad E^0 = 1.23V$ Equation 3.

However, the voltage drops with an increase of current density, and the curve can be divided in three main regions of voltage losses associated with the following processes: 1) *activation losses* – reaction kinetics on the electrodes; 2) *ohmic losses* – ion transport across the electrolyte; 3) *mass transport (concentration) losses* – spread of fuel and oxidant supply and product removal from the GDE. Therefore, the practically obtained voltage can be calculated as:

$$V = E^0 - \eta_{act} - \eta_{ohm} - \eta_{conc}$$ *Equation 4*

Even though the process within a FC can be divided into regions, actual electrochemical reactions take place on so called "three-phase interface" – the interface between a *catalyst* (where a molecule gets split into e^- and ions, or vice versa), an *electrode* (for a reactant supply and e^- transport to current collectors) and *electrolyte* (for ion transport). This interface plays a critical role in the process performance of a FC. There are a few challenges recognized with this respect:

- To maintain balance between solid, liquid and gaseous phase in the porous electrode structure. If the porous electrode wets with an excessive amount of electrolyte leaching from the polymer membrane, the electrode may "flood" suppressing the mass transport and consequently reducing electrochemical performance.
- To engineer a significant number of catalyst sites within the interface which are electrically and ionically connected to the electrode and the electrolyte, respectively, while being efficiently exposed to the reactant gases. In some cases it requires incorporation of a zone next to the catalyst with exhibits mixed conductivity.

The performance improvement can therefore be derived from a development of each single component and the "three-phase interface" itself. Thus, there is plenty of research focused on improving kinetics of both HOR and ORR by investigating the possible catalysts and catalyst alloys apart from the noble metals, manipulating particle size and reducing the catalyst loading in the GDE. Another direction of research is to develop more rigid, chemically stable materials for membrane fabrication with good conductive properties and low cost. Third common research direction faces the development of GDL structure manipulating with the thickness, pores size, coating with water repellent layer etc. Additionally, lots of studies are dedicated to the hardware design optimization such as FC geometry and simulations with various operating conditions such as flow rates, temperature, gas humidity, back pressure and others.

1.3. Why HT-PEMFC?

Important to note that a fuel cell is a device which converts a chemical energy of hydrogen and oxygen into electrical energy while generating heat or power as a byproduct. Theoretical efficiency (η_{max}) is around 83-90% which is higher than for a heat engine due to the fact that the energy conversion is not Carnout-limited for fuel cells [12]. The thermodynamic efficiency under isothermal conditions can be calculated as following:

$$\eta_{max} = \frac{W_{max}}{\Delta H} = \frac{E \times I \times \Delta t}{\Delta H} = \frac{\Delta G}{\Delta H} = \frac{1 - T\Delta S}{\Delta H}, \qquad \textit{Equation 5}$$

where ΔH, ΔS, ΔG are the changes in enthalpy, entropy and Gibbs energy respectively,
W_{max} is the maximum work that is generated,
TΔS reflects the byproduct heat.

Combined heat and power generators (CHP) are based on this principle of cogenerated heat recovery, which otherwise would be wasted. That increases the total system efficiency which is typically 55-65% in a contrast with the current power generation of up to about 40-45%.

LT-PEMFC are limited by the temperature of 90°C since the common and commercially available polymer membranes are based on perfluorosulfonic acid (PFSA) which makes the membranes performance strongly depend on humidification level (this phenomenon will be discussed in the next subchapter). Because of the low operating temperature, the electrochemical reactions kinetics is sluggish and requires a catalyst with pronounced electro-catalytic activity. However, there are only few materials which are able to provide sufficient activity in this temperature range. These materials are usually carbon supported noble metal (e.g. Pt/C) which are rare and expensive. Therefore, lots of studies are dedicated to reduce the catalyst loading on the electrodes while maintaining sufficient FC performance.

Another important disadvantage of a LT-PEMFC associated with the Pt catalyst is its sensitivity to poisoning by CO and sulfur species which can be found as traces in hydrogen fuel.

Additional key flaws of a LT-PEMFC are heat and water management. The first one is determined by a narrow operating temperature window. That makes thermal management especially difficult at high current densities. The water management is a challenge since the sufficient polymer electrolyte humidification should be provided while ensuring there is no flooding.

To some extent, some of these disadvantages can be counteracted by lowering operating current density and increasing electrode catalyst loading, but both increase cost of the system. If hydrocarbon fuels are used, the extensive fuel processing required negatively impacts system size, complexity, efficiency, and system cost [6].

An attractive approach to improve the performance of FC while reducing the costs is moving to elevated temperatures above 100˚C. This shift has the following potential advantages: 1) enhanced electrochemical kinetics for both electrode reactions; 2) simplified water management since water is manipulated only in vapor state (steam); 3) simplified cooling system due to the increased temperature gradient between the fuel cell stack and the coolant; 4) waste heat recovery as an energy source; 5) increased CO tolerance [10]. The latter advantage would allow to fuel a FC with a hydrogen after a reforming unit thereby reducing the cost for hydrogen purification. Moreover, integration

of a reforming unit within a FC stack has been broadly discussed recently [11]. The attractiveness of this approach initiated lots of research work for the past years.

Enhanced electrochemical kinetics

As discussed before, there are two electrochemical reactions happening on the electrodes: HOR and ORR. The exchange current density for ORR (10^{-8}-10^{-9} Acm^{-2}) is much smaller than for HOR (10^{-3}-10^{-4} Acm^{-2}), and the overall electrochemical kinetics of a PEMFC is determined by ORR [10].The overpotential for HOR is negligibly small compared to ORR in case of sufficient anode humidification. However, at the elevated temperatures above 100˚C, there is a challenge to humidify the anode.

The kinetics on both electrodes can be typically described by the Tafel equation:

$$E = E_{rev} + b\ log i_0 - b\ log i \qquad \textit{Equation 6}$$

$$b = -2.3\frac{RT}{\alpha nF} \qquad \textit{Equation 7}$$

where E is an electrode potential, E_{rev} is a reversible potential, b is a Tafel slope (Figure 7), i is a current density, i_0 is an exchange current density, n is a number of electrons transferred in the rate determining step and α is the transfer coefficient.

Increase of temperature was found to 1) slow down the decrease in E_{rev}, 2) increase b at low current densities, 3) increase i_0 *(exchange current density in te following graphics)*.

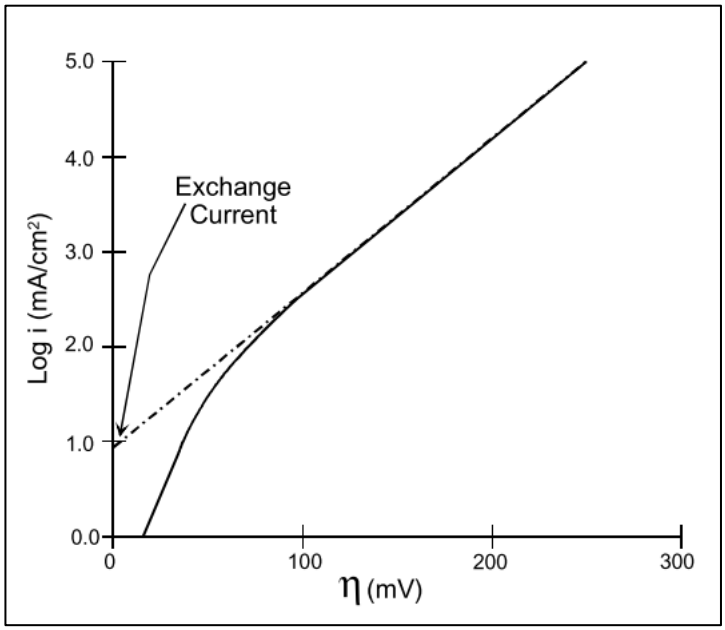

Figure 7 - Example of a Tafel plot. Reprinted from [6]

Increased CO tolerance

On-site generated hydrogen as a reformate of different organic fuels using water-gas shift reaction, preferential oxidation, membrane separation or methanol oxidation often contains traces of CO which tend to get adsorbed on Pt catalyst sites. They occupy the site responsible for HOR as shown in Figure 8 and reduce the activity of Pt or Pt containing alloys.

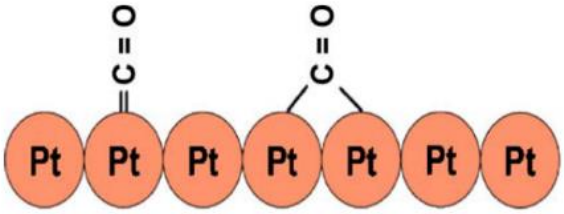

Figure 8 - Pt catalyst sites poisoning mechanism by CO species. Reprinted from [10].

It is known that for PEMFC operating at 80˚C, CO concentrations > 10 ppm cause a significant performance loss, while at 130˚C the tolerance of Pt catalyst is increased to 1000 ppm [13]. This phenomenon can be explained by the fact that adsorption of CO on Pt sites is associated with a negative entropy and higher exothermic effect than H_2 adsorption, so increasing the temperature disfavors this process [14–16]. There are lots of scientific works published which studies Pt competitive adsorption by CO and H_2 [17–19]. Figure 9 shows a loss in voltage as a function of current density at different temperatures and different CO concentrations.

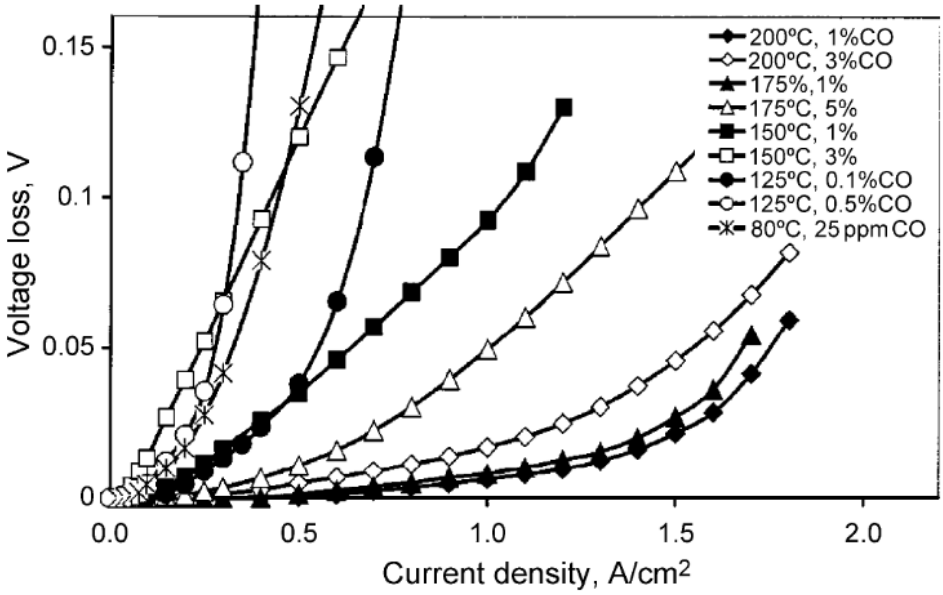

Figure 9 – The influence of the temperature on Pt catalyst tolerance towards CO species. Reprinted from [15].

Improved water management

As stated above, typical polymer electrolytes used in LT-PEMFC require a high level of humidification for high performance due to their chemical structure. At the same time, water is constantly produced at the cathode side during the operation, and results into a gradient of water concentration across the electrolyte. That causes a back diffusion of water from the cathode to the anode side. Simultaneously, water is carried in the opposite direction – from the anode to the cathode side – by protons. This process is called electro-osmotic drag [10]. These two mechanisms co-exist within the polymer membrane and determine the net water flux (Figure 10).

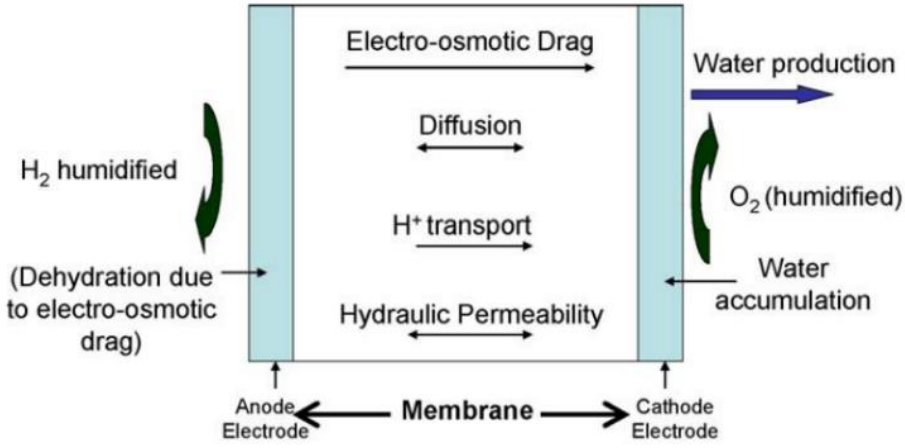

Figure 10 - Water diffusion processes within a polymer membrane electrolyte of a hydrogen fuel cell. Reprinted from [10].

The performance loss occurs when either the anode gets dehydrated due to water loss during electro-osmotic drag, or the cathode gets flooded since back diffusion is not fast enough or oxygen/air flow rate is too low to remove the excess of liquid water. When operating at temperatures above 100˚C, fuel and oxidant flows do not get humidified, and the polymers with lower dependence on humidification are used. That simplifies the system and allows better control over performance loss.

Improved heat management

As discussed above, the energy which has not been converted to electrical is harvested as heat. Thus, a typical PEMFC exhibit an electric efficiency of 40-50% at 80˚C, therefore high amount of heat needs to be removed in order to avoid electrolyte and electrodes dehydration [20]. Therefore, a typical FC stack must reject all the heat produced via the cooling system. This capability of the system at temperatures below 100˚C in very inefficient. To ensure a rapid heat transfer, heat exchanges with large surface areas are used. On the contrary, for the temperatures above 100˚C the heating system can be simplified due to a higher temperature gradient between the coolant and a cooling agent. Moreover, this rejected heat with a temperature over 100˚C can be utilized for steam

formation. Hence, most of the energy is used in either way which improves the overall energy efficiency of the system.

1.4.State-of-the-art membranes for fuel cells

As discussed earlier, the polymer membrane is one of the key elements of PEMFC. The main functions of the membranes are: 1) separation of anode and cathode compartments preventing gas crossover; 2) ion transport and electronical insulation. State-of-the-art membranes for LT-PEMFC are based on PFSA which are sold under commercial names of Nafion® [21], Flemion® [22], Gore® [23], Aquivion® [24], 3M™ [25] and others. Figure 11 represents a typical chemical structure of PFSA (Nafion as an example). The polymeric ions and absorbed electrolyte phase-separate from the fluorocarbon backbone into approximately spherical clusters connected by short narrow channels. The polymeric charges are most likely embedded in the solution near the interface between the electrolyte and fluorocarbon backbone. This configuration minimizes both the hydrophobic interaction of water with the backbone and the electrostatic repulsion of proximate sulfonate groups [26].

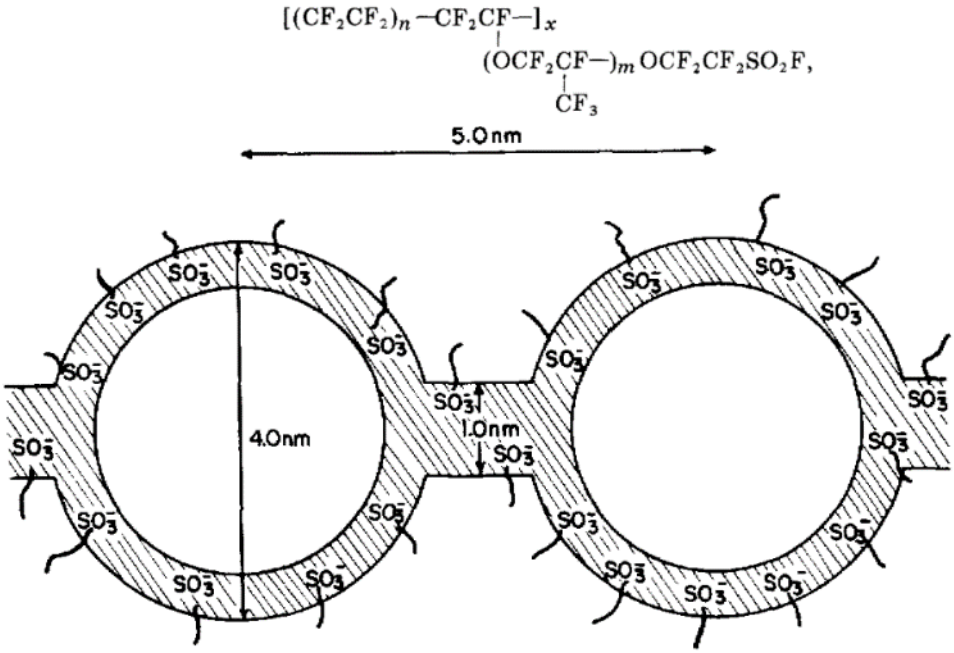

Figure 11 - Chemical structure of perfluorosulfonic acid (Nafion) membrane and its cluster-network model. Reprinted from [26].

That means that a PFSA membrane has an heterogenous structure with conductive ion-clusters which are spread across the non-conductive fluorocarbon network. The fluorocarbon backbone provides long-term stability in both oxidative and reductive

environments, which results into over than 60 000 hours operation of Nafion membrane [27]. Typical ion conductivity of 0.1 S cm^{-1} is provided by the mentioned ion-clusters which highly depends on water uptake. That property requires PSFA type membranes to be highly humidified in order to minimize resistance. At operating temperatures above 100 °C humidification becomes an issue and significant performance loss is observed. One of the ways to solve this problem is to increase backpressure several times, which would increase the complexity of the setup [28].

In order to support the desired performance at dry or low humidity conditions, various research groups have been working on supplying the existing PFSA membrane with water-retaining properties via anchoring functional organic groups such as sulfates to the backbone [29], mixing-in inorganic fillers such as graphene oxide, silica, zirconium phosphate etc. [30–37] or doping with low-volatile liquid phase phosphoric acid, ionic liquids etc. [19,38,39]. Such additives and doping agents help PFSA retain water to support conductive properties, although operating temperatures above 120 °C are still not feasible also due to thermal stability of the polymer. Another drawback of PFSA membranes is their high cost.

Alternatives to the sulfonated fluorocarbon can be non-fluorinated hydrocarbons such as sulfonated polyetheretherketone (SPEEK) [17,40–47], polysulfones (PS) [48–53], polyimides (PI) [54–57], polybenzimidazoles (PBI) [58–61] and others. Most of them can be referred to a class of materials called acid-based polymer membranes. They have been extensively studied by multiple research groups over the past decade. These hydrocarbon backbones have good physical properties and thermal stability, and graphted functional groups provide ion conductivity. Typical proton conductivity for such polymers is below 10^{-3} S cm^{-1} at room temperature [28].

The most actively researched material for HT-PEM application since 1980s has been poly 2,2'-m-(phenylene)-5,5'-bibenzimidazole (Figure 12).

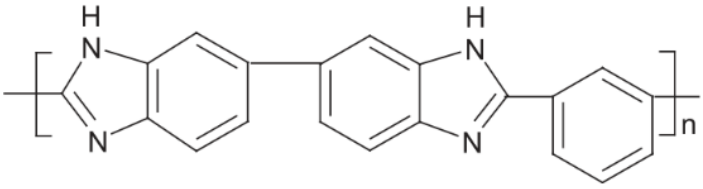

Figure 12 – Structure of polybenzimidazole

PBI is an amorphous thermoplastic with good thermal stability (T_g = 425±436 °C) due to the presence of benzene rings with side groups [28]. Additionally, it exhibits good chemical stability and good fabrication properties. PBI as a polymer does not exhibit ion conductivity. However, it is a basic polymer and therefore, can react with strong acids which facilitate proton transport across the membrane. For a good proton transport along the anionic chain, the acid must be amphoteric with both proton donating and accepting

properties. The most interesting acid for doping of PBI among others is phosphoric acid (PA) which exhibits low volatility, good thermal stability and high conductivity at high concentrations. The PA-doped PBI (PA-PBI) complex has been studied for a few decades [50,62–64]. The proton transport mechanism in such acid-base complex is well described by Melchior et al. [65]. Doped PBI can contain up to 90%wt. of PA embedded in its network. Mechanical stability such as tensile strength of thin films of PA-PBI decreases with an increase of doping level (DL), although it remains sufficient even at DL=40 mol_{PA} per unit of PBI, while elongation at break increases. PA doping substantially minimizes the water vapor pressure and allows PEM operation up till 210 °C, although the impact of water content on the level of conductivity is well pronounced. Thus, at temperatures above 200 °C significant dehydration of PA is observed, which leads to a risk of formation of phosphates with reduced conductive properties. Thermal degradation of PA-PBI at elevated temperatures has been well studied [62].

Recently, ionic liquids (IL) have been widely considered as ion conductors alternative to acids due to their superior thermal stability, negligible volatility, wide electrochemical operation window and high ion conductivity [66]. Various IL doped polymers (including PBI) have been fabricated and tested for potential HT-PEMFC application [44,67–69]. Hosting of IL by polymer frameworks is well described by Iojoiu et al. [70]. Lately, IL have been extensively studied for various electrochemical applications such as fuel cells, batteries, capacitors and supercapacitors.

1.5. Ionic liquids as alternative electrolytes

IL are salts with melting temperature below 100 °C. Two main subsets of IL are protic ionic liquids (PIL) and aprotic ionic liquids (AIL). In this work the focus will be on PIL which by definition are compounds formed by neutralization of certain Brønsted bases by Brønsted acids via proton transport (Equation 7).

$$B + A \rightarrow HB^{+} + A^{-} \qquad \textit{Equation 8}$$

Hence, these structures consist of proton donor (cation) and proton acceptor (anion) sites essential to build up a hydrogen-bonded network [71]. The stronger acid/base is used, the higher pK_a of the IL and therefore, the enhanced the proton transport. The most common cations for PIL are primary, secondary, or tertiary ammonium ions, mono- or di-imidazolium ions or guanidinium ions (Figure 13).

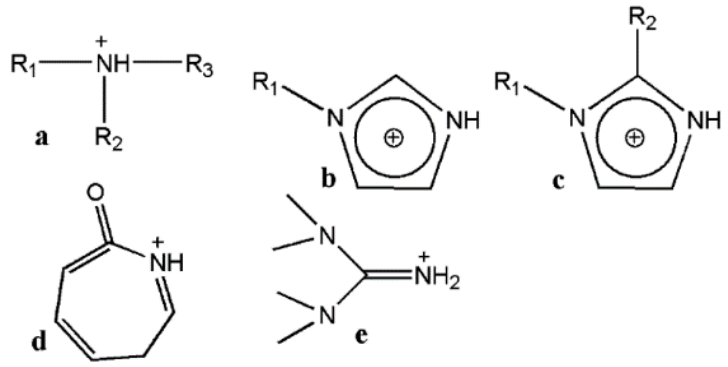

Figure 13 - Typical cations in protic ionic liquids. Reprinted from [71].

The most common anions are carboxylates, nitrate, hydrogen sulfate ions, or fluorinated ions such as bis- (trifluoromethanesulfonyl)imide (TFSI), trifluoroacetic acid (TFA), and bis(perfluoroethylsulfonyl)imide (BETI), tetrafluoroborate, or hexafluorophosphate (Figure 14).

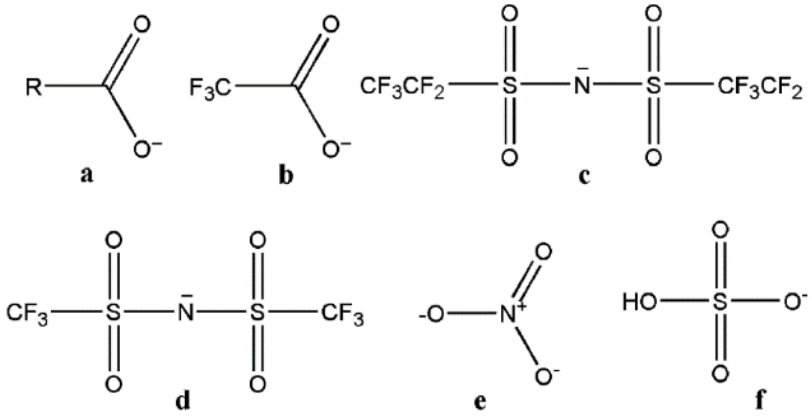

Figure 14 - Typical anions in protic ionic liquids. Reprinted from [71].

In case the proton transport from acid to base is not complete, there are some other species other than cation and anion present in the mixture of a PIL, reducing the ionicity of the liquid. It was found out that there is a complicated system of aggregation and segregation in PIL with different energy barriers required to form either a single ion or a cluster and the amount of water present in the PIL often has a significant effect on the physico-chemical properties of the PIL. Therefore, one of the important properties of the PIL is their hydrophilicity/hydrophobicity.

Thus, Anouti et al. studied the effect of water present in various PIL and found out that addition of water greatly enhance conductive properties of the PIL [72]. This enhancement happens due to viscosity decrease and therefore, increase of the charge mobility [73]. At the same time water can dilute PIL decreasing the concentration of charge carriers, and moreover, can wash PIL away from the PEM electrolyte. Since water

is the product of O_2 reduction on the cathode side, and as we learnt above, it can diffuse in the polymer membrane, it is beneficial to use hydrophobic PIL for PEM fuel cells applications [74].

Another important propertiy of PIL is ion conductivity. In most PIL the proton transport occurs via vehicular mechanism: PIL with the highest conductivities are those with highest fluidities (Figure 15). The conductivities of IL at room temperature range from 1.0×10^{-4} to 1.8×10^{-2} S cm^{-1}. Conductivities of on dialkylimidazolium cations are known to have higher ionic conductivity than those based on tetraalkylammonium, pyrrolidinium, piperidinium and pyridinium cations. The origin of the anion also plays a key role. Thus, such anions as F^- and Br^- limit the stability to 2–3 V whereas bis(trifluoromethylsulphonyl)imide anions (NTf2) is oxidized at a high anodic potential (4.5 V) [75]. IL based on tetraalkylammonium cations exhibit enhanced stability of cathodic reduction of 4.0–5.7 V.

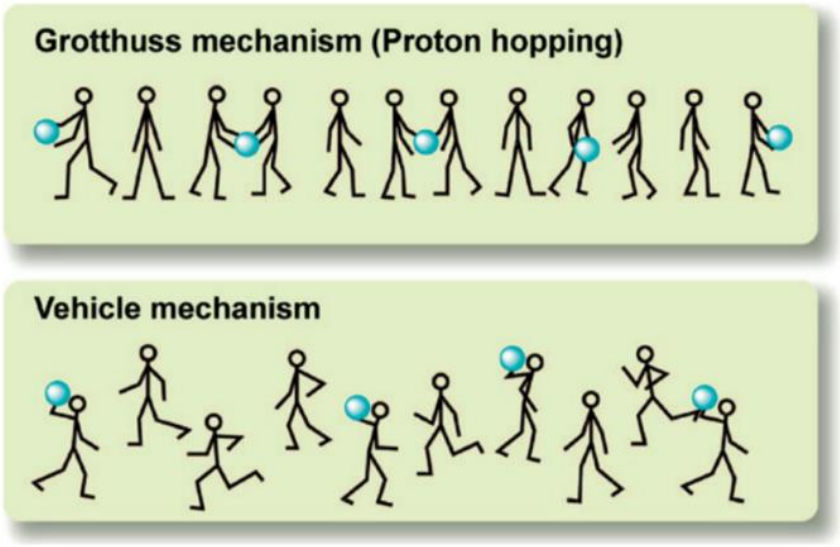

Figure 15 - Illustration of two mechanisms of proton transport: Grotthus (in acidic aqueous solution) and vehicle (in protic ionic liquids). Reprinted from [76].

The properties of IL can be modified by e.g. changing the length of the alkyl chain of the cation, or by the covalent tethering of task-specific functionalities to one or both of the constituent ions [77]. Therefore, IL are considered as tunable and task-specific media.

1.6.Ionic liquids immobilized in the membranes

Since IL are liquid at FC operating temperatures, they are required to be confined in the solid matrix. There are two main ways to immobilize IL: chemical grafting or physical mixing with the polymer or adsorption inside the pores on inorganic nanoparticles.

Chemical grafting can be done directly to the polymer backbone during the post-treatment, to inorganic particles with the surface functional groups or by polymerizing various monomers in the presence of IL (Figure 16).

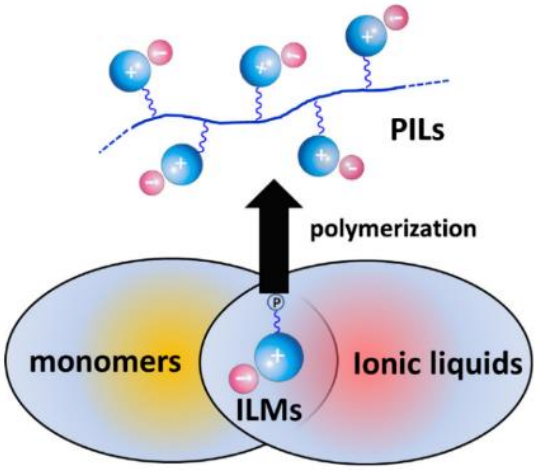

Figure 16 - Ionic liquid membranes. Reprinted from [78].

As one of the examples, Yan et al. fabricated membranes by polymerization of PIL-based microemulsion [79]. Authors studied different IL based on [OTf] anion. Styrene was used as a monomer for co-polymerization via cross-linking under UV light irradiation. Such membranes showed ion conductivity up to 1×10^{-1} S cm^{-1} at 160°C. Authors proposed that this conductivity was achieved due to well-connected PIL nanochannels by warned about potential disruption in long-term HT-PEMFC operation due to progressive IL release.

One of approaches is the modification of commonly used Nafion membranes by incorporating different cations through a proton exchange mechanism between the membrane and the ionic liquids. De Yuso et al. studied the effect of the incorporation of n-dodecyltrimethylammonium (DTA^+) in protonated Nafion 112 membranes[80]. After reaching an equilibrium value of 68% for the DTA^+ , the contact angle studies showed a reduction in the hydrophobic character of the Nafion 112/DTA^+. The X-ray photoelectron spectroscopy (XPS) and thermogravimetric data showed a higher thermal stability and a lower water loss for modified samples heated at 120°C.

Diaz et al. studied the performance of Nafion 112 membranes impregnated with different ILs: 1-butyl-3-(4-sulphobutyl)-imidazolium trifluoromethanesulphonate ([HSO_3-BBIm][TfO]) and 1-methyl-3-(4-sulphobutyl)-imidazolium bis(trifluoromethylsulphonyl)imide ([HSO_3-BMIm][Tf_2N]) [81]. An IL with an imidazolium cation was selected due to its high electrochemical stability. Moreover, sulphonic groups were added to the cation to facilitate proton transport. Suitable anions, such as NTf_2 and OTf, were selected due to their high ionic conductivity. IL have a degradation temperature above 300°C, which made them suitable for fuel cell applications. A higher current density was obtained when the Nafion membrane was impregnated with [HSO_3-BBIm][OTf], reaching 217 mA cm^{-2} without humidifying the inlet gases at 25°C.

Di Noto et al. studied the properties of Nafion 117 membranes doped with triethylammonium methanesulphonate (TMS) and triethylammonium fluorobutanesulphonate (TPFBu) [82]. The water content of TPFBu is less than that of TMS due to its hydrophobicity, agreeing with the lower water content of Nafion doped with TPFBu relative to Nafion doped with TMS. The IL uptakes of the membranes impregnated with TMS and TPFBu were 20 and 39 wt%, respectively.

Liew et al. prepared a proton conducting polymer electrolyte based on poly (vinyl alcohol)(PVA)/ammonium acetate (CH_3COONH_4)/1-butyl-3-methylimidazolium chloride (BmImCl) through a solution casting technique [83]. As expected, the ionic conductivity increased with the mass loading of the IL. The increased ionic conductivity is due to the strong plasticizing effect of the IL which softens the polymer backbone, increasing the flexibility of the polymer chain. The plasticizing effect promotes the mobility of the polymer chains and therefore, enhances a Grotthus mechanism of the short-distance proton transport. Additionally, IL acts as a carrier of protons improving the ionic conductivity through vehicular mechanism. The highest ionic conductivity of 5.74×10^{-3} S cm^{-1} was achieved with 50 wt% BMImCl loading which resulted into maximum power density of 18 mW cm^{-2} at room temperature during PEMFC test.

Eguizábal et al. developed composite membranes based on 1-H-3-methylimidazolium bis(trifluoromethanesulphonyl)imide ([HMI][Tf_2N]) encapsulated in large pore commercial zeolites and PBI for HT-PEMFC application [84]. The conductivity of this material outperforms pristine PBI most likely due to the presence of the HMI cations and NTf_2 anions on the external surface of the zeolite crystals. Both ions favor acid-base interactions with the H_3PO_4–PBI system and a Grotthuss type mechanism through the IL network. An ionic conductivity of 5.4×10^{-2} S cm^{-1} at 200°C was achieved with the optimal membrane composition.

Another promising method of immobilization of IL inside the polymer films is their physical confinement. It can be done via two main approaches: 1) direct mixing of the polymer solution with IL followed by the casting procedure or 2) formation of the porous polymer film with the further impregnation with IL via immersion (Figure 17). Those approaches lead to the formation of two different structures accordingly: 1) quasi-solidified IL membranes (QSILM) and 2) supported IL membranes (SILM) [85].

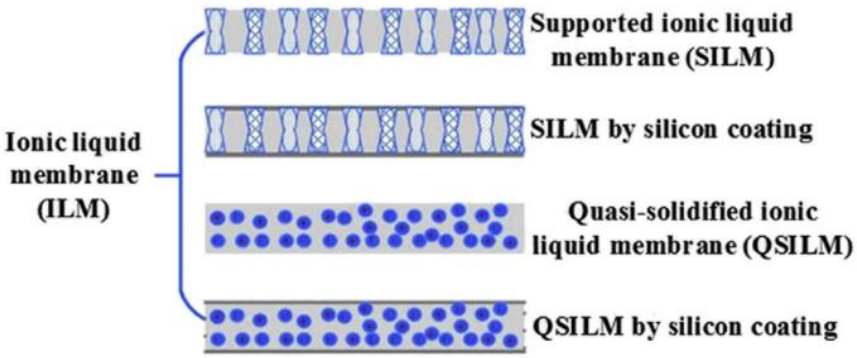

Figure 17 - Two main approaches for ionic liquids immobilization inside the polymer film. Reprinted from [85].

QSILM can be prepared by polymerizing various monomers in the presence of IL or by generating a simple mixture of polymers with ILs [86]. In this way a composite membrane based on an alkylimidazolium phosphate IL and SPEEK was prepared using a solution casting method by Jothi et al. The thermal stability of SPEEK/lL composite membranes is higher than that corresponding to pristine membranes. Addition of IL to SPEEK enhanced the ionic conductivity, reaching approximately 3.0×10^{-3} S cm^{-1} at 145°C under anhydrous conditions when 50 wt% IL was incorporated into the polymer matrix. This membrane was tested in a fuel cell at various temperatures under non-humidified conditions. At 145°C, the OCV was reported to be 0.83 V, and the maximum power density was 203 mW cm^{-2}.

Ye et al. developed gel-like composite membranes based on H_3PO_4/1-methyl-3-propyl-methylimidazolium dihydrogen phosphate ($PMIH_2PO_4$)/PBI for HT_PEMFC application. The fabricated films exhibited a proton conductivity of 2.0×10^{-3} S cm^{-1} at 150°C under anhydrous conditions. The increase in conductivity was observed after water vapor absorption [87]. The authors proposed that $PMIH_2PO_4$ may act as a proton transfer bridge, a plasticizer for PBI and water retainer. It also may interact with the hydrogen bonds in the system.

SILM structure of 1-H-3-methylimidazolium bis(trifluoromethanesulphonyl)imide immobilized in the porous PBI was demonstrated by van de Ven et al. The composite membrane was prepared via delayed precipitation technique and proton conductivity of 1.86×10^{-3} S cm^{-1} was achieved for the composite at 190°C [88]. The performance of these membranes exceeded that of Nafion 117 at temperatures above 90°C. Power densities of 39 mW cm^{-2} were obtained at 150°C with H_2/O_2.

Another example of SILM is the membrane based on porous PI impregnated with trifluoro methansulfonic acid (TEA) developed by Langevin et al. [89]. The authors proposed a technique of porous film fabrication based on vapor induced phase separation (VIPS). The test at 130 °C discovered proton conductivity of the composite membranes

(20 mS cm^{-1}) below, but very close to, that of the pure ionic liquid (31 mS cm^{-1}). Storage modulus exceeded 200 MPa up to at least 150 °C.

1.7. Ionic liquids immobilized on the catalysts

Next to confinement of IL in electrolytes, they have been also actively studied in catalysis. As discussed in Chapter 1.1, one of the major drawbacks of a LT-PEMFC Pt catalyst is poisoning of its surface sites by nonreactive oxygenated species and the sluggish ORR kinetics. As proposed by Tian et al., water molecules are considered as a major source of oxygenated species [90]. A group of Etzold et al. demonstrated a facile method of protecting reactive Pt sites from surface oxidation by a hydrophobic IL 1-butyl-3-methylimidazolium bis(trifluoromethanesulfonyl)imide ($[C_4C_1Im][NTf_2]$) [91]. Authors demonstrated accelerated ORR kinetics for IL-modified Pt/C catalyst, claiming a reduced overpotential and therefore, an enhanced activity. Authors attributed this effect to higher accessibility of Pt sites protected by the hydrophobicity conveyed by IL (Figure 18). The reported mass activity of the catalyst outperformed pristine catalyst three times (1.01 A mg^{-1}_{Pt}@0.9 V).

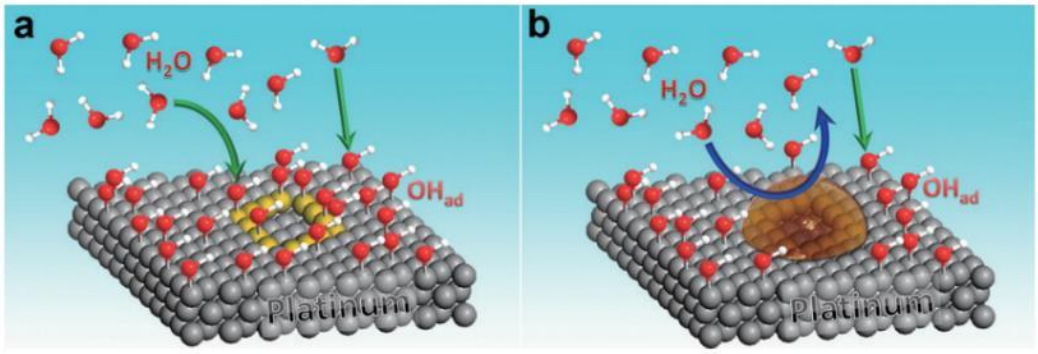

Figure 18 - Scheme for the interfacial microenviroments at a) Pt/C, and b) Pt/C-SCILL, showing that the IL would selectively locate at the defect sites and protect the Pt sites from hydroxy species. Reprinted from [91].

The concept of the formation of such a structure called solid catalyst with ionic liquid layer (SCILL) was earlier proposed by Kerchen et al. [92].

However, most of imidazolium-based IL were discovered to be able to only provide rather low fuel cell performance. Gao et al. have studied the influence of cations of ILs on Pt/C catalyst by cyclic voltammogram. It was found that imidazolium cation results in smaller electrochemical active surface areas (EAS) of Pt/C than those of trimethylethyl amide and pyridinium [93]. This decrease is believed to cause significant fuel cell performance decrease.

1.8. Motivation for the work

Since at elevated temperatures over 120 ºC water cannot longer facilitate proton transport, there is a need to develop an alternative non-water-based electrolyte. At this development stage nothing can surpass phosphoric acid doped PBI in terms of conductivity in HT-PEMFC. However, durability issues associated with thermal degradation of phosphoric acid and poisoning of Pt based catalyst compel scientists to search for more thermally stable electrolytes like ionic liquids.

This work is focused on development of the high-performance cation-exchange polymer membrane electrolyte for high temperature application (T>100°C). As discussed above, the desired electrolyte should have satisfying thermal and mechanical stability, exhibit sufficient proton conductivity in the range of HT-PEMFC operating temperatures and moreover, maintain this conductivity over a lifetime. Additionally, the membrane should be easy in handling in order to ensure fabrication of the membrane-electrode assembly (MEA).

PBI is selected as a basic polymer due to its good thermoplastic properties. Since PBI is an ion insulator, the desired proton conductivity is intended to be reached via incorporation of ionic liquids and acids inside the polymer network. Ionic liquids are designed to: 1) be thermally stable at T<250°C, 2) be protic and exhibit high ion conductivity, 3) have wide electrochemical operating window and 4) be hydrophobic in order to ensure their retention during exposure of the membranes to water. Ionic liquids are produced inhouse via the neutralization reaction of purchased Brønsted bases by Brønsted acids via proton transport.

The essential physico-chemical properties of the membranes are checked before MEA fabrication. GDE is fabricated in-house via spraying of the catalyst ink over the commercial GDL. It is expected that the viscosity of the IL reduces at the elevated temperatures. Therefore, the influence of the ionic liquids on the electrochemical activity of the catalyst is studied in order to ensure the fuel cell operation in case of the leakage of the IL from the polymer electrolyte.

Finally, MEA is fabricated and tested in the fuel cell at various operating conditions. Such characteristics as polarization curves and stability (potential degradation) are measured.

The goal of this work is to study the influence of the selected IL on the characteristics of the fuel cell components and the overall fuel cell performance, to select the most suitable IL for the potential HT-PEMFC application and propose the fabrication procedure of their immobilization inside the polymer matrix. Two main approaches of immobilization – quasi-solidified ionic liquids membranes (QSILMs) and supported ionic liquids membranes (SILMs) - were investigated and compared.

2. Experimental

Key materials

Table 2 – List of key materials used in this work

Abbreviation	Full name	Supplier	Purity
C_1Im	1-methylimidazole	IoLiTec, Germany	>98%
dema	N,N-diethylmethylamine	TCI, Germany	>98%
C_2Im	ethylimidazole	IoLiTec, Germany	>98%
TMG	1,1,3,3-tetramethylguanidine	Alfa Aesar, USA	99%
NTf_2	bis(trifluoro)methylsulfonyl imide (acid form)	IoLiTec, Germany	80%
[dema][OTf]	diethylmethylammonium trifluoromethanesulfonate	IoLiTec, Germany	98%
H_3PO_4	Phosphoric acid	J.T. Baker, USA	85-87%
PBI	polybenzimidazole M_w=45.000 g mol^{-1}	Danish Power Systems (DPS), Denmark	
PVP K30	polyvinylpyrrolidone M_w=40kDa	Sigma Aldrich GmbH, Germany	
PVP K90	polyvinylpyrrolidone M_w=360kDa	Sigma Aldrich GmbH, Germany	
GDE	gas-diffusion electrode 1.3 mgPt cm^{-2}	Danish Power Systems (DPS), Denmark	
GDL	gas-diffusion layer type H23C2	Freudenberg, Germany	
Pt/C	Pt nanoparticles supported on carbon black (catalyst)	Johnson Matthey, UK	

Ultrapure water was made by a Puranity 15 UV VWR water purification system, equipped with 0.22 mm filter from VWR. Other essential chemicals were purchased from Sigma Aldrich GmbH, Germany

Synthesized ionic liquids

For this research work the following ILs were designed in collaboration and synthesized by Dr. Daniel Rauber (Saarland University). Figure 19 shows the structure of the selected ILs and Table 3 lists their physico-chemical properties.

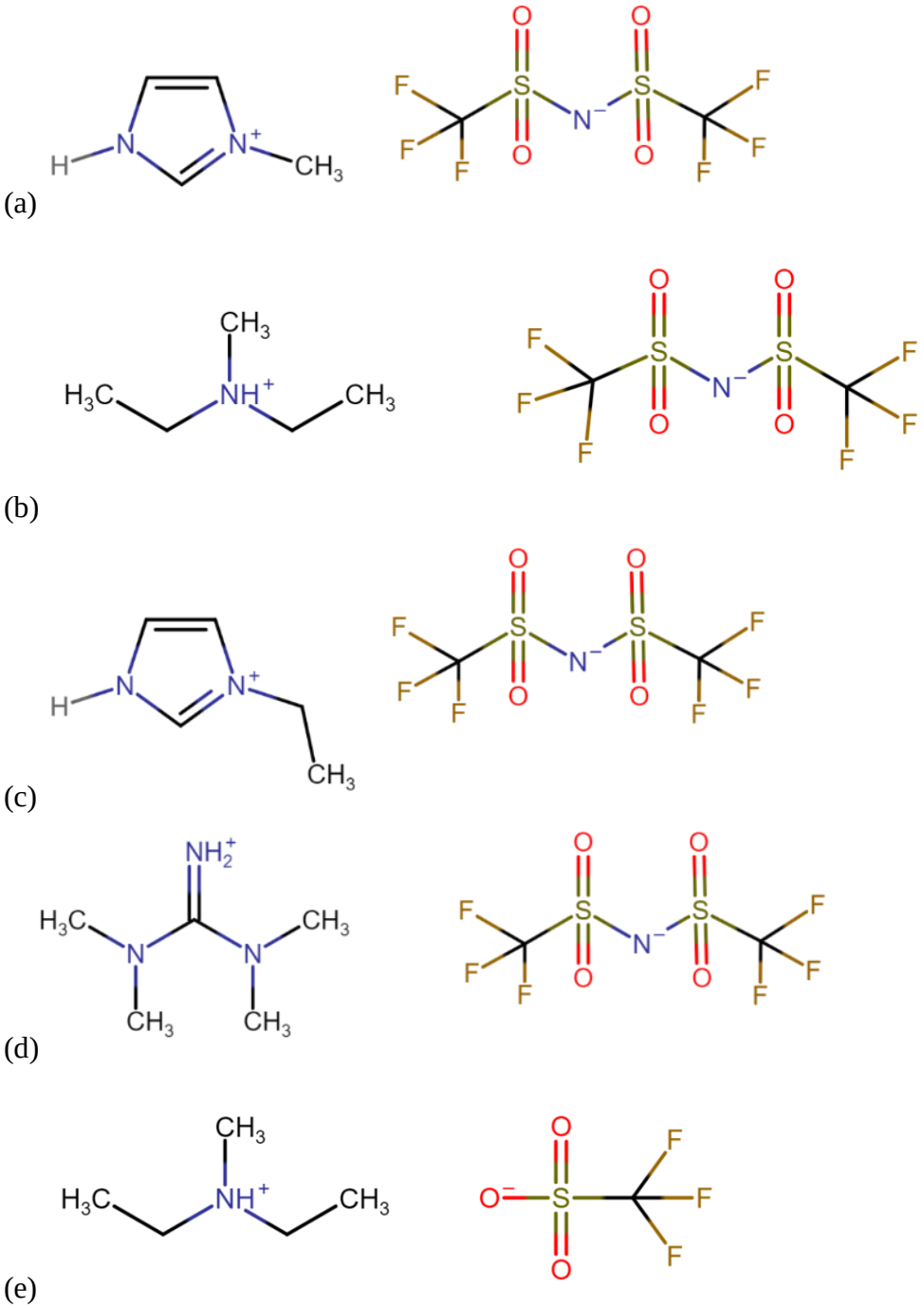

Figure 19 - Structures of the ionic liquids studied in this work: (a) [C_1Im][NTf_2], (b) [dema][NTf_2], (c) [C_2Im][NTf_2], (d) [HHTMG][NTf_2], (e) [dema][OTf]

Table 3 - Investigated ionic liquids and their physical-chemical properties

Abbreviation	Name of IL	Ionic conductivity (30°C), mS cm^{-1}	M_W, g mol^{-1}	Melting point, °C	ΔpKa*
IL1	$[C_1Im][NTf_2]$	7.2	363.27	49	17.0
IL2	$[dema][NTf_2]$	6.1[94]	367.00	25[95]	20.5
IL3	$[C_2Im][NTf_2]$	6.63[94]	376.00	< RT	18.5
IL4	$[HHTMG][NTf_2]$	3.1	381.00	-	23.9
IL5	[dema][OTf]	8.1	237.24	< RT	17.5

*pKa data are reported by Miran et al. in [96] for [dema] and $[C_2Im]$ and in [97] for [OTf] and $[NTf_2]$. pKa data for [HHTMG] are reported by Caine et al. [98]

For the synthesis of the ionic liquids, listed in Figure, the corresponding base (1.00 eq.) was dissolved in pure water (20 mL per 1 mL of base). To the resulting homogenous solution bis(trifluoromethanesulfonyl)imide (80% aqueous solution, 1.05 eq.) was added dropwise under ice cooling for about 30 min to form a second, hydrophobic phase. After additional stirring for 2 h, the aqueous phase was removed and the organic residue was dissolved in dichloromethane (15 mL per 1 mL of initial base) and extracted 4 times with water. The organic solvent was removed by rotary evaporation and the residue dried in oil-pump vacuum at 50ºC for two days. The identity and purity of the resulting ionic liquids was confirmed by NMR spectroscopy (which was left out of this work but can be checked in Supporting Information of the published work) [99].
Since the IL were used for high temperature operation later, the most promising IL were tested for bulk ionic conductivity. The bulk conductivities of the dry ILs have been measured by impedance spectroscopy using a SP-150 potentiostat from BioLogic (France) and a commercial sealed conductivity cell from WTW (Germany) consisting of two rectangular platinized platinum electrodes with nominal cell constant of 0.5 cm^{-1}. The cell constant was calibrated using commercial conductivity standards. Impedance measurements were recorded with amplitudes of 5, 10 and 15 mV and frequencies in the range of 200 kHz to 1 Hz in 50 logarithmic steps. The determined resistances with maximum deviation of 1% were averaged. The temperature was controlled using a Proline RP 1845 thermostat from LAUDA (Germany) with a maximum temperature deviation of 0.01ºC. The impedance measurements were carried out in the temperature range 25º<T<125ºC, due to limitations of the experimental setup. The uncertainty of the conductivity measurements as judged from commercial conductivity standards is estimated to be 2%.

The obtained values were fitted by the Vogel-Fulcher-Tammann equation:

$$\sigma = \sigma_0 \cdot e^{\frac{B}{T-T_0}}, \qquad \textit{Equation 9}$$

where σ_0, B and T_0 are material-dependent fitting parameters.

The obtained fitting parameters are given in Table 4 and the fitted curves are shown in Figure 20.

Table 4 - VFT fitting parameters for the specific conductivities of the dried bulk ILs

Ionic liquid	σ_0 / mS cm-1	B/K	T_0/K	R_2
IL2 [dema[NTf_2]	599.5	-583.2	171.7	0.99998
IL4 [HHTMG[NTf_2]	677.7	-664.8	179.7	0.99990

The Vogel-Fulcher-Tammann (VTF) equation is commonly used to describe the thermal dependence of the IL's specific conductivity since these fragile glass formers commonly show deviations from the Arrhenius law [100,101].

The extrapolated conductivities at 200ºC amount to 86 and 70 mS cm^{-1} for [HHTMG][NTf2] and [dema] [NTf2] respectively (Figure 20).

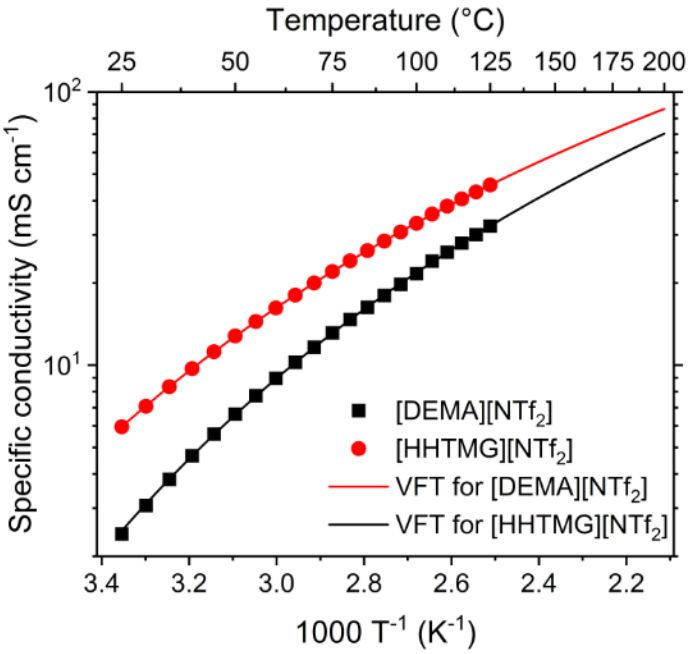

Figure 20 - Specific conductivities of our ionic liquids measured at 25-125°C (data points) and extrapolated to 200°C according to Vogel-Fulcher-Tammann (Equation 8) (drawn lines).

2.1.Ionic liquids immobilized into the polymer electrolyte. Structure of quasi-solidified ionic liquid membranes.

2.1.1. Membrane casting

Quasi-solidified ionic liquid membranes (QSILMs) were produced via direct blending and co-casting (Figure 21). The optimisation of the fabrication process and studies on the influence of the origin and content of IL on the composite membranes were accomplished in three steps.

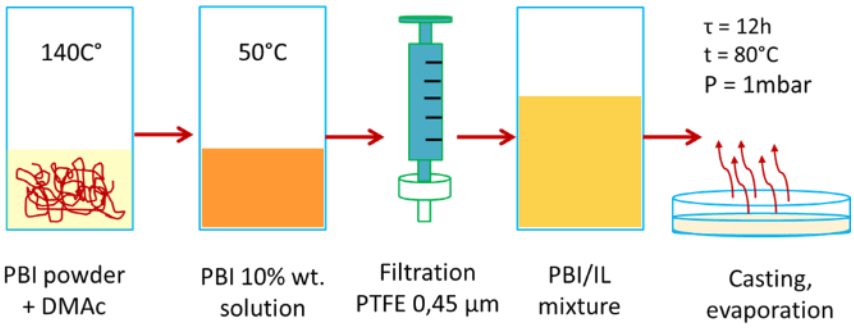

Figure 21 - Fabrication of quasi-solidified ionic liquid membranes via direct blending, casting and evaporation

A. Polymer solution preparation and IL/PBI mixture preparation

The commercial powder of PBI powder was dissolved in a certain amount of DMAc at 160 ºC for 24 h under vigorous stirring to obtain 7%wt. solution. After cooling to ambient temperature, the solution was filtered through 0.45 µm PTFE filter to remove undissolved impurities.

B. Optimization of IL content

The IL1 was mixed with the polymer solution in different IL/PBI ratios (0-2 with a step of 0.1) and left with stirring for at 24 h. After obtaining homogenous mixtures, composite membranes were casted in Petri dishes with flat bottoms and left in an oven at 80 ^{0}C for 24 h to ensure the solvent evaporation. The residual solvent was removed by evacuation (10 mbar) at 80ºC during 6 hours. After drying, all membranes were immersed in distilled water in order to remove the traces of the solvent and peel of the membranes from the glass substrate (Petri dish).

C. QSILMs samples fabrication

Selected ILs were mixed with the polymer solution in the following PBI/IL proportion: 1:1, 1:2 and 1:3. The composite membranes were fabricated as described above. In order to obtain samples of a bigger area for a fuel cell test, ILs/PBI mixtures were casted on a glass plate with a Doctor's knife. After drying as described above, all membranes were peeled off from the glass plate in water and dried in the gel-drier at 55°C for 4 h to obtain flat films. QSILMs were named as "*X.Y*", where *X* is related to the number of IL and *Y* is related to IL/PBI ratio in a composite membrane.

2.1.2. Acid treatment

In order to achieve necessary conductivity, QSILMs were doped with PA via two routes (Figure 22).

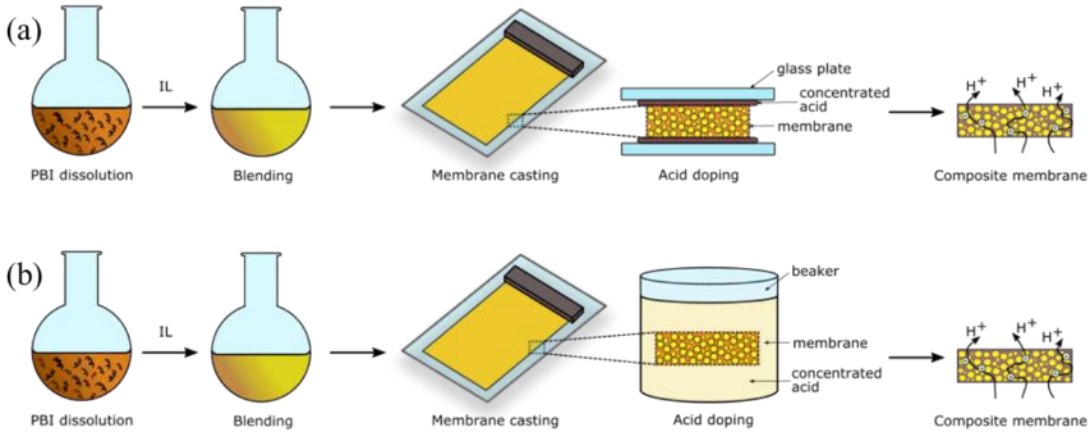

Figure 22 - Doping of quasi-solidified ionic liquids membranes

A. In thin PA film and in concentrated PA solution.

The doping of QSILMs in thin film was performed in the following way. The samples with dimensions of 12×18 mm^2 were dried in a vacuum oven at 120 ^{0}C and 1 mbar overnight and the weights W_1 were measured afterwards. Then the samples were placed between two objective glasses with thin layers containing certain amount of 85 wt% PA from both sides (Figure 22a) and left for 3 days to assure complete diffusion of PA into the membranes.

B. In bulk concentrated PA solution

Alternatively, all the samples were immersed into bulk 85%wt. PA for different periods of time from 15 min to 8h (Figure 22b).

C. Acid doping level (ADL) determination

The excess of PA was wiped off with blotting paper. In order to get rid of the remaining water, the samples were dried at 120 ^{0}C in the vacuum oven overnight, and the weights W_2 of the doped membranes were measured. Pristine PBI membrane was doped accordingly and considered as a reference membrane. The acid doping level (ADL) was calculated as following:

$$ADL = \frac{(W_2 - W_1) \cdot M_{PBI}}{M_{PA} \cdot W_{PBI}} \qquad \textit{Equation 10}$$

Pristine PBI membranes were doped with PA accordingly as reference membranes. After the optimization of ADL level, the doped QSILMs samples of a bigger surface were fabricated for the further fuel cell tests.

2.2.Ionic liquids immobilized into the polymer electrolyte. Structure of supported ionic liquid membranes.

2.2.1. PBI support fabrication

Polymer porous supports can be formed either by templating, porogen exlusion or phase inversion. There are several known approaches in phase inversion such as: 1) thermal-induced phase separation, 2) nonsolvent-induced phase separation/wet-casting (delayed immersed precipitation), 3) evaporation (dry-casting), 4) dry wet casting, 5) nonsolvent vapor-induced phase separation, 5) reaction and 6) shear-induced phase separation [102]. All the mentioned processes utilize different driving forces to have a control over the formation of a certain structure (symmetric or asymmetric). In this work, most of those approaches have been tried to form a stable porous PBI support.

A. Porogen exclusion

The porous PBI membrane was prepared using a modified procedure suggested by Li et al [103]. The polymer was added to NMP in order to obtain 5wt% solution. The mixture was left under continuous stirring at 175°C for 18 h until PBI was completely dissolved. The solution was cooled to 80°C and galactose powder was added in weight ratio of PBI/galactose = 1 : 1.5 followed by vigorous stirring for 4 h. The final dark-brown solution was casted onto a clean glass plate with a casting bar and heated in the oven in two steps: 80°C for 24 h followed by 140°C for 2h. The glass plate with a dry dark film on it was immersed in DW for 24 h and dried at 120°C for 12 h in a vacuum oven afterwards.

B. Vapor-induced phase separation (VIPS)

Four different PBI films named pPBI@1-4 were fabricated using procedures inspired and modified from the procedures that other research groups had reported earlier.

pPBI@1-2

Thus, the fabrication procedures for pPBI@1,2 were inspired by the work of Langevin et al. [89]. The proposed procedure was optimized in order to take into account the properties of PBI. The PBI powder (12 wt%) was added to NMP with LiCl (2 wt%) as the additive to prevent agglomeration. The mixture was left under continuous stirring at 175°C for 20 h until PBI was completely dissolved. Obtained dark-brown liquid was cooled to ambient temperature, filtered through PTFE filter (10 μm pore size) and split into half.

One portion was left untouched until casting (solution #1) and another one was modified as following. The solution was heated up to 80°C and PVP K90 (4 wt%) was added

slowly and left under vigorous stirring for 2 days until homogeneous viscous solution was obtained. The solution (solution #2) was cooled to ambient temperature and used for casting the membrane as following.

Solutions #1 and #2 were casted on the clean glass plate with Doctor's blade (200 µm gap) and placed into an humidity chamber at 25°C and 50% relative humidity (RH) for 6 h in order to induce phase inversion with water vapor as non-solvent (Figure 23). Thereafter the glass plates were immersed in water bath in order to peel off the freestanding polymer films followed by water/ethanol (50vol% : 50vol%) bath. The films were called pPBI@1 and pPBI@2 respectively.

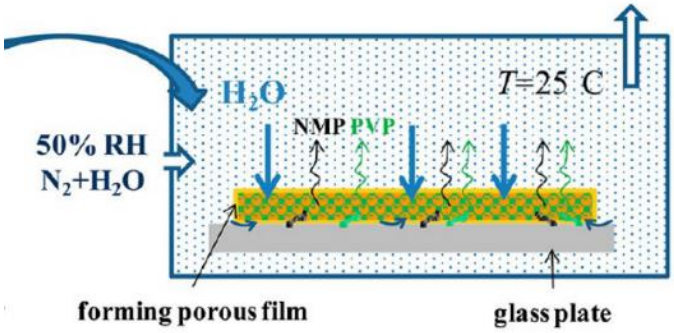

Figure 23 - Visualization of VIPS technique. Reprinted from [89].

pPBI@3

Sample pPBI@3 was casted from the solution #2 with Doctor's blade (300 µm gap) and placed into humidity chamber at 50°C and 80% RH for 1 h in order to induce phase inversion with water vapor as non-solvent. Thereafter the glass plates were immersed in water bath in order to peel off the freestanding polymer film followed by water/ethanol (50vol% : 50vol%) bath. The conditions of humidity chamber for pPBI@3 were reproduced from the work of Luo et al. [104] with a slight change in duration of VIPS process.

pPBI@4

The fabrication procedure for pPBI@4 were inspired by the work of Yuan et al. [105]. Thus, solution #3 was prepared by dissolving 8wt% of PBI powder in the certain amount of DMAc at 80°C for 36 h and filtered through 10 µm PFFE filter after cooling to ambient temperature. Afterwards solution #3 was casted with Doctor's blade (300 µm gap) and placed into humidity chamber at 50°C and 100% RH for 20 min in order to induce phase inversion with water vapor as non-solvent. Thereafter the glass plates were immersed in water bath in order to peel off the freestanding polymer film followed by water/ethanol (50vol% : 50vol%) bath. The sample was named as pPBI@4.

C. Delayed immersion precipitation in a solvent/nonsolvent mixture

PBI porous support was prepared using the modified procedure suggested by van de Ven et al. [88]. 1 g of PBI powder and 0.17 g of LiCl were dissolved in 8.8 ml of NMP at 175 °C under vigorous stirring for 24 h in order to obtain 10wt% solution. After cooling down to ambient temperature the solution was filtered through a 5 µm PTFE syringe filter. 0.15 g of PVP K30 were added slowly to the solution reheated up to 175 °C and stirred for 1 h. After the dissolution of the low molecular weight PVP, 0.15 g of PVP K90 were added and stirred at 175 °C for 24 h. After cooling to ambient temperature a viscous dark brown polymer solution was obtained.

The solution was casted onto a clean glass plate using a casting bar with a gap of 0.18 mm. The casted solution was then immersed into NMP/water (50vol% : 50vol%) coagulation bath for 30 min. After that the membranes were washed several times in pure water for 12 h to wash off the traces of NMP, PVP and LiCl and stored in DW until ILs impregnation.

2.2.2. Impregnation of IL into PBI support

Petri dishes filled with ILs were heated up till 50 ^{0}C in an oven to obtain $[C_1Im][NTf_2]$ and [HHTMG][NTf_2] in liquid state and decrease the viscosity of [dema][NTf_2] and $[C_2Im][NTf_2]$. The porous PBI support (pPBI) was immersed in absolute ethanol (99%) for at least 30 min in order to remove water from the pores. Samples of pPBI were quickly wiped with a tissue to remove the ethanol from the surface and were immersed into the molten ILs. The Petri dishes were gradually heated in an oven to 100 ^{0}C under 50 mbar vacuum and left overnight followed by 10 mbar vacuum for 1 h and 1 mbar for 10 min in order to replace ethanol with the corresponding ILs. After cooling to room temperature the membranes were removed from the bulk ILs and wiped with a tissue to remove the excess of ILs from the surface. The composite membrane containing $[C_1Im][NTf_2]$ was wiped with ethanol since this IL solidified on the surface at RT. The porous support (further named as pPIL) containing ILs was obtained and SILMs were named as pPIL**X** where **X** indicates the number of the IL presented in Table 3.

2.3.Ionic liquids immobilization onto the catalyst

2.3.1. Solid catalyst with ionic liquid layer (SCILL)

In order to study the effect of an IL onto the catalyst utilized in GDE (10% Pt/C), the catalyst was covered by the IL and electrochemical characteristics were measured. Catalyst particle covered with the IL was named SCILL (Solid Catalyst with Ionic Liquid Layer). The impregnation was done as following: 1) 90 mg of Pt/C (10 wt% Pt) was dispersed in 10 mL of i-propanol and 50 µL of [dema][NTf_2]; 2) the dispersion was intensively stirred at room temperature for 24 h and 3) ultrasonicated for 20 min. Obtained ink was placed in the flask of the rotary evaporator and evacuated in steps of 1) 137 mbar for 60°C, 2) 8 mbar, 60°C; 3) $2 \cdot 10^{-3}$ mbar, at room temperature overnight.

2.3.2. GDE treatment with phosphoric acid

Doping of GDE with phosphoric acid by pipetting from an aqueous solution

Firstly, 10wt% aqueous H_3PO_4 solution was prepared. Secondly, a weight of a clean pristine GDE (DPS) was measured (W_1) and a certain amount of the solution was applied to the surface of the GDE so that the loading of H_3PO_4 would be 10 mg cm^{-2}. Finally, GDE was dried at 90ºC for 24 hours, and the final weight was measured (W_2). The real loading was measured as a relative difference between W_1 and W_2.

Doping of GDE with phosphoric acid in contact with PA-doped PBI membrane

Firstly, commercial GDE were treated with PA using the following procedure: 1) commercial PBI membrane was immersed in concentrated PA until maximum doping level at RT was achieved; 2) the excess of PA was wiped off the membrane with paper tissue; 3) the membrane was sandwiched between two GDEs using a metal brick to ensure the contact between the surfaces and left for 1h to let PA diffuse to the GDEs; 4) the GDEs were removed from the membrane surface and stored on a Petri dish until the further usage. PA doping level of the GDEs was determined as the relative weight difference between pristine GDE and the treated one. The influence of PA was studied in the single fuel cell test using self-fabricated membranes.

2.3.3. Ionic liquid deposition onto commercial GDL/GDE

Doping of GDE with ionic liquid by pipetting from an ethanol solution

Firstly, 100 mg of IL was diluted with 4 mL of ethanol. Secondly, a weight of a clean pristine GDE (DPS) was measured (W_1) and a certain amount of the solution was applied to the surface of the GDE so that the loading of H_3PO_4 would be 2 mg cm^{-2}. Finally, GDE

was dried at RT for 1 hour, and the final weight was measured (W_2). The real loading was measured as a relative difference between W_1 and W_2.

Catalyst and catalyst/ionic liquid deposition by means of spraying

Secondly, GDEs were fabricated by coating of the commercial GDLs with the catalyst ink using a spraying robot (Figure 24). The catalyst ink was prepared as following: 1) 126 mg of commercial Pt/C catalyst (active carbon with pore volume of 1.02 mL/g as the support) was mixed with 9 mL of ethanol and 62.5 µL of IL6 was added; 2) the mixture was sonicated for 1 h until the dispersion obtained. The dispersion is not stable due to hydrophobic nature of the IL, therefore, the ink was sprayed immediately. The syringe is filled with the fresh ink dispersion and connected to the spraying device with a capillary. The spraying robot is programmed to pump the ink and deposit it onto the GDL by means of pressure following the defined pattern. GDL is fixed on the aluminum heating plate which is heated to 100ºC. The chamber is closed due to safety requirements and preventing any dust particles be co-deposited on the GDL surface.

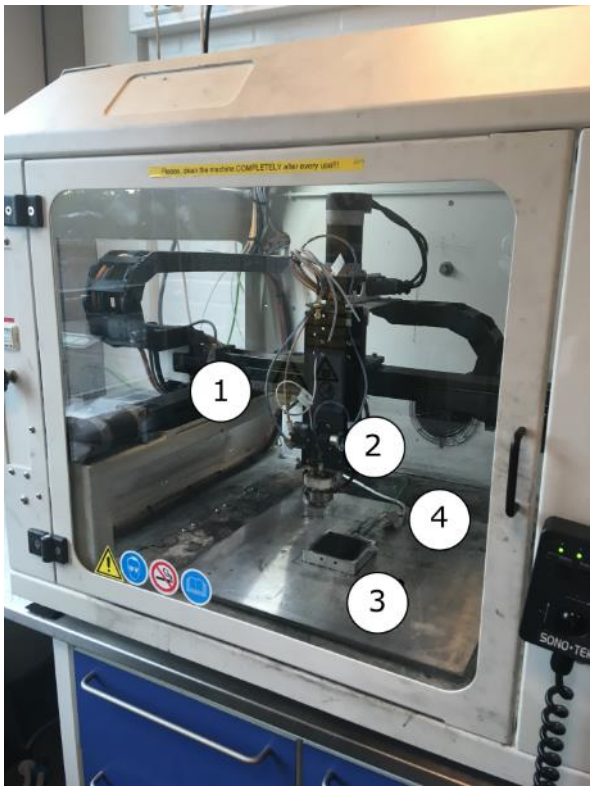

Figure 24 - Spraying robot (property of DTU Energy, Lyngby); (1) robot's moving arm; (2) ultrasonic nozzle; (3) heating plate with a sample fixed on the top and (4) heating rods connected to the plate. Ink is pumped by the glass syringe purchase from Trajan Scientific and Medical

2.4.Membrane-electrode assembly fabrication, single fuel cell test and durability test

2.4.1. Membrane-electrode assembly fabrication

The membrane electrode assemblies (MEA)s containing QSILMs with active area of 4 cm^2 were prepared by means of hot pressing using a Specac Atlas™ 15T Hydraulic Press coupled with Specac 4000 Series™ High Stability Temperature Controller (Figure 25). The composite membranes were pressed between commercial gas-diffusion electrodes (GDE) at 150 °C and 100 kg cm^{-2} for 10 min. The electrodes were doped with 1.7 mg_{PA} cm^{-2} for the better adhesion. The MEAs containing SILMs with active area of 25 cm^2 were assembled in a different cell without preliminary hot pressing.

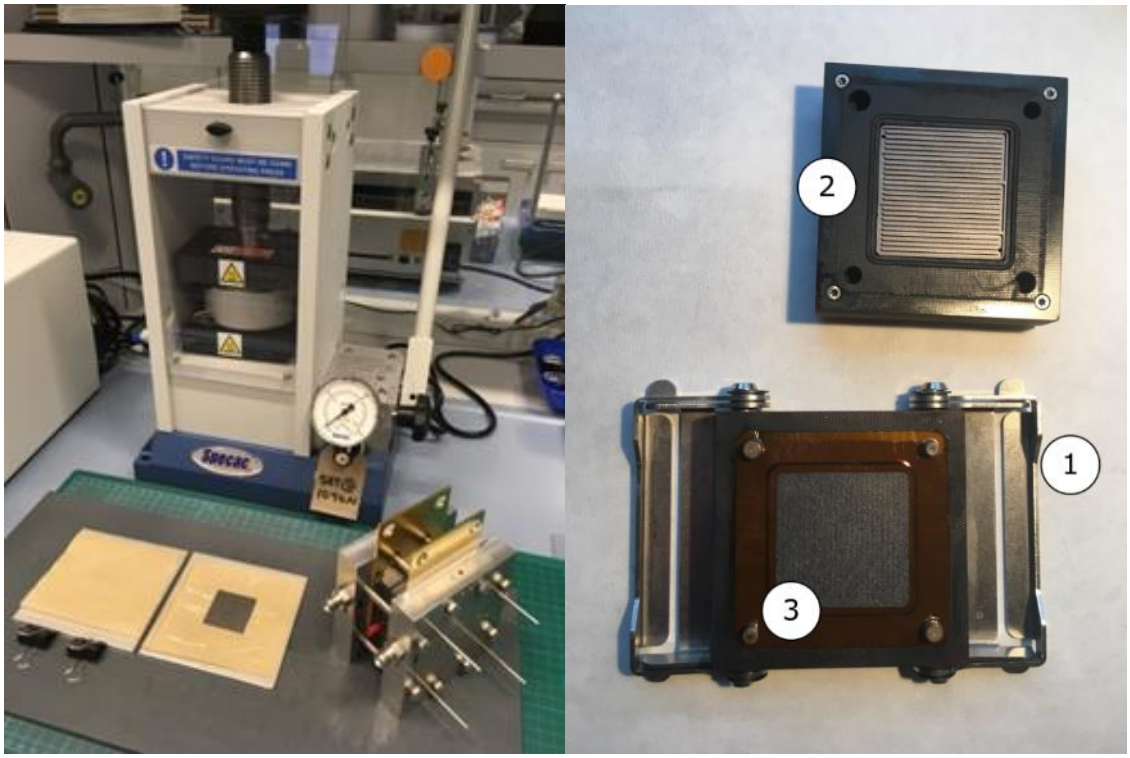

Figure 25 – (left) Hot press for membrane-electrode-assembly fabrication; (right)Fuel cell of 25 cm^2 active area for the test of porous SILM membrane (property of DTU Energy, Lyngby): (1) fuel cell housing; (2) graphite plates with flow pattern; (3) self-fabricated MEA with Kapton® gasket

2.4.2. Single fuel cell test

The performances of the MEAs were evaluated by measuring polarization (I-V) curves using a test station presented in Figure 26. The obtained MEAs were sandwiched with the clamping torque 2 N m^{-1} between two carbon plates with serpentine flow pattern and two end plates with metal rods for heating to high temperatures (Figure 27). The anode side was supplied with hydrogen at a flowrate of 60 mL min^{-1} and cathode side was supplied with air flow of 180 mL min^{-1}. Prior to obtaining the polarization curves the MEAs were preconditioned at 0.2 A cm^{-2} until constant voltage was reached. Polarization curves were recorded in galvanostatic mode.

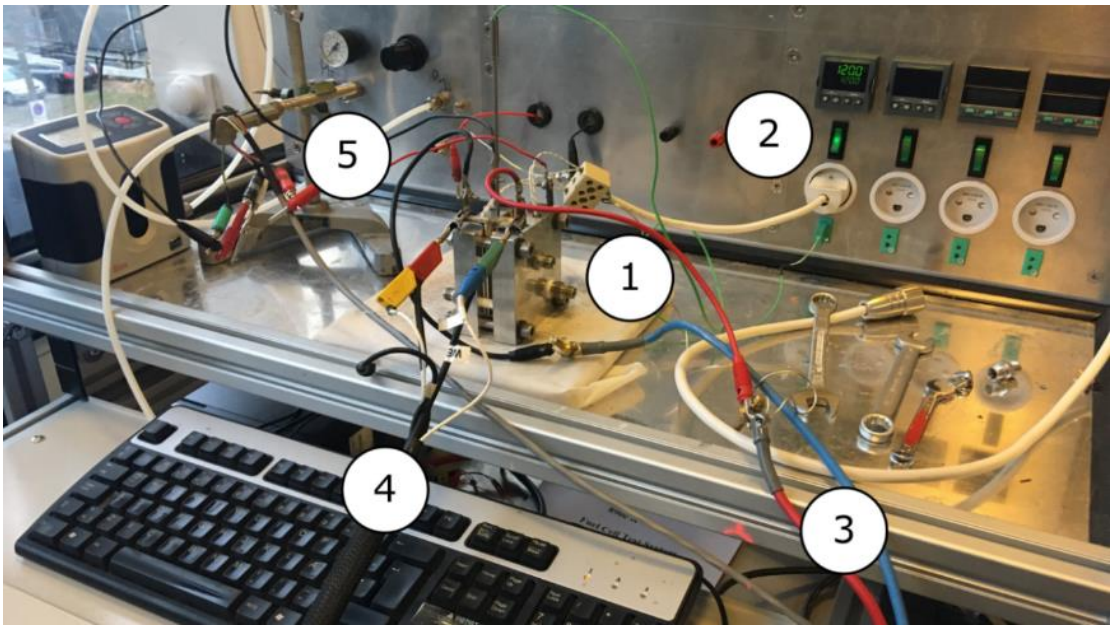

Figure 26 - Fuel cell station (property of DTU Energy, Lyngby): (1) fuel cell; (2) heating rods and a thermocouple connected to temperature controller; (3) load cables connected to Scribner complex of 885 Potentiostat and 890ZV Test Load; (4) cable connection for BioLogic Potentiostat for impedance measurements; (5) H_2 and air lines

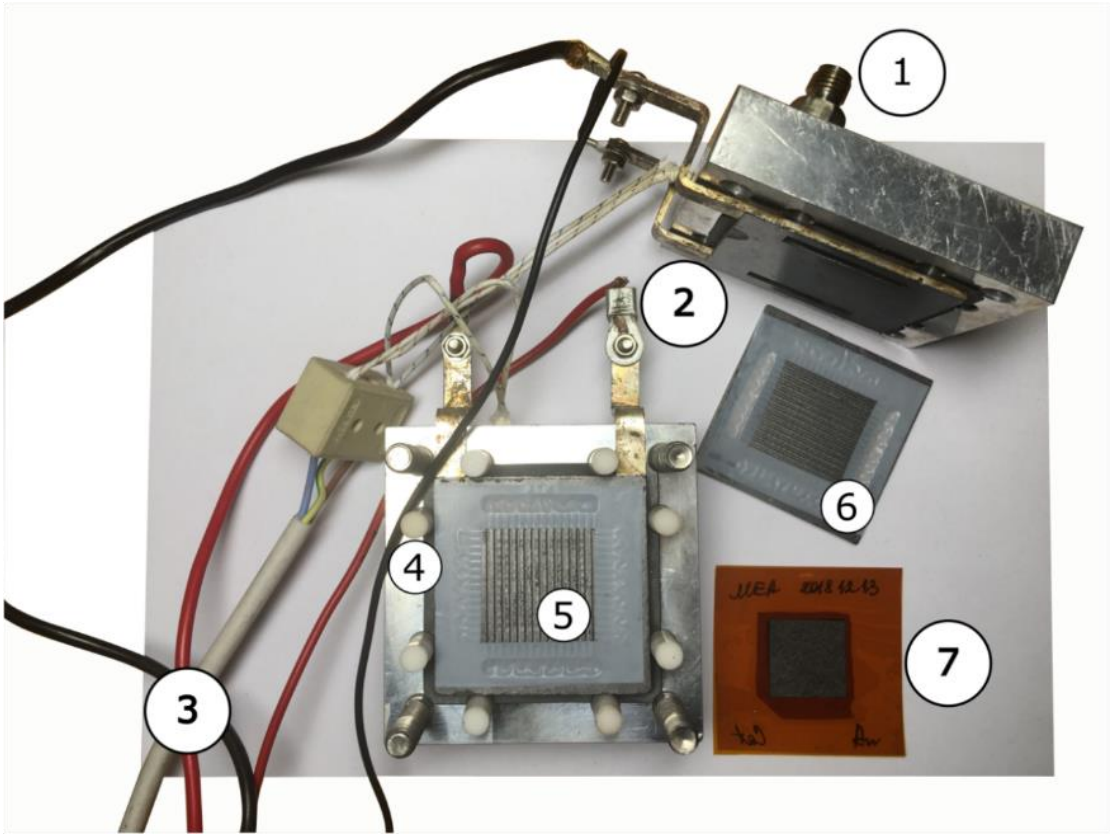

Figure 27 - Fuel cell of 5 cm2 active area for the test of blended QSILM membrane (property of DTU Energy, Lyngby): (1) end plates in gas inlet and outlet from the opposite sides; (2) current collectors; (3) load cables; (4) heating rods; (5) graphite plates with serpentine flow pattern assembled perpendicular to each other; (6) PTFE gasket; (7) self-fabricated MEA with Kapton® gasket

2.4.3. Fuel cell durability test

After a single fuel cell test, durability of the MEA was checked as following: 1) the cell was heated up to 200ºC under the flow of H_2 (40 mL min^{-1}) at the anode side and air (80 mL min^{-1}) at the cathode side. Potential was continuously measured at 0.2 A cm^{-2}. Electrochemical impedance spectra (EIS) were detected in order to monitor the state of the cell.

2.5.Characterization techniques

Fourier-transform (FT-IR) spectroscopy

FT-IR spectroscopy is a common technique to study chemical bonds within material. It allows a researcher to detect vibrations of functional groups and interconnections between them in order to reproduce the structure of the composition. In current work FT-IR spectroscopy was used to prove the existence of ILs inside the composite membranes and investigate possible chemical bonding between ILs and the hosting polymer. FT-IR analyzer Shimadyu IRSpirit (Japan) was used to investigate transmittance spectra of the composite membranes in the wavenumber window of 4000 - 400 cm^{-1}.

Scanning electron microscopy (SEM)

SEM is commonly used to obtain information on the surface and cross-section morphology of a sample. It is an essential tool for membranes studies since it detects possible damages in the structure such as pinholes and cracks. It also provides information on thickness, homogeneity and phase separation. In current work SEM was used to analyze the distribution of ILs within polymer matrices. The samples were gold coated using Emitech K675X sputter equipment operating at 125 mA during 45 s in a 10 mbar argon atmosphere. SEM pictures were taken using a FEI scanning electron microscope (QuantaTM 250 FEG) operating at 5 kV. Cross-section SEM image of the MEA after a fuel cell operation was done using Zeiss microscope.

Fluorescence microscopy

Fluorescence Microscopy was carried out using an Olympus IX71 coupled with the fluorescent lamp Olympus U-RFL-T to get pictures of fluorescence of the QSILMs structures. Extinction was applied in a blue range of spectra with λ=360-370 nm and emission was detected at λ>420 nm.

Energy-dispersive X-ray (EDX) spectroscopy

EDX spectroscopy is frequently used as an extension tool to SEM for elemental analysis of the scanned specimen. The fundamentals of the technique rely on the fact that each chemical element has a unique atomic structure which results into different position of electromagnetic emission peaks in the spectrum. The position can be predicated by Moseley's law. In order to receive an emission peak, the sample is initially excited by a focused electron beam, the released X-ray energy is thereafter converted into a voltage signal on the X-ray detector, a pulse processor measures that signal and sends the data further to the analyzer. In scope of this work EDX was used to detect the chemical elements inside the fabricated membranes in order to identify the presence of the incorporated liquids.

Thermogravimetric analysis (TGA)

TGA is used to analyze thermal stability of the studied materials in a certain range of temperatures and gas atmosphere. In the current work a Netzsch TG 209F1 Iris analysis system was used to determine the thermal behavior of the composite membranes. Samples were analyzed in the temperature range from 30 to 800 ^{0}C at the heating rate of 10 K min^{-1} under an air flow of 40 mL min^{-1}.

Brunauer–Emmett–Teller (BET) method

The BET method serves as a common tool to measure the specific surface area of materials. It also indicates the total volume of the pores and their average size. The technique is based on recording the isotherm of nitrogen adsorption on a solid surface of a sample. In this work BET was used to estimate the open porosity of the composite membrane specimen. Preliminarily all the samples were dried in the oven at 120°C for 24 h and afterwards 9 point measurements were conducted.

Tensile strength

Stress-strain curves were recorded by a Cometech machine Model QC-508E (Taiwan), equipped with a 50N load cell to analyze rigid properties of the membranes. Room temperature and humidity were recorded. The membrane specimen with a length L_0=4 cm, width w_0=1 cm and thicknesses d_0 were clipped between two clamps which were pulled apart with a speed of 1mm min^{-1} until 1% specimen elongation to determine Young's modulus followed by 10 mm min^{-1} to determine tensile strength and elongation at break afterwards. At least five repetitions were done for each sample.

Force F was recalculated to stress (σ) as following:

$$\sigma[MPa] = F/(w_0 \times d_0) \qquad \textit{Equation 11}$$

Elongation was (ε) defined as the gauge length in percentage according to:

$$\varepsilon[\%] = (L - L_0)/L_0 \qquad \textit{Equation 12}$$

Young Modulus [GPa] was calculated as a linear slope of the initial part of the curve in the stress/elongation diagram. The linear behavior at the beginning of the measurement indicates the reversible behavior of the material. Tensile strength [MPa] was measured as maximum load before the break. Each parameter was evaluated as average for 5 samples of the same specimen.

Electrochemically active surface area (EASA)

The EAS area can be evaluated from the charge required to reduce a monolayer of protons on Pt (hydrogen adsorption) and calculated from cyclovoltammograms as follows:

$$EASA\ \left(\frac{cm^2_{Pt}}{q_{Pt}}\right) = \frac{q_{Pt}}{\Gamma \times L} \qquad \textit{Equation 13}$$

where q_{Pt} is the voltammetric charge density in C $cm^{-2}_{electrode}$;

$$q_{Pt}\left(\frac{C}{cm}\right) = \frac{s}{\vartheta} \qquad \textit{Equation 14}$$

s – integrated area of the peak in mA V cm^{-2} (Figure 28);

v – scanning speed in cm^2;

Γ = 210 µC cm^{-2} - reference value of the hydrogen desorption signal (Q_H);

L is the Pt loading in g cm^{-2}.

Figure 28 shows a typical CV curve used for EAS calculation

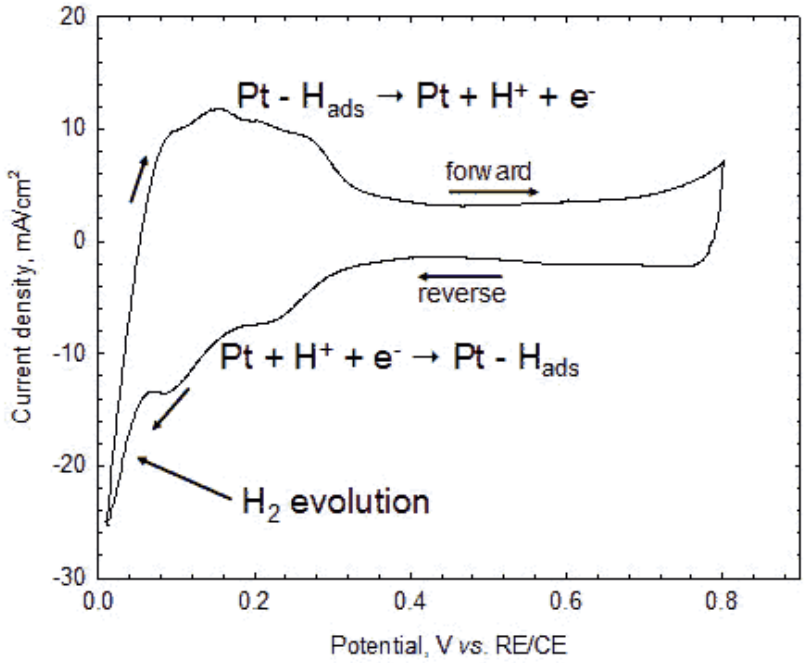

Figure 28 - Cyclic voltammogram of PEM fuel cell catalyst layer for EASA analysis by hydrogen adsorption/desorption. Conditions: Scan rate = 40 mV/s; Cell: 35 °C; 100% RH anode/cathode; 1 atm [106]

EASA was determined by cyclic voltammetry (CV). The glassy carbon (GC) surface was firstly pretreated (cleaned) in N_2 saturated electrolyte 0.1 M HClO4 at 0-1.3 V vs. HRE (hydrogen reversable electrode) for 20 cycles at the ramp of 100 mV s^{-1}.

After that the SCILL (10%wtPt/C+IL2) ink was prepared as following: 1) 45 mg of SCILL was dispersed in 5.06 g of DW, 1.0 g of i-propanol with addition of 0.03 g of

Nafion (5 %wt. alcohol solution); 2) the dispersion was placed in the ultrasonic bath for 10 min until visually homogeneous black dispersion was formed. At the next step, 50 µL of the dispersion was dropped onto the GC surface of 15 mm in diameter, resulting into Pt loading of 36.1 µg per GC (20.4µg cm^{-2}).

The electrochemical cell (Figure 29) was a conventional three-electrode system: a working electrode (WE), a counter-electrode (CE) and a reference electrode (RE). GC covered by a catalyst sample acted as a WE which was immersed in the electrolyte solution and rotated at the defined speed by a motor. A Pt spiral was used as a CE and a reversible hydrogen electrode (RHE) was used as a RE. The working beaker with the electrolyte was purged with N_2 30 min (bubbling). CV curves were recorded at 1600 rpm rotating speed while cycling between 0.05-1.3 V at the scanning ramp of 10 mV s^{-1}. The ink with the reference catalyst (10%wtPt/C) was prepared and characterized identically.

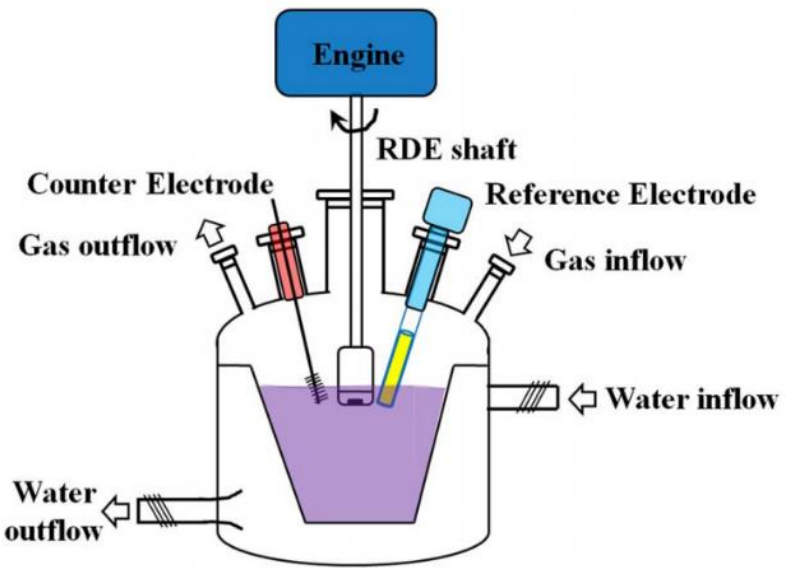

Figure 29 - Three-electrode system connected to the motor for Rotation Disk Electrode experiments. Reprinted from [107].

Conductivity

Ion conductivity is one of the main properties of the polymer electrolyte. In order to measure in-plane conductivity, an appropriate cell was self-fabricated. The cell has a Teflon interior with four platinum wires for four-probe connection and stainless steel metal end plates connected to the heating elements and a gas line. Two outer wires are used to apply a current and marked as working (W) and counter (C) electrodes The inner ones are used as potential probe and marked as reference (R) and sense (S) electrodes

(Jakobsen, Jensen, Cleemann, & Li, 2016). The samples of 10×20mm^2 were fixed between four wires as shown on the Figure 30.

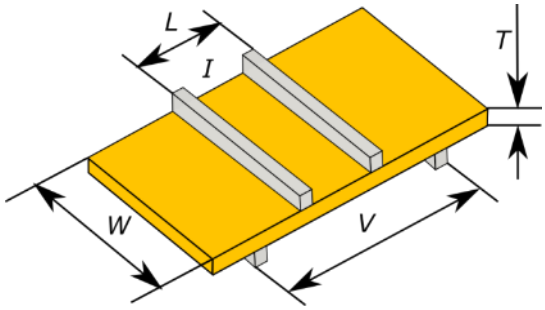

Figure 30 - The position of the membrane and the electrodes inside the Teflon cell designed and fabricated in-house for ionic conductivity measurements

The outer and inner wires are located at the different sides of the membrane to measure the resistance in the plane of the membrane avoiding measurements of the surface conductivity. The thickness of the samples was measured with a micrometer. The cell was connected to a Bio-Logic SP-150 potentiostat (Bio-Logic Science Instruments, France), to perform cyclic voltammetry in H_2 flow at high temperatures (80-180 ^{0}C) without humidification for SILMs and with RH=5% for QSILMs. Resistance was taken as a *I-V* slope in a range of -0.3V < ΔE < 0.3V with a rate of 10 mV s^{-1}. The proton conductivities for all the membranes were calculated from:

$$\sigma = \frac{L}{R \cdot W \cdot T} \qquad \textit{Equation 15}$$

Here σ is the proton conductivity in S cm^{-1}, L is the distance between inner electrodes (L=0.425cm), R is the measured resistance in Ohm, W is the width and T is the thickness of the membrane in cm.

Two different devices were used to measure the conductivities of the samples: 1) a commercially available Scribner 740 test system – for the samples with conductivity values < 0.1 mS cm^{-1} (Figure 31), and 2) a self-made cell – for the samples with conductivity values > 0.1 mS cm^{-1} (Figure 32) integrated in the built unit (Figure 33).

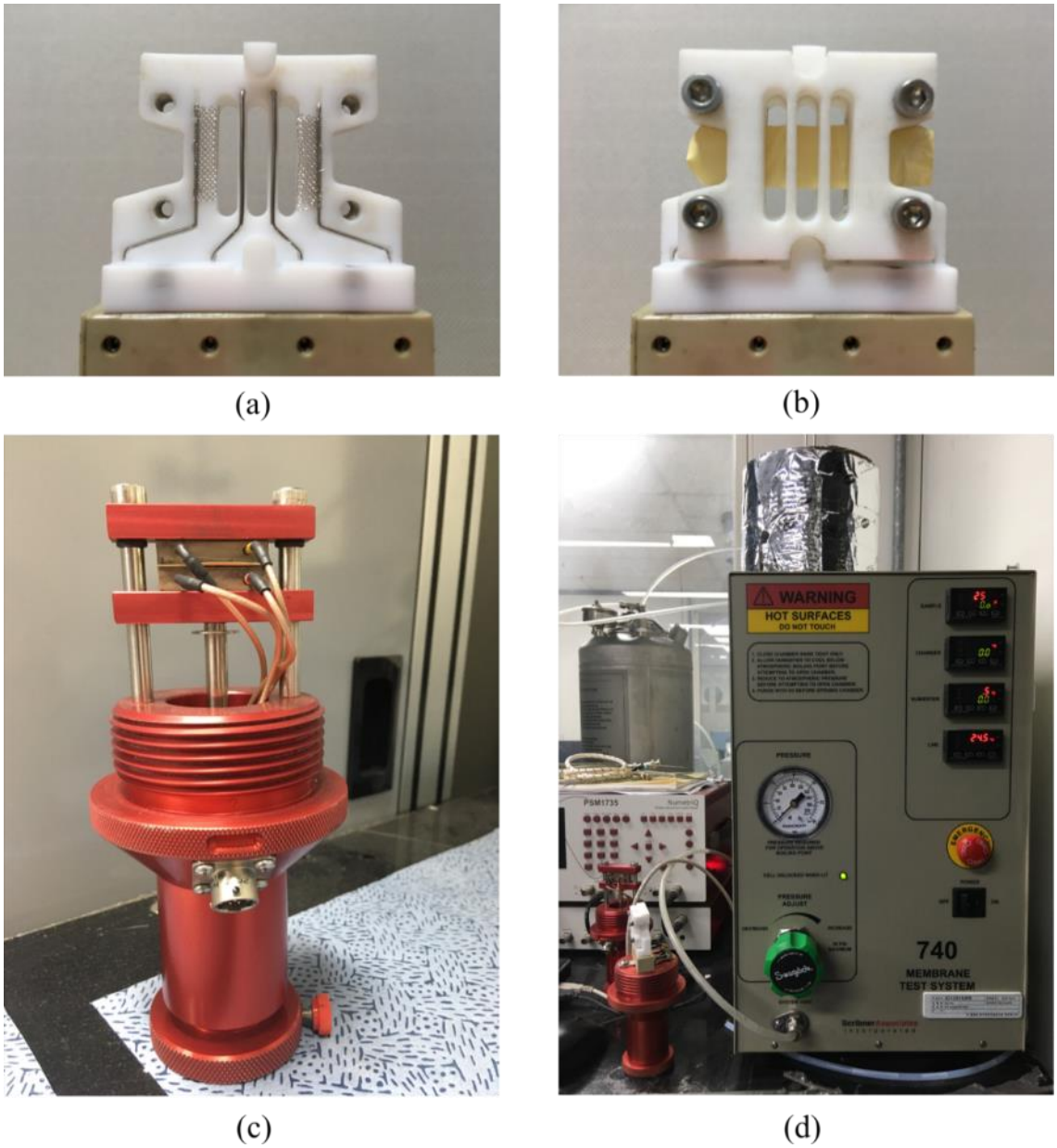

Figure 31 - Scribner 740 test system (property of KIST Fuel Cell Research Center, Seoul): (a) open PTFE cell for in-plane conductivity measurements with 4-probe-connection; (b) closed PTFE cell with the QSILM fixed on the top of four Pt wires; (c) closed cell for

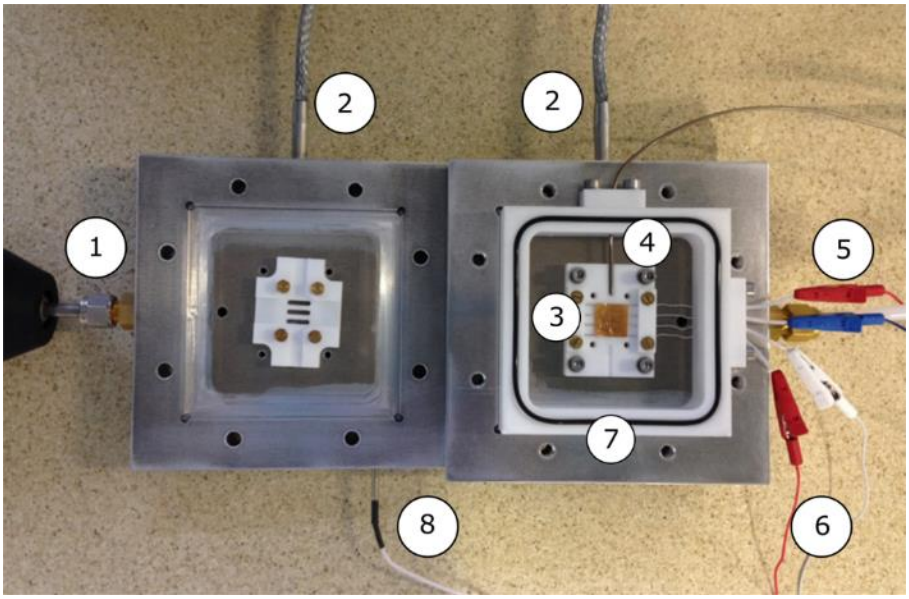

Figure 32 - In-plane conductivity measurements cell: (1) gas inlet (connected to humidity controller); (2) heating rods; (3) PTFE cell with 4 Pt wires 0.5 mm each; (4) thermocouple for temperature check inside the PTFE cell; (5) gas outlet; (6) 4-probe-connection to BioLogic potentiostat; (7) rubber sealing; (8) thermocouple for end plate temperature control

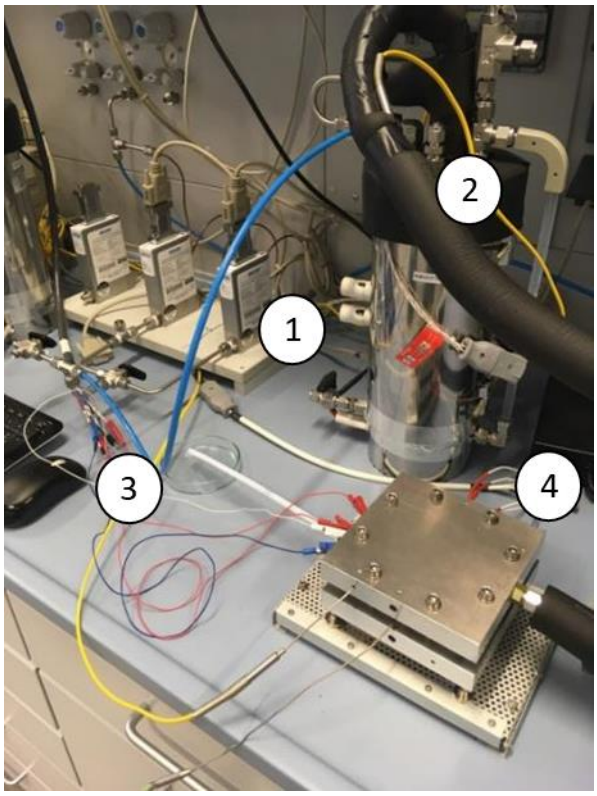

Figure 33 - Self-made cell connected to (1) - mass flow controllers; (2) gas humidifier (bubbler); (3) cables of potentiostat; (4) heating

3. Results and discussion

3.1.Supported ionic liquid membranes

3.1.1. Membrane fabrication and characterization

First of all, in order to prepare freestanding SILMs, homogeneous porous PBI support with good mechanical properties must be fabricated. Therefore, two common phase inversion techniques of pore formation within thin polymer films were investigated: *1) vapor induced phase separation (VIPS)* and 2) *delayed immersion precipitation in a solvent/nonsolvent mixture (DIP).* As mentioned before, both processes utilize different driving forces to have a control over the formation of a certain structure (symmetric or asymmetric). The crucial factors that must be optimized in order to achieve a porous structure in PBI film are the origin of the solvent, the concentration of the polymer solution, the presence/absence of a porogen and its concentration, and the thickness of the casting bar's gap in accordance to the conditions in a humidity chamber or a non-solvent concentration in the precipitation bath.

VIPS technique for porous PBI support fabrication

Phase inversion is strongly influenced by relative humidity in VIPS [102]. The impact of such parameters as relative humidity, temperature, time and porogen on morphology was studied by means of cross-section SEM (Figure 34). Additionally, mechanical properties of the obtained membranes were evaluated. Table 5 shows the main parameters of the porous PBI support fabrication via VIPS technique and appearance of the membranes.

Table 5 - Conditions of porous PBI support preparation via vapor induced phase separation technique

Sample	Solvent	PVP	Doctor's blade gap, mm	Parameters of humidity chamber			Observations
				T, °C	RH, %	*τ*, h	
pPBI@1	12wt%NMP+ 2wt%LiCl	-	0.2	25	50	6	Continuous, brittle after water bath
pPBI@2	12wt%NMP+ 2wt%LiCl	+	0.2	25	50	6	Freestanding, cracked on a carbon tape due to drying out
pPBI@3	12wt%NMP+ 2wt%LiCl	+	0.3	50	80	1	Continuous, brittle after water bath, cracked in air
pPBI@4	8wt%DMAc	-	0.3	50	100	0.3	Continuous after casting, impossible to peel off

From the SEM images it is possible to see that during the process of VIPS the polymer solidifies with formation of micro- and macro voids and therefore, a friable structure. There is no visible polymer net which would hold the structure and make the support rigid, therefore the membranes were observed to break either during washing process or directly after removal from the water bath due to dry out. The only freestanding membrane among the samples was pPBI@2 which exhibits a dense morphology (Figure 35a). However, the semi-opaque appearance of the film gives the indication of the potential nano size pores or avoids formation which cannot be clearly seen on SEM images (Figure 34).

The fact that it was impossible to reproduce the porous structures that have been reported by previously mentioned groups, can be due to the difference between the chemical structures and molecular weights of the initial polymers. Thus, it is visible that for the selected polymer of a certain molecular weight VIPS technique is not a desired technique of a stable porous structure formation. Therefore, another approach – DIP – was investigated as an alternative fabrication technique.

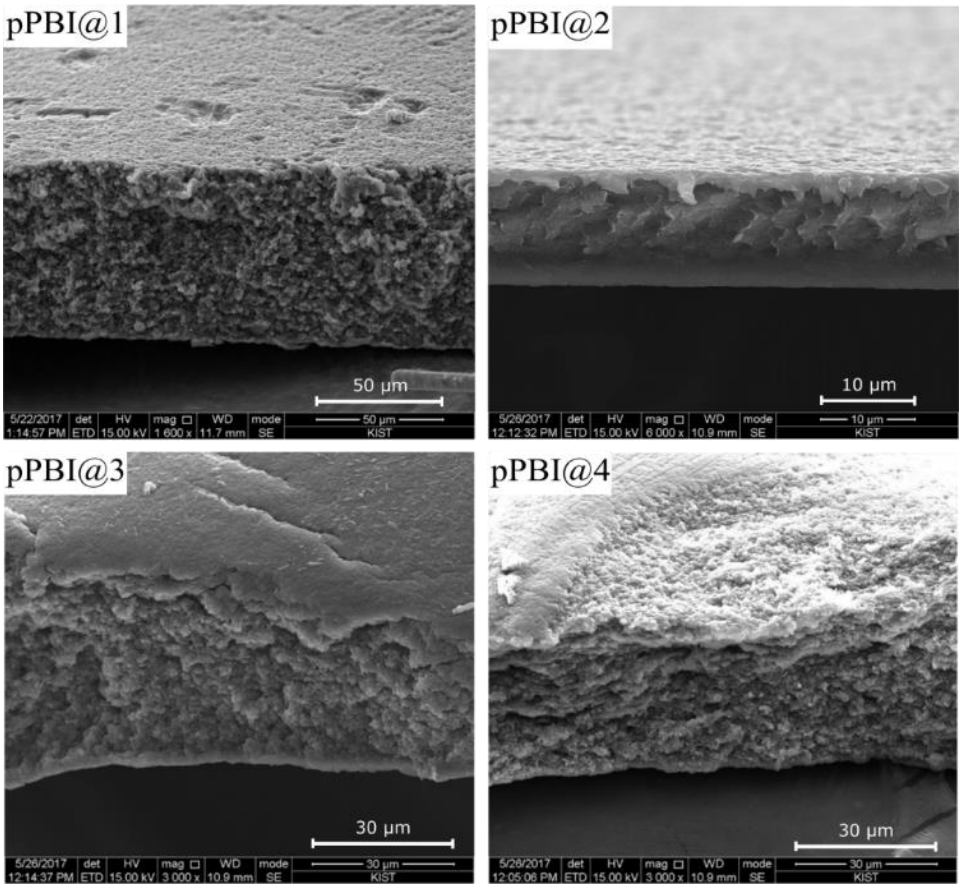

Figure 34 - Cross-section SEM images of the polybenzimidazole film p-PBI@X obtained via vapor induced phase separation technique

The above described part of the work was done in Korean Institute of Science and Technology, Fuel Cell Research Center (Seoul, South Korea).

DIP technique for porous PBI support fabrication

Alternatively, the sample of a PBI film was prepared via DIP approach (Figure 35b). A freestanding membrane with visually homogeneous semi-opaque structure was obtained. Since the membrane obtained via DIP approach exhibited better visual mechanical stability and the related technique does not require such special equipment as a humidity chamber, all the further samples were fabricated according to DIP approach.

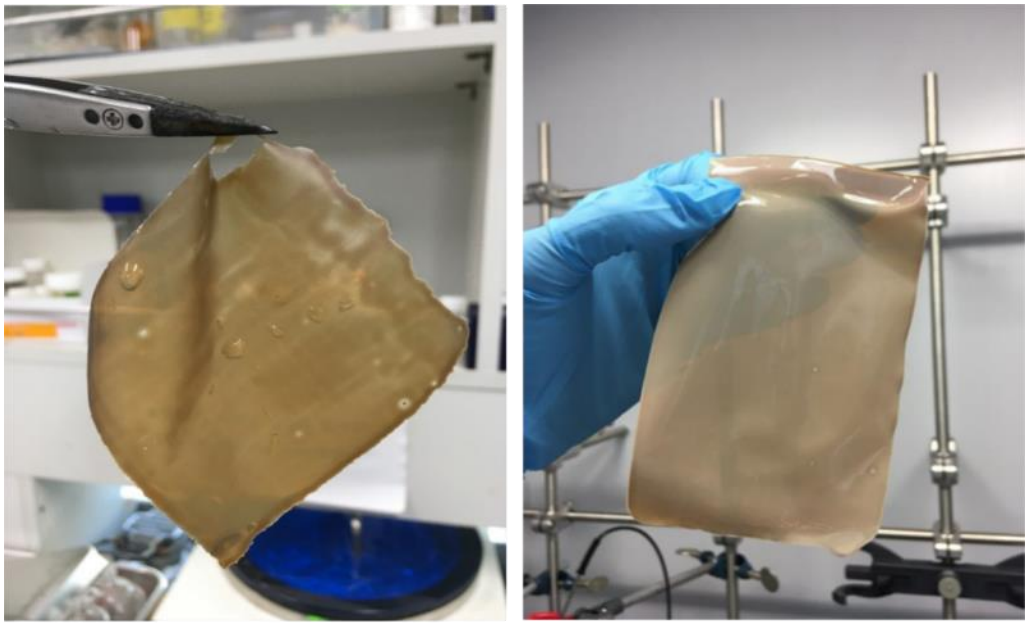

(a) (b)

Figure 35 - Polybenzimidazole support freestanding membranes obtained via a) vapor induced phase separation (pPBI@2); b) delayed immersion precipitation (pPBI@5)

The membrane was observed to quickly dry out in the air after removing from the ethanol bath. This induced shrinking and becoming transparent as the evidence of collapse of the pores which is supported the SEM image (Figure 36). Therefore, the procedure was developed in the way of direct replacement of ethanol inside the pores by corresponding ILs while skipping the drying step as proposed by van de Van et al [88]. Since the investigated ILs are all soluble in ethanol, they can easily diffuse inside the pores. When the Petri dishes are heated in the vacuum oven at 100°C and 50 mbar, the ethanol slowly evaporates from the pores, which get therefore gradually filled with the ILs. The appearance of bubbles indicates the evaporation process. Increasing the vacuum ensures the maximum possible loading of ILs. No shrinking or brittleness was observed for the samples wetted with ILs which have negligible vapor pressure. This optimization of the process ensures the remaining of a porous structure without losing visual mechanical stability of the films.

The morphologies of the porous support and the SILMs were investigated using SEM. Figure 36 represents the surface images and the cross-section images of the membranes.

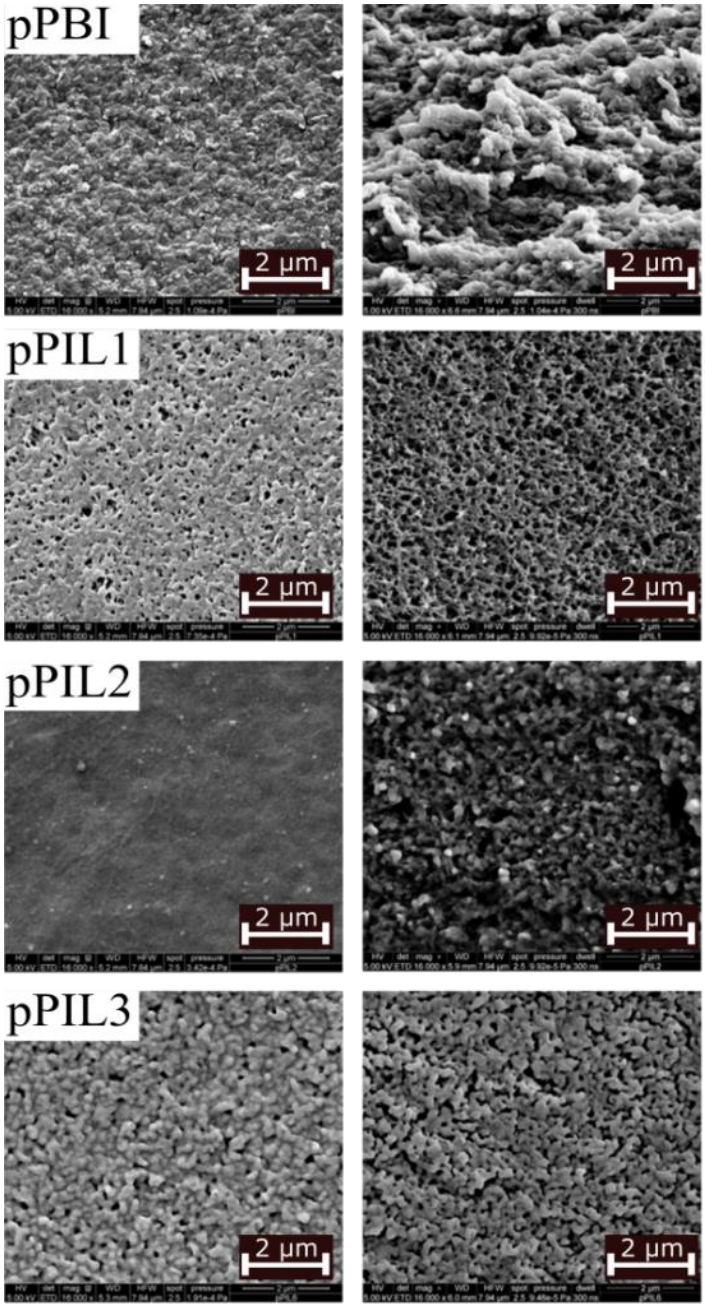

Figure 36 - SEM images (×16 000) of the surfaces (left) and cross-sections (right) of the fabricated SILMs

Cross-section images of SILMs demonstrate a network of channels of ILs confined in PBI matrices. Since $[C_1Im][NTf_2]$ is solid at room temperature, a discontinuous layer of the salt can be observed on the membrane's surface even after wiping the membrane with absolute ethanol. We conclude that $[C_1Im][NTf_2]$ does not penetrate into the membrane properly due to its high viscosity and instead remains on the surface. This causes poor mechanical properties and the membrane cannot be exploited for MEA preparation. The result does not correlate with the work of van de Ven et al. who observed on SEM images

that pores of PBI support got filled with $[C_1Im][NTf_2]$ and successfully prepared the MEA [88]. This may occur due to impregnation of the porous support in n-hexane at the last step that they implemented. The porous support we obtained was highly brittle after n-hexane bath which made further impregnation of ILs difficult. Thus, in our work we eliminated this step, in order to maintain the pores of the support continuously filled.

In contrast to the IL mentioned above, $[dema][NTf_2]$ and $[C_2Im][NTf_2]$ act in SILMs as plasticizers enshrouding the polymer network. Due to their plasticizing effect, they increase segmental motion of PBI chains that makes PBI backbone more flexible to help ion transfer. The main difference between the samples can be observed on the surface of the membranes. The sample pPIL3 has partially open surface porosity (Figure 36) while the sample pPIL2 has a dense surface layer formed by total coverage of PBI pores with the correspondent IL (Figure 36).

Unfortunately, measurement of the surface area and pores distribution showed unreliable results, since during the heating process a condensate was formed even above 180ºC. It can be explained by the increasing viscosity of ILs immobilized in open pores. Since they are hydrophobic, washing samples with water would not ensure the total removal. Washing the samples with ethanol, on the other hand, would collapse the pores. For all the samples, the specific surface area was low (the data are not sufficient for the graphical demonstration). Low surface area can be associated with the following factors: a) low porosity or no macroporosity; b) pores are narrower than 0.4 nm, where N_2 cannot penetrate. Therefore, the estimation of the pore size was done only based on SEM cross-section images.

The loading for SILMs was done by washing with ethanol followed by drying and measurement of the weight loss. The loading values were calculated: for pPIL1 it is 435 ± 142 wt%, for PIL2 – 463 ±9 wt% and for pPIL3 – 312 ± 21 wt%. Therefore, the loading distribution for pPIL1 is ±33% whereas this is only 1.9% for pPIL2 and 6.8% for pPIL3 (Figure 37). This large difference to the samples containing IL1 indicates that there is no control over the amount of IL wiped from the surface and the pores with ethanol. Therefore, we believe that ILs which are solid at room temperature are not suitable for reproducible production of SILMs structures.

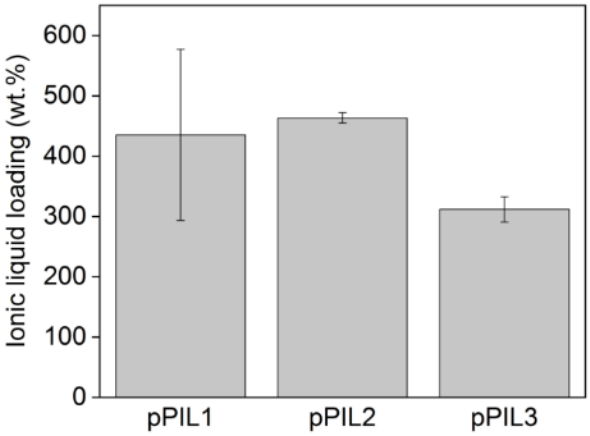

Figure 37 - Ionic liquids loading in the fabricated SILMs

The chemical structures of SILMs were investigated by FT-IR spectroscopy (Figure 38). As shown, all the samples display characteristic peaks of PBI at the wavelength 800-500 cm^{-1} which include the peaks of imidazole and benzene rings. Moreover, all of them have peaks of 1360-1335 cm^{-1} and 1170-1145 cm^{-1} representing antisymmetric and symmetric stretch vibrations of SO_2 groups in sulfonamides which corresponds to [NTf_2] anion and indicates the presence of ILs in the SILMs.

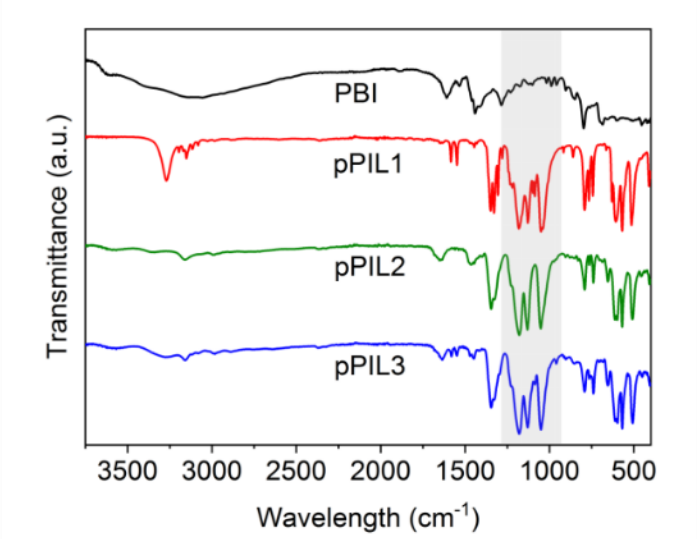

Figure 38 - FT-IR spectra of the fabricated SILMs

Thermogravimetric curves in Figure 39 shows that the PBI support quickly adsorbs water from air through the open pores structure. Hence, 7.8% of the weight loss at 200°C occurs due to water evaporation. Composite membranes exhibit < 1% of the weight loss at 200 °C (0.6% - pPIL1, 0.4% - pPIL2, 0.2% - pPIL3) since the macropores on the surface are blocked with ILs which corresponds to the finding from SEM images.

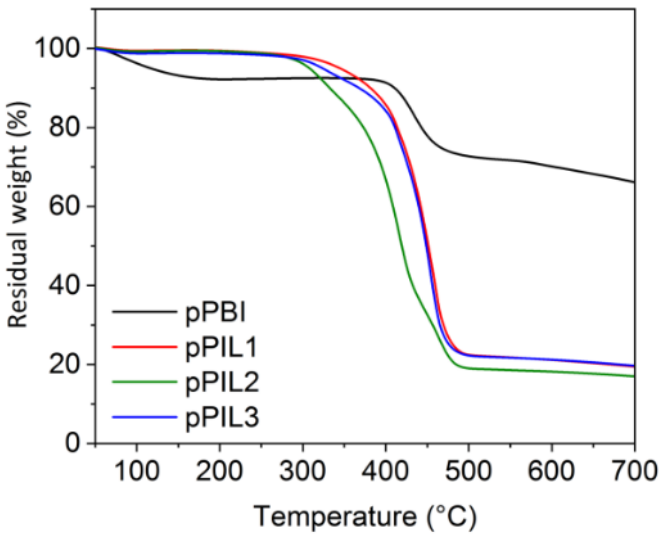

Figure 39 – Thermogravimetric curves of the SILMs measured in air

Although the decomposition temperature of pure PBI is more than 500 °C [60], TGA analysis shows that thermal decomposition of PBI support starts at around 390 °C. The possible reason for that are some traces of PVP inside the pores which were not washed off. SILMs are thermally stable up to 280 °C and therefore can be exploited in HT-PEMFC.

In-plane conductivity at elevated temperatures and anhydrous conditions was measured for all SILMs. These conditions are similar to those in the HT-PEMFC. The results on conductivities are presented in Figure 40. Conductivity values of pPIL1 could not be reproduced because of diversity of loading of IL1 with high melting temperature. This problem can be overcome by using such ILs as [dema][NTf_2] or [C_2Im][NTf_2]. Since their melting points are lower than room temperature, they do not crystalize on the surface. Therefore, there is no need to wipe the membrane with ethanol which provides control over the reproducible loading. Among the investigated SILMs, pPIL2 exhibited the highest conductivity which reached 20.74 mS cm^{-1} at 180 °C.

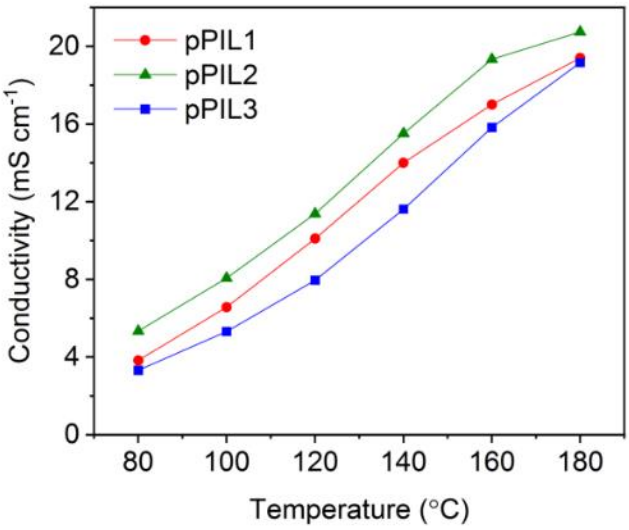

Figure 40 - In-plane conductivity of the SILMs (the lines are given as a guide for eyes)

Langevin et al. [89] suggested vapor induced phase separation (VIPS) as a method to prepare a polyimide porous support. Reported SILM containing triethylammonium trifluoromethanesulfonate salt [TEA][OTf] exhibited through-plane conductivity at 130 ^{0}C of about 20 mS cm^{-1} which is 64% of the conductivity of the pure IL. However, [TEA][OTf] possesses hydrophilic properties and can therefore easily be washed out of the open pores. Due to this fact a durability test is necessary to estimate the lifetime of the membrane.

3.1.2. Single fuel cell test and hydrogen pump experiment

After development of free-standing composite membranes with a high IL loading, the MEA with pPIL2 as a membrane electrolyte was successfully fabricated by means of hot press to ensure the contact between the membrane and GDEs and the fixed positions of the electrodes. MEA showed no visual damage (Figure 41 left).

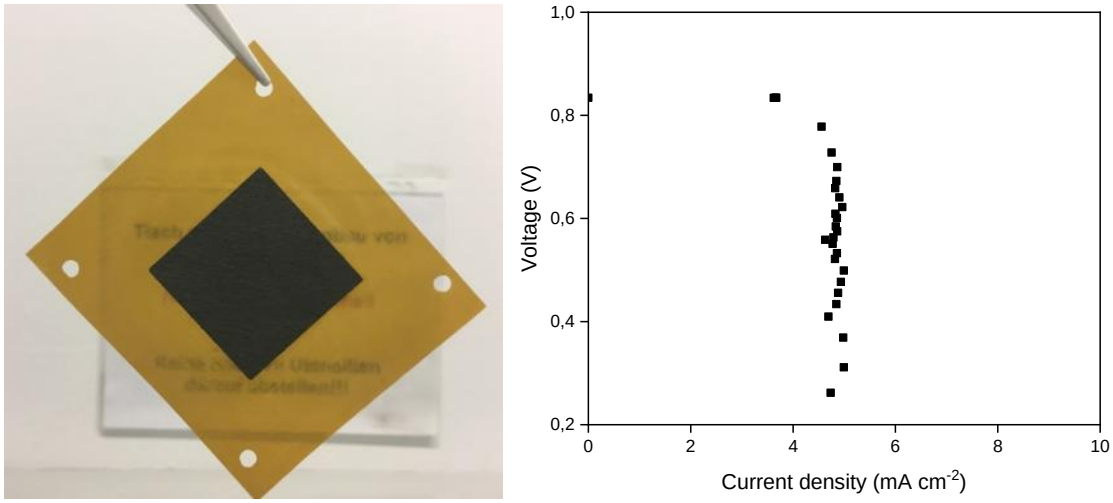

Figure 41 – (left) Self-fabricated MEA with pPIL2 as a polymer membrane electrolyte; (right) Polarization curve of that MEA-pPIL2 at 160 ºC

In order to evaluate the performance of the MEA, efforts of making polarization curves were made. The OCV at 160°C was 0.83 V and stable over time. However, an immediate voltage loss was observed once a small current was applied. It is worth to mention, that after switching off the current the OCV was recovered to the previous value. The repetition of the current load gave the same result as shown in Figure 41. In their work Smith and Walsh experienced similar behavior with [dema][TfO] [108]. After a comprehensive electrochemical analysis, they proposed that PILs cannot support sustainable current flow in the absence of acidic or basic additives.

pPIL2 of 4 cm^2 was sandwiched between two commercial DPS gas-diffusion electrodes with torch of 1 N m^{-1}. The MEA was heated up to 120 C and an OCV of 0.7 V was measured. However, when a current density of 7.5 mA cm^{-2} was applied, the voltage response dropped to 0.3V (Figure 41 right). Further tests were not possible.

In order to discover the presence of proton transport across the membrane, two experiments were conducted: hydrogen pump and EMF. During hydrogen pumping from both sides of the membrane, the current response was measured in dependence of the voltage (Figure 42a). It can be observed that the current does not follow the shape of potential, but rather gives spikes and reduces till a constant value of 0.25 mA.

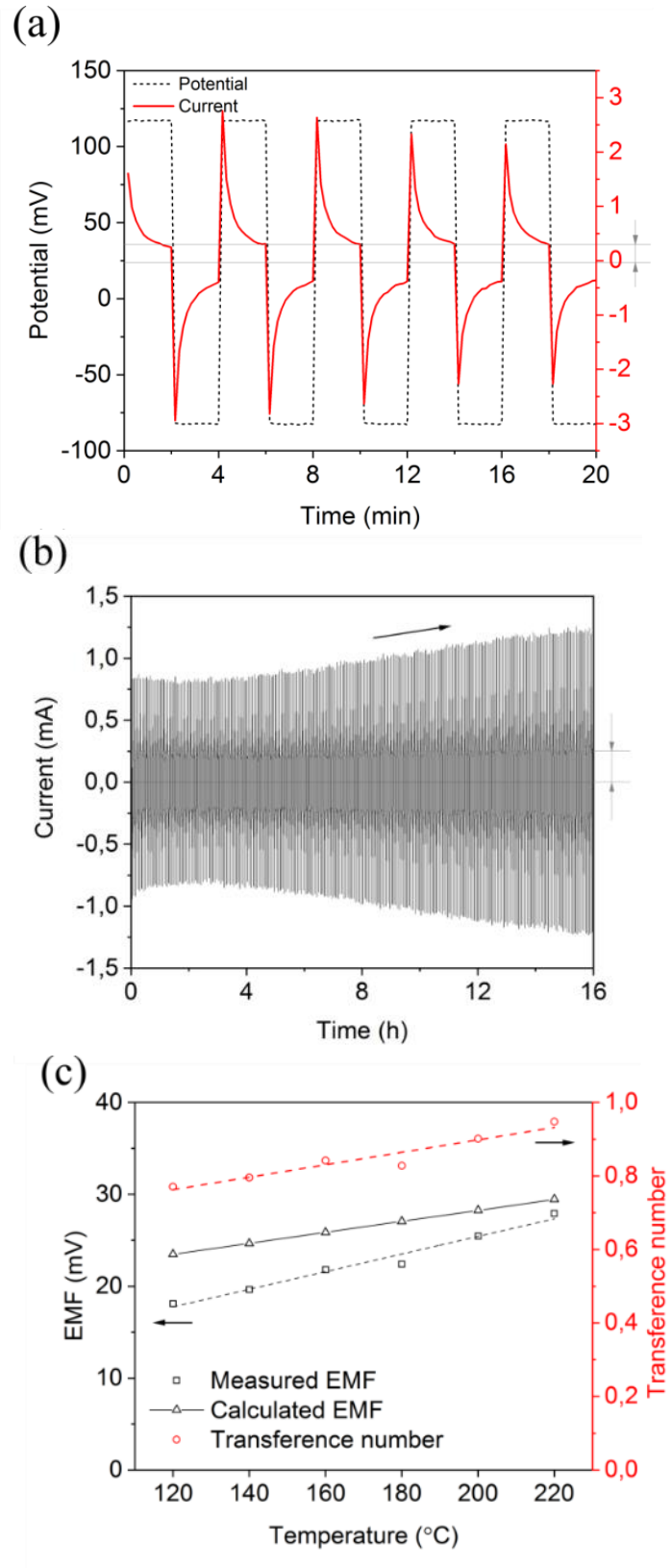

Figure 42 - Hydrogen pump experiment: (a) short-term and (b) long-term, (c) electromotive force dependence on temperature of MEA_pPIL2 at 120 ºC

These peaks of current can be related to the capacitance formed on the interface between the membrane and the electrodes. In order to investigate the long-term behavior, the cell was left for 500 cycles (Figure 42b). It can be observed that the capacitance slightly decreases at the beginning but after 4 h of operation starts increasing in values. A possible reason for this phenomenon could be the influence of the IL which is kept inside the open channels of the membrane. When the MEA is heated up, the IL's viscosity decreases and the IL likely leaches out covering the surface of the electrodes and possibly penetrating the carbon support. When the layer of IL is above a certain thickness, poor gas solubility or poisoning effect of the catalyst can take place and the capacitance on the interface increases.

The value of the constant current can be low when conductivity is determined by the motion of ions rather than protons. Conductivity measurements do not give distinct information on the origin of the conductivity. In order to check the nature of the ion transport, the experiment on EMF was conducted. Under operation with hydrogen on both sides at different partial pressures, the OCV of the cell was measured as shown below:

H_2 (1 bar), Pt | pPIL3 | Pt, H_2 (0.25 bar) *Equation 16*

The EMF obtained as a function of temperature is shown in Figure 42c. It can be seen from the figure that the obtained EMF was close to the theoretical values calculated from the Nernst equation. The ratio of the measured EMF to the theoretical value was assumed to be the proton transference number [108] and was found to be in range from 0.77 to 0.95. This indicated the prevalence of the protonic nature of the ionic conductivity of pPIL2.

After confirmation of proton transport across the membrane and exclusion of noticeable gas permeability which can cause a mixed potential and therefore a drop in OCV, we assume that this phenomenon can originate from the vehicle mechanism of conductivity which dominates in the membranes. This means, the protons are transported by cations moving from the anode to the cathode side when current is applied. When protons are delivered, they react with oxygen of the air on the catalyst resulting in water formation. Along with it, deprotonated cations are located on the cathode side and stay inactive for further proton transport since there is no force to drag them back to the anode side. After all the cations are consumed, there is no conductivity across the membrane anymore and therefore no performance. When current is removed, deprotonated cations diffuse back to attach new portion of protons from hydrogen fuel, and the original OCV value is recovered.

In their work Smith and Walsh experienced similar behavior with [dema][TfO] [108]. The increase of the transfer number with the temperature increase during EMF experiment in this work also correlates with their assumption that equilibrium concentration of parent acids and bases in PILs can increase due to exposure to heating. The researchers also mentioned that in diethylmethylammonium-containing PILs the

yield of nonstoichiometric composition can occur due to the loss of the most volatile component [109,110]. Therefore, such effects could potentially provide the shuttles required to transport protons between the anode and cathode of fuel cells. They also previously observed a drastic increase in the ORR-onset potential in [dema][TfO] as the PIL temperature was raised from 25 to 160 °C as was demonstrated previously, indicating that the ORR proceeds via different routes at high and low temperatures [111].

After a comprehensive electrochemical analysis, they proposed that PILs cannot support sustainable current flow in the absence of acidic or basic additives. Therefore, nonstoichiometric mixtures of PILs and their parent acids or bases should be further studied as potential electrolytes in SILMs structures.

3.1.3. Post-operational MEA characterization

After the MEA based on pPIL2 was tested in a single fuel cell, its structure and composition were analyzed by cross-section SEM (Figure 43) and EDX (Figure 43). SEM shows the intended difference in the catalyst loading on the anode (0.4 mg_{Pt} cm^{-2}) and cathode (0.6 mg_{Pt} cm^{-2}). More catalyst was loaded on the cathode, since ORR is more complicated than HOR, and therefore requires more catalyst for the activation. The figure shows that during higher magnification more energy is used in the electron beam, which damages the cathode and causes cracks.

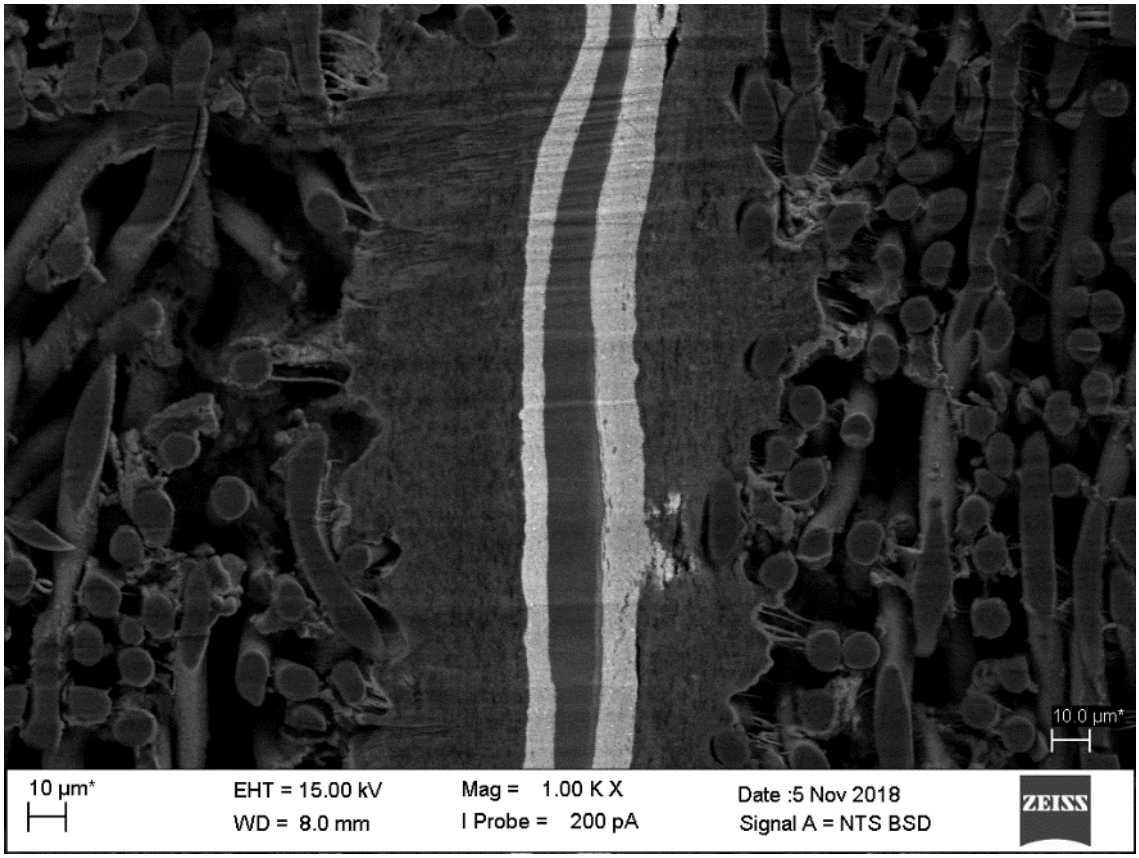

Figure 43 – Cross section SEM image of the MEA fabricated with pPIL2, anode with 0.4mg$_{Pt}$ cm^{-2} and cathode 0.6mg$_{Pt}$ cm^{-2} , captured after a single fuel cell test.

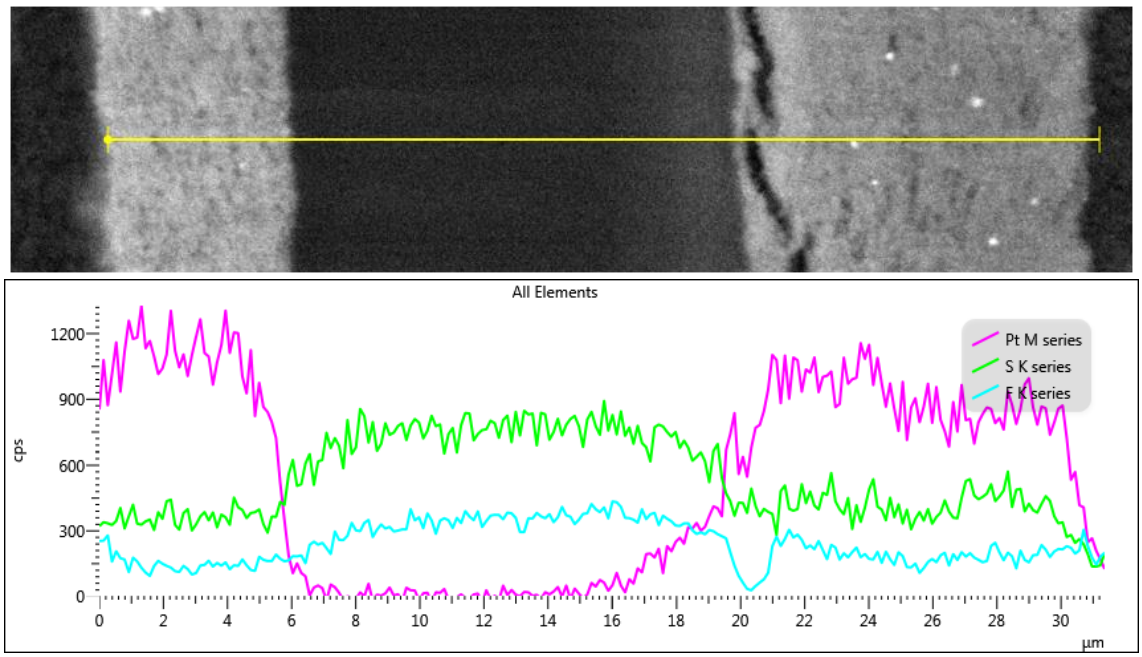

Figure 44 – (top) Cross section SEM image of the MEA fabricated with pPIL2, anode with 0.4mg$_{Pt}$ cm^{-2} and cathode 0.6mg$_{Pt}$ cm^{-2} captured after a single fuel cell test; (bottom) EDX showing elemental distribution within the MEA such as Pt, S and F.

For the anode side one can see a sharp Pt front on the EDX map (Figure 46). It is clear that Pt did not diffuse neither to the membrane, nor to the mesoporous layer of the GDL. Interesting observation was done looking at the F map. Fluor is present not only in the membrane, but also in the mesoporous layer of the GDL, indicating the possible application of PTFE ionomer. This monomer is typically present in GDL for LT-PEMFC and gives hydrophobic properties to the mesoporous layer.

It is important to note that the EDX mapping shows a significant sulfur diffusion from the membrane to the catalyst layer. Sulfur species are known to be poisonous towards the precious metals such as Pt. Therefore, the immediate loss of the performance can be caused be the catalyst poisoning by the excess of the mobile anion $[NTf_2]^-$ present in the IL. The sulfur front on the anode side is not as sharp as at the cathode side. That might give an indication that $[NTf_2]^-$ anion moves towards the anode during a fuel cell operation.

It is clear from the cross-section SEM image and EDX spectrum that Pt has diffused to into the membrane from the cathode side. The Pt slope is as sharp at the cathode side of the EDX spectrum as it is at the anode side. The pale shiny Pt front takes up to a quarter of the total membrane thickness, however, it is not clearly visible for the whole length of the membrane. Therefore, this local Pt diffusion into the membrane might be caused by the small local thickness of the dense carbon support (mesoporous layer) of the gas-diffusion layer. Fluorine and sulfur which are the footprints of the IL5 are more present

in the membrane. However, there is still a certain level of fluorine and sulfur measured in the catalyst layer of both anode and cathode, indicating the leakage of IL6 from the membrane to the electrodes. Figure 44 shows the map of Pt, F and S elements.

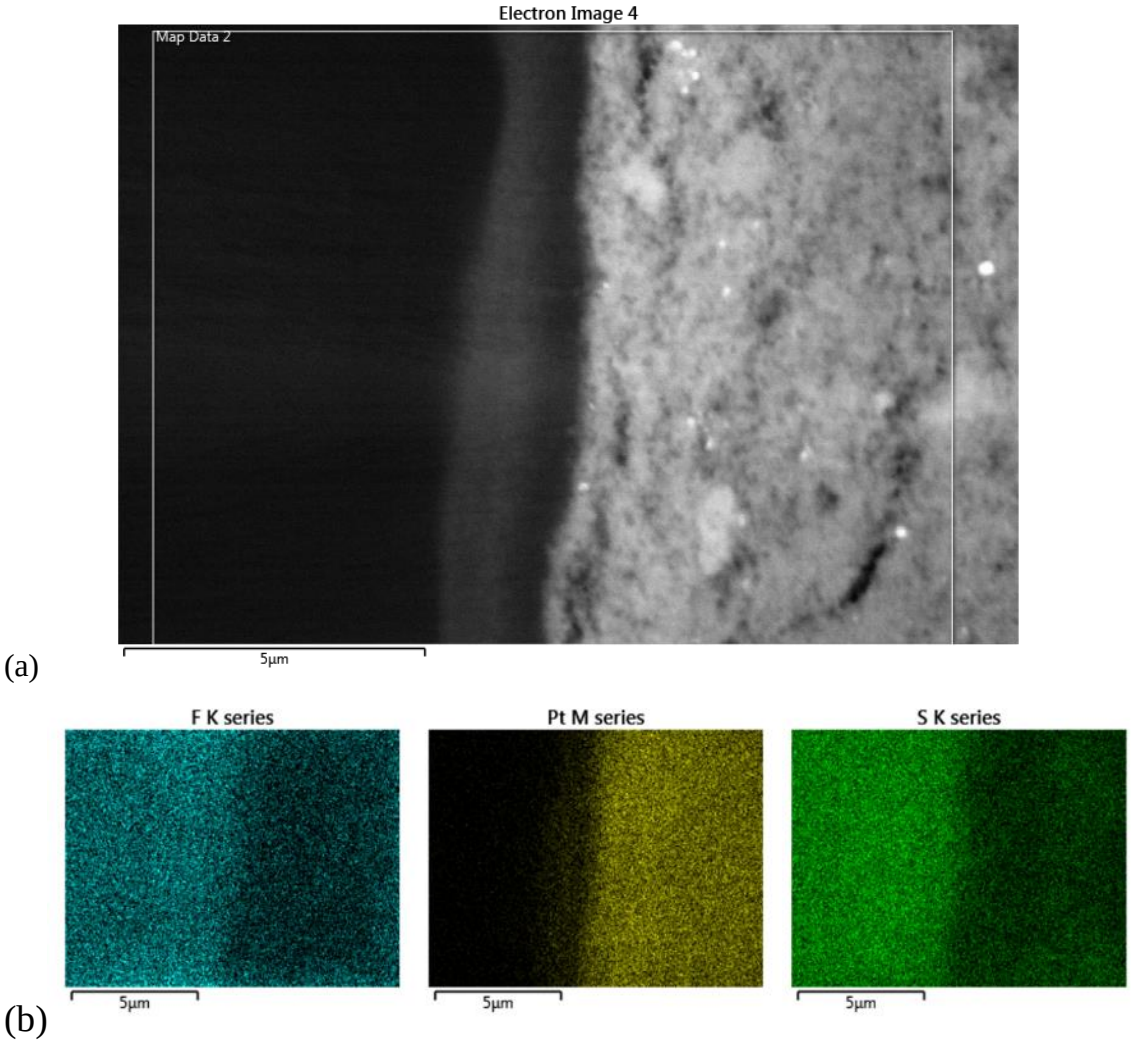

Figure 45 – (a) A fragment of the cross-section SEM image and (b) EDX scan of the MEA cathode side showing the map of elemental distribution

(a)

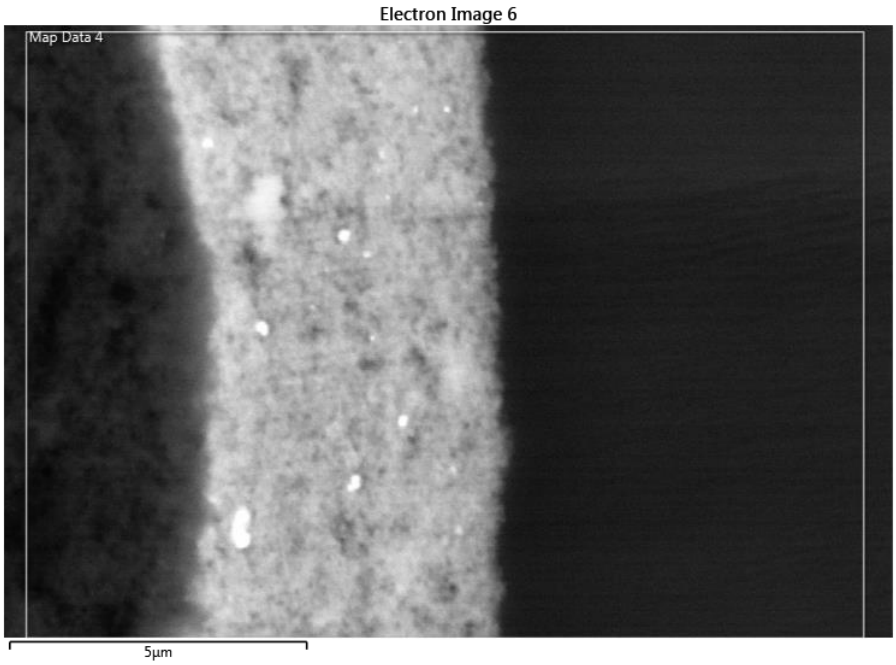

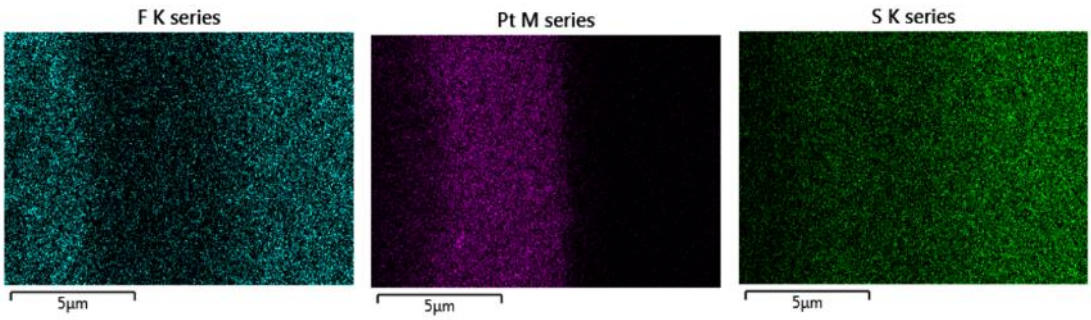

Figure 46 - (a) A fragment of the cross-section SEM image and (b) EDX scan of the MEA anode side showing the map of elemental distribution

3.2.Quasi-solidified ionic liquid membranes

3.2.1. Membrane characterization

In order to study the influence of the IL content on the properties of the membranes, small area samples containing 0-67%%wt. were casted (Figure 47). All investigated ILs have hydrophobic properties which prevents them being dragged with water produced on a cathode side during the fuel cell operation.

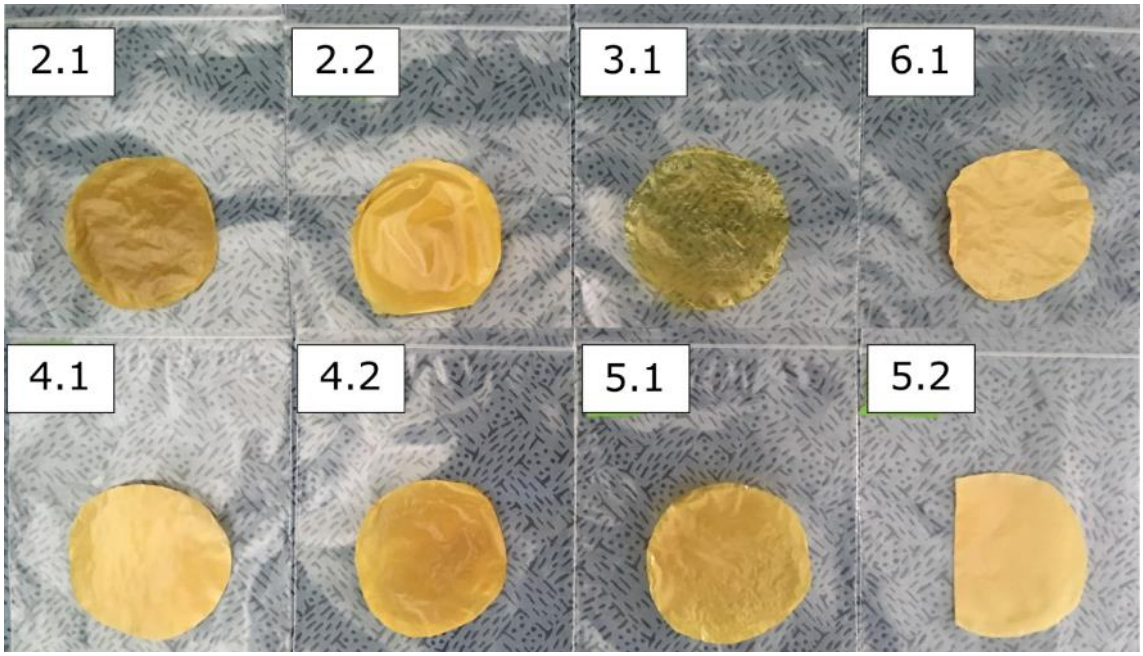

Figure 47 - The samples of fabricated QSILMs with various ILs and their content

It was found that composites with the ratio IL/PBI over 0.5 demonstrate the formation of a porous structure while the addition of less amount of ILs leads to formation of a dense structure like an initial polymer. Figure 48 shows the influence of the ILs concentration which is increasing from left to right in the row for one of the fabricated samples. At this point of the study, the samples were broken without using liquid N_2, hence the cross-section images are not neat.

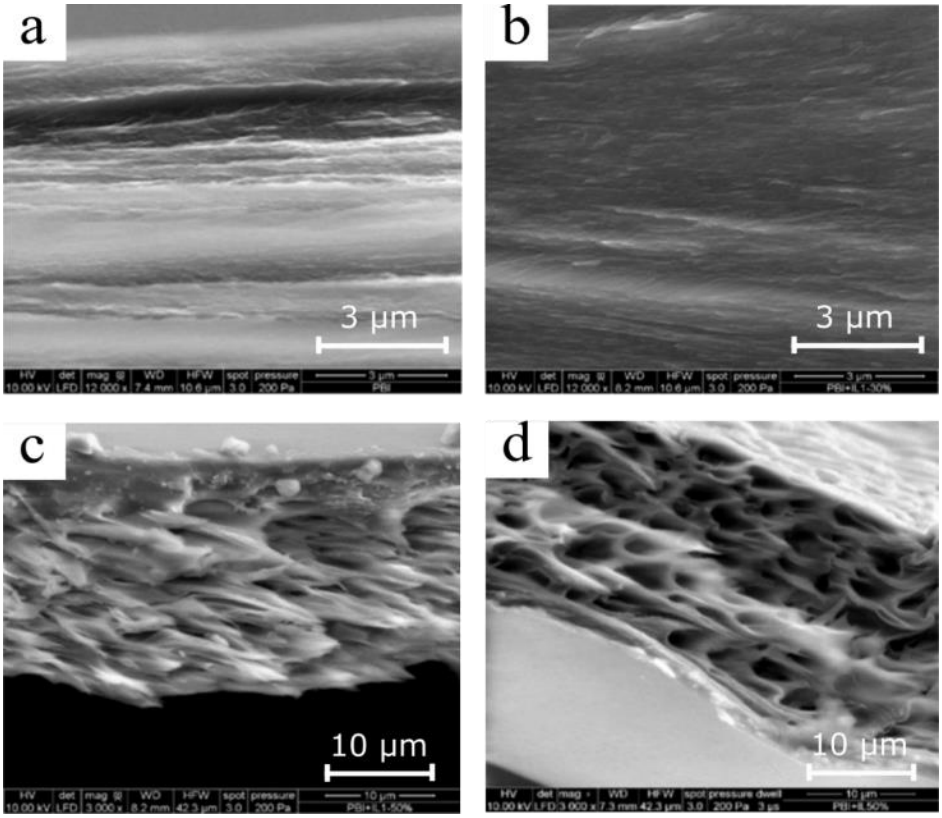

Figure 48 - SEM microphotographs of (a) pristine PBI membrane; and QSILMs with [C_1Im][NTf2]/PBI ratios: (b) 0.3; (b) 0.5; (c) 1

Since [dema][OTf] is probably the most explored IL for electrochemical application, it was decided to study the trend of a thermal decomposition of QSILM sample based on that IL (Figure 49).

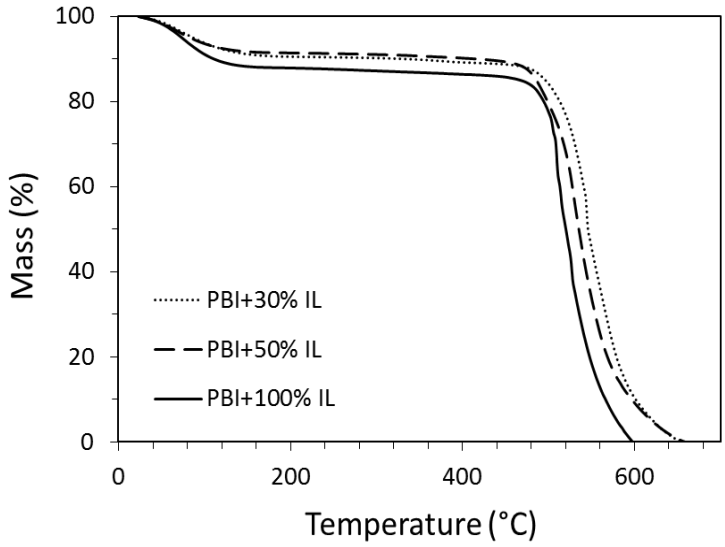

Figure 49 - TGA curves of the QSILMs containing based on PBI polymer and [dema][OTf] ionic liquid

The first decomposition slope corresponds to the loss (ca. 13% for pristine PBI and 10% for the QSILMs) of adsorbed water from the air. The second slope is related to the decomposition of the material. It can be concluded that the temperature of a polymer decomposition slightly decreases after impregnation with the IL. It happens because the temperature of IL decomposition is significantly lower (ca. 300ºC) than those of a PBI. Important to note that after fabrication of a QSILM at this IL content, the membrane decomposes as a single material, which might indicate a chemical interaction between PBI backbone and IL2. Nevertheless, all the samples demonstrate good thermal stability up to 500^0C and thus can be exploited for high temperature applications.

The new ionic liquids such as [C_2Im][NTf_2] and [HHTMG][NTf_2] were designed for the impregnation into the polymer framework. [C_2Im][NTf_2] were chosen since it is liquid at room temperature unlike [C_1Im][Tf_2N] which makes its handling easier. [HHTMG][NTf_2] has 2 free places for proton exchange so it's suspected to exhibit higher proton conductivity. The data on the IL above were not published before. [dema][NTf_2] was used from the previous studies.

The samples of bigger area were fabricated for the further detailed investigation (Figure 50) in various PBI/IL proportions (Table 6). The structures of membranes containing different concentrations of immobilized ILs were characterized by SEM technique (Figure 51).

Table 6 - Compositions of the scaled-up QSILMs with the selected ionic liquids

Sample	Immobilized IL	Content of PBI, mol%	Content of IL, mol%	IL/PBI ratio
2.1	[dema][NTf2]	50	50	1
2.2	[dema][NTf2]	33	67	2
4.1	[HHTMG][NTf2]	50	50	1
4.2	[HHTMG][NTf2]	33	67	2

Samples 2.3 and 4.3 were not rigid enough for the test.

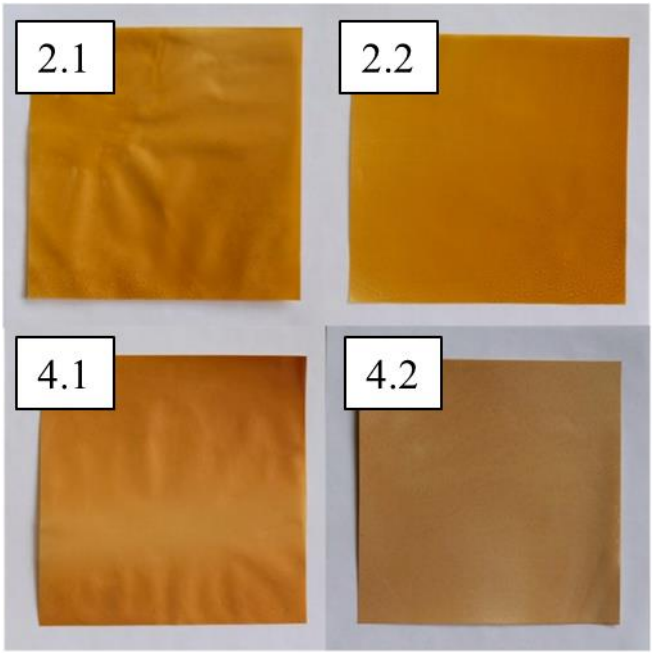

Figure 50 - The samples of fabricated QSILMs with two different loadings of 2.1, 2.2 – [dema][NTf_2] and 4.1, 4.2 – [HHTMG][NTf_2]

Strain-stress curves were recorded to analyze the mechanical properties of the samples. The compositions of QSILMs and the calculated characteristics are listed in Table 7.

Table 7 - Mechanical properties of QSILMs

Sample	Tensile Strength	Young's Modulus	Elongation at break
m-PBI	72.3 ± 5.0	1124.2 ± 72.7	33 ± 20
2.1	28.2 ± 4.4	504.8 ± 28.5	87 ± 5
2.2	11.3 ± 1.1	185.4 ± 5.8	67 ± 11
4.1	24.4 ± 2.3	578.5 ± 13.3	47 ± 9
4.2	11.2 ± 0.8	252.8 ± 6.1	57 ± 11

It can be seen that ILs act as plasticizers making the PBI backbone more flexible. The tensile strengths for QSILMs containing one portion of IL and double portion of IL are similar to those of phosphoric acid doped PBI membranes at room temperature which amount to 500-700 mol%, respectively [113].

The morphologies of QSILMS were investigated using SEM. Figure 51 represents the cross-section images of the membranes. The images exhibit a “sponge-like” structure of

the membranes where ILs are confined in the 3D polymer network. A thin layer of dense PBI is formed on the upper surface and the thickness of the layer as well as the pore size decreases with an increase of IL content. Hence, we assume it is beneficial to increase the loading of IL in order to avoid formation of a nonconductive PBI layer from one side. Even though [HHTMG][NTf_2] crystallizes at room temperature, no damage in structure can be observed during SEM analysis. For the blending procedure the state of the IL plays a role since all the studied ILs are soluble in DMAc.

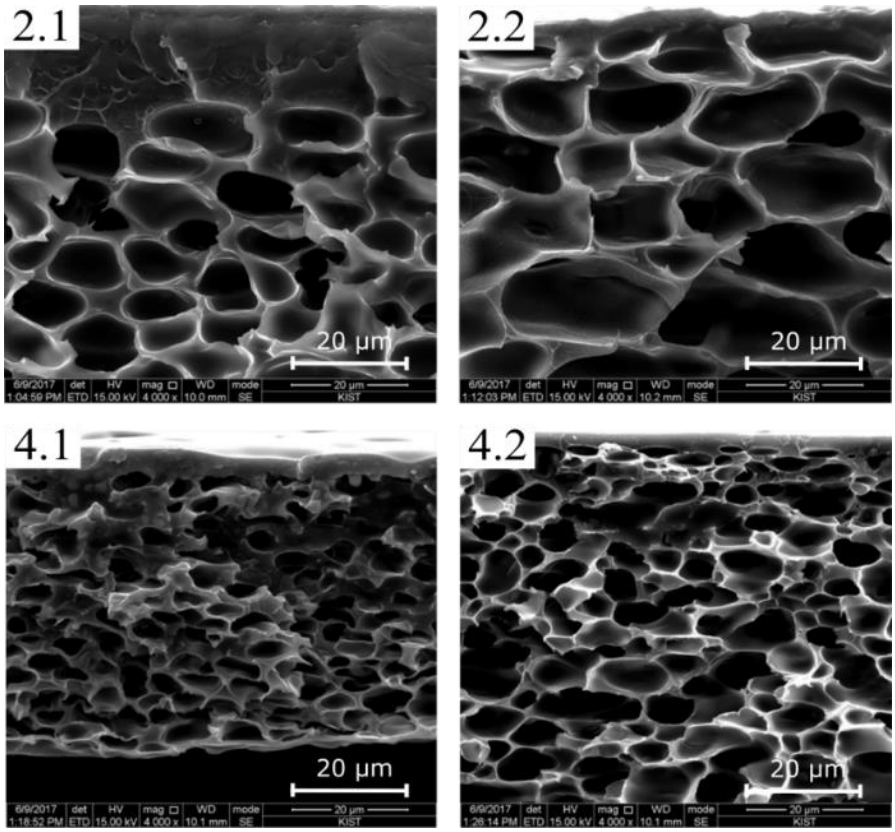

Figure 51 - SEM cross-section of QSILMs (×4000)

The presence of ILs in the channels of the membranes was confirmed by recording FT-IR spectra (Figure 52). As well as SILMs, all pristine QSILMs samples display characteristic peaks of the PBI backbone at the wavelength 800-500 cm^{-1} and peaks of 1360-1335 cm^{-1} and 1170-1145 cm^{-1} representing SO_2 groups in sulfonamides.

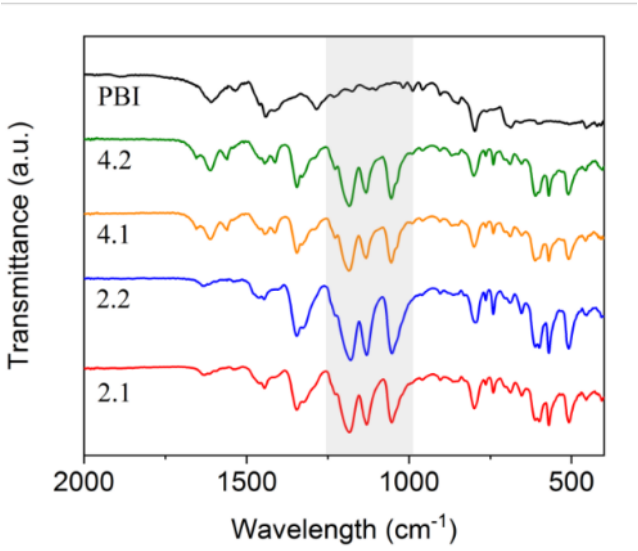

Figure 52 - FT-IR spectra of the fabricated QSILMs showing characteristic peaks

Figure 53 exhibits the dependence of ionic conductivities of pristine QSILMs on temperature measured in the self-made cell in the range of 80-180 °C. For all the tested membranes conductivities increased with an increase of temperature. Membrane 4.2 exhibited the highest value among others and reached $0.3 \cdot 10^{-3}$ S cm^{-1} which is three order lower than state-of-the-art PBI membrane doped with PA. Wang and Hsu reported conductivity of about $0.5 \cdot 10^{-3}$ S $cm^{-1}$for QSILM-based aprotic IL PBI/2[C_6C_1Im][OTf] at anhydrous conditions at 160-180 ^{0}C [8]. Nevertheless they found out that the increase in IL content and operating temperatures improves the conductivity which could reach 0.016 S cm^{-1} for PBI/4[C_6C_1Im][Otf] at anhydrous conditions at 250 ^{0}C.

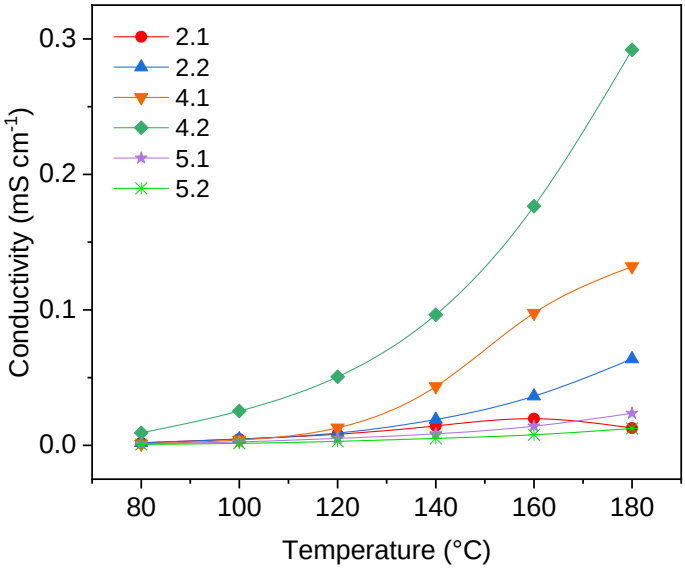

Figure 53 – Ionic conductivities of QSILMs (lines are given as a guide for eyes)

In order to understand the origin of poor conductive properties of pristine QSILMs, samples were investigated by means of fluorescence microscopy. It is known that PBI exhibits fluorescence in a broad range of spectra and several research groups used this property to study the agglomeration of BPI [114,115]. Figure 54 shows an image from the microscope with fluorescent lamp in black and white field. Fluorescence can be observed on the interface of phase separation between the Ils and the polymer. The membranes exhibit "quinoa-like structure" with segregated globules of the Ils within the polymer matrix. There are no interconnected channels of the Ils as could be assumed from cross-section SEM images, but rather closed pores insulated by nonconductive polymer walls. This continuous polymer film blocks proton transport between conductive globules, hence the membranes act as insulators. As to our best knowledge, fluorescence of PBI never was used as a tool to analyze the morphology of PBI films and phase separation. The theory on segregated globules can be also supported by the image from confocal microscopy (Figure 55).

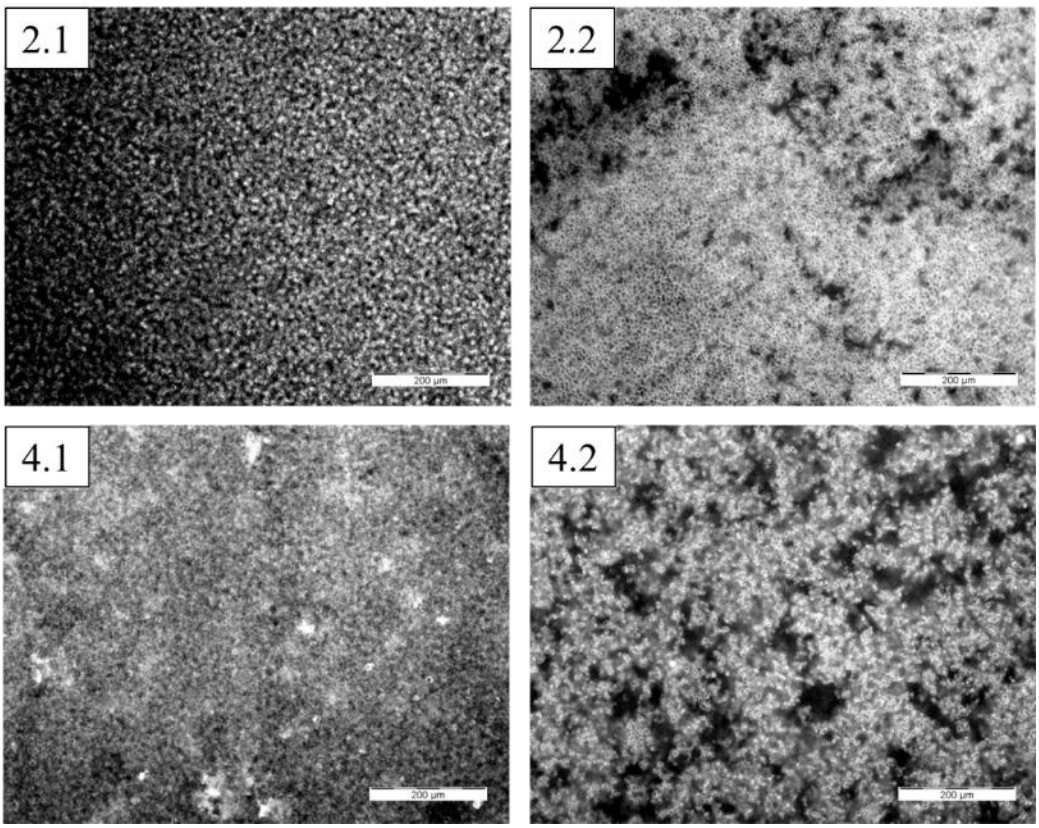

Figure 54 - Images of pristine QSILMs from fluorescence microscopy (×10). Scale bar corresponds to 200 µm.

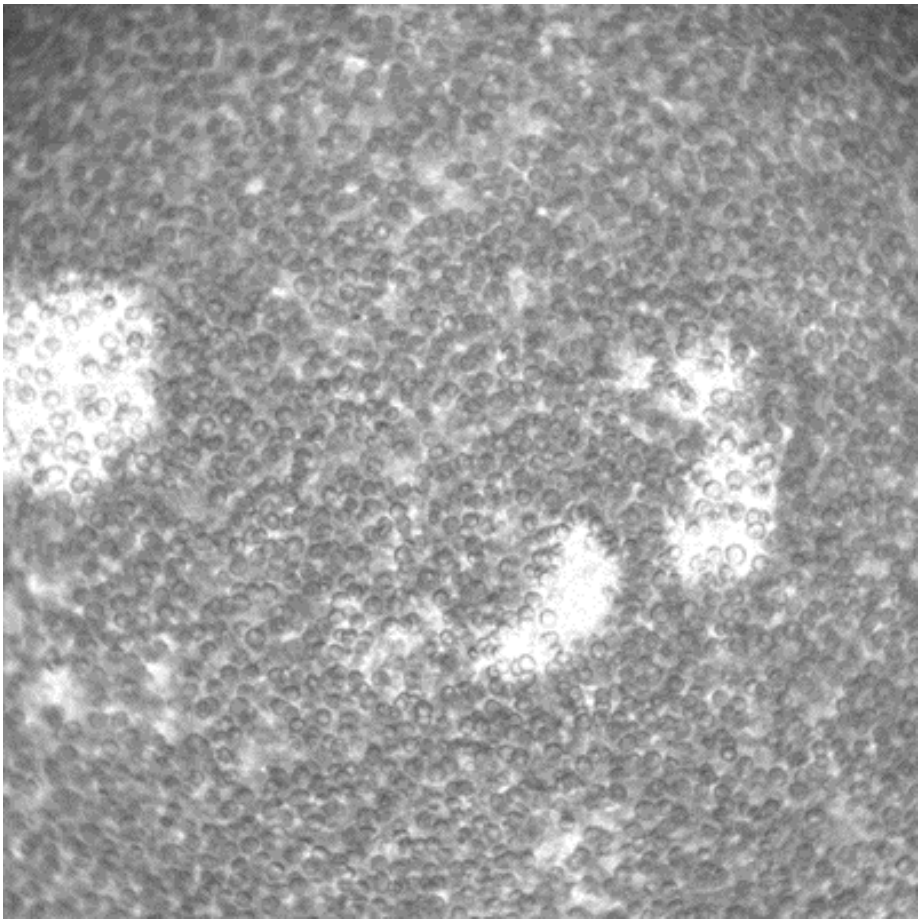

Figure 55 - Fluorescence confocal microscopy of QSILM 2.1 at λ = 514

These images taken by the innovative approach of fluorescence microscopy helped understanding the phase separation between the polymer and the ILs.

In order to support continuous transport of protons across the membranes, the PBI network has to gain conductivity via protonation or grafting of the functional groups. Therefore, all pristine QSILMs were doped in PA via two approaches shown in Figure 22 and their conductivities were checked at the same conditions as previously described. The compositions of the doped membranes are listed in Table 8.

The influence of doping level on the conductivity of the QSILMs was studied as following. In order to reach low DL ($\theta < 6$) the QSILMs were doped in a thin film of a certain amount of PA as shown in the Scheme 2a. After doping thin films of PA, conductivities increased by two orders of magnitude and reached maximum values of about 0.06 S cm^{-1} for QSILM with the $[HHTMG]^+$ cation at 180 °C. Figure 56 comparatively analysis the conductivities of the different QSILMs with low DL. The conductivities for QSILMs containing $[HHTMG]^+$ cation as a part of IL exhibit twice as high conductivity values as those carrying $[dema]^+$ cation. No influence of the IL content on the conductivities was observed for both ILs.

Table 8 - Compositions of the doped QSILMs (means doped in thin film)*

	Sample	PBI, %mol.	IL, %mol.	H_3PO_4, %mol.	ADL
Thin film doping	PBId*	34.5	0	65.5	1.9
	1.1d*	14.5	14.5	71.0	4.9
	1.2d*	13.2	26.3	60.5	4.6
	2.1d*	14.1	14.1	71.8	5.1
	2.2d*	14.1	28.2	57.7	4.1
Bulk doping	1.1d	9.1	9.1	81.8	9.0
	1.2d	7.8	15.6	76.6	9.8
	2.1d	10.8	10.8	78.5	7.3
	2.2d	8.6	17.2	74.1	8.6

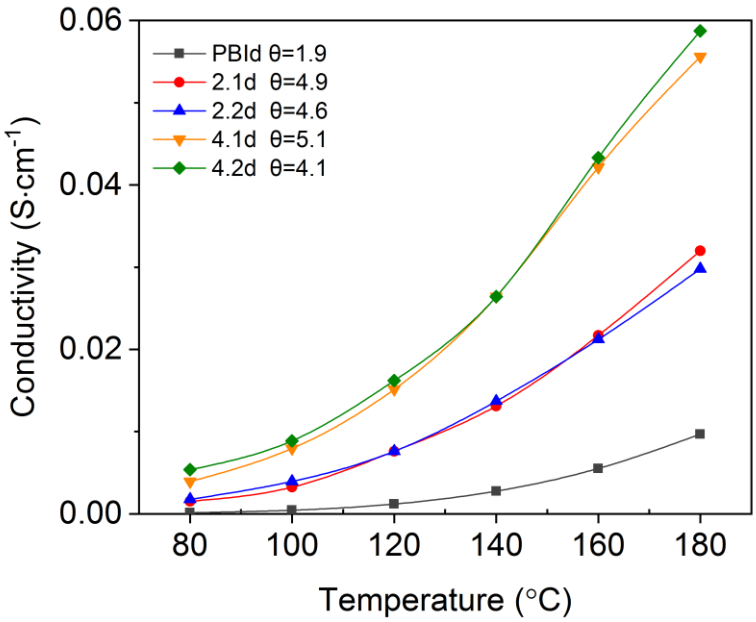

Figure 56 - Conductivities of QSILMs doped with phosphoric acid solution

In order to reach higher DL, sample 4.1 was doped in concentrated PA solution for different periods of time from 15 min to 8h as shown in the Scheme 2b. DL and corresponding conductivities were recorded. Figure 57 shows the conductivity dependence on the amount of adsorbed PA from the concentrated solution.

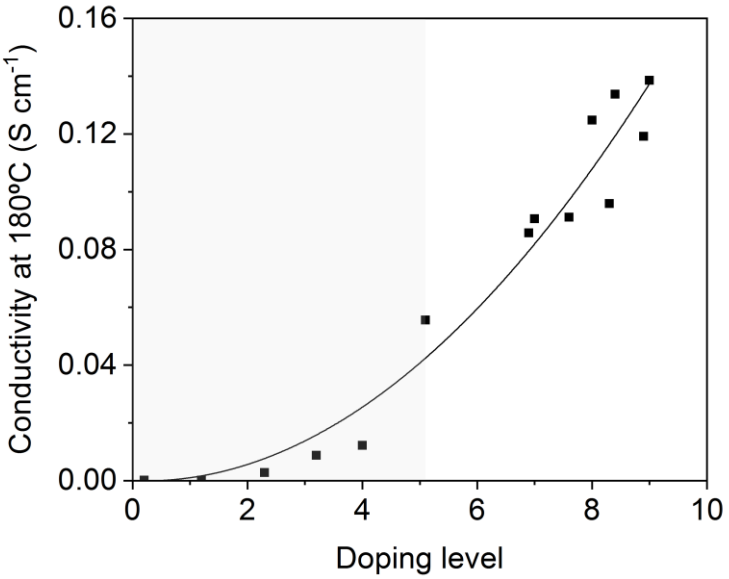

Figure 57 - Dependence of conductivity values on the doping level for the sample 4.1

As expected, immersion technique allows higher DL which results in higher conductivities accordingly. Maximum DL of 9 mol of PA per repeat unit was obtained after 4 h of treatment and yielded an in-plane conductivity of about 0.14 S cm^{-1} at 180 °C which is higher than fully humidified Nafion at the operation conductions of low temperature fuel cells. We assume that QSILMs immersed in concentrated PA solution reach higher DL due to better diffusion of the acid molecules inside the polymer matrix. Hence, QSILMs doped via this route were used for the further analyses and fuel cell tests.

The fact of boost in conductivity after doping with the acid supports the theory of phase separation within QSILMs assumed from fluorescence pictures. After doping of the polymer backbone, protons are provided with continuous pathways between phases of the polymer network and segregated globules of ILs, and therefore QSILMs achieve good conductive properties. The process can be compared with dropping of solid polymer bridges between isles of electrolytes. This is the first time fluorescence microscopy is used for investigating the structure of PBI based composite membranes.

Previously a few research groups have already made an effort of combining ILs and PA as mixed electrolyte. For example, Ye at al. proposed gel-type PBI membrane containing 1-methyl-3-propyl-methylimidazolium dihydrogen phosphate ($[C_1C_3C_1][H_2PO_4]$) as ionic liquid and additional PA [87]. Maximum reported conductivity for PA/ $[C_1C_3C_1][H_2PO_4]$ /PBI membrane (2/4/1) reached 0.002 S cm^{-1} at 150 °C under anhydrous conditions and 0.009 S cm^{-1} at 10% relative humidity. In this work we could obtain conductivity values one order of magnitude higher under the similar conditions for doped QSILMs.

Rewar et al. fabricated the blended PBI membrane containing polymeric IL poly(diallyldimethylammonium) trifluoromethanesulfonate P[DADMA][TfO] and doped with PA [67]. They reported a maximum through-plane conductivity of 0.07 S cm^{-1} at 150 °C for PBI with 45 wt% of P[DADMA][TfO] and a doping level of 23 mol PA per repeat unit. This doping level is twice higher than the doping level we used in our work for QSILMs which can lead to leaching of free PA into GDE. As was mentioned before, no leaching was observed for doped QSILMs at room temperature.

Lin et al. produced cross-linked phosphoric acid doped 1-vinyl-3-butylimidazolium bis(trifluoromethylsulfonyl)imide [VBIm][NTf_2] based composite membranes [116]. Maximum conductivity reached 0.04 S cm^{-1} at 180 °C for the sample containing 35 wt% [VBIm][NTf_2], 35 wt% VIm35 and 134 wt% PA uptake.

Membranes containing $[HHTMG]^+$ cations exhibited lower performances in fuel cell tests than those with $[DEMA]^+$ cations despite having higher conductivities. However, it should be stressed that the membrane 1.1d was 70 μm thick, whereas the membrane 2.2d was 100 μm thick. Rewar et al. [67]observed a maximum performance for the composite PBI membrane containing 25 wt % of [DADMA][OTf] and 107.3 wt % PA uptake and reached 0.5 W cm^{-2} at 160 °C in H_2/O_2 fuel cell. No data on the tests under higher temperatures and air flow on the cathode side were provided. These authors reported the utilization of Nafion solution during the catalyst ink preparation which is not favorable for operation at the temperatures above 100 °C as was discussed before. Therefore, fuel cell tests remain the main tool to evaluate the performance of the membrane.
We suppose that QSILMs structures with acid post-doping are beneficial for immobilization of ILs inside a polymer matrix due to its closed pore structures preventing them from leaching out during the operation in a fuel cell. Moreover, we assume that acid post-doping has a tremendous effect on the conductive properties of the studied QSILMs not only due to the protonating PBI backbone back but also due to diffusion of free PA in the closed pores filled with ILs providing non-stoichiometry to the electrolyte.
Thus, Smith and Walsh [108] thoroughly studied beforementioned [dema][TfO] as electrolyte for non-humidified fuel cells by means of comprehensive electrochemical analysis. In their work they concluded that protic ILs cannot support proton shuttling between the electrodes of fuel cells due to its preliminary vehicle mechanism of a proton transport and require inclusion of dissolved acidic or basic proton shuttles in order to be utilized as electrolyte. According to the mechanism that was proposed in their work, I assume the following mechanism for our IL.
For protic ILs [dema][NTf_2] and [HHTMG][NTf_2], the ionization (protonation-deprotonation) occurs by proton exchange between the proton donor and acceptor:

a) dema + $Tf_2NH \rightarrow DEMAH^+ + NTf_2^-$
b) HHTMG + $Tf_2NH \rightarrow HHTMGH^+ + NTf_2^-$

The driving forces are

a) $\Delta pK_a[dema]^+ = pK_a[dema]^+ - pK_a[NTf_2]^- = 10.5 – (−10) = 20.5$ [97]
b) $\Delta pK_a[HHTMG]^+ = pK_a[HHTMG]^+ - pK_a[NTf_2]^- = 13.9 – (−10) = 23.9$ [98]

Free energy for the ionization is then given by:

a) $\Delta G^0 = –2.303\ RT\ \Delta pK_a = –117.0$ kJ/mol
b) $\Delta G^0 = –2.303\ RT\ \Delta pK_a = –136.4$ kJ/mol

If assembled into an electrochemical cell this free energy corresponds to a reversible potential:
a) $\Delta E^0 = –\Delta G^0/nF = 1.2$ V
b) $\Delta E^0 = –\Delta G^0/nF = 1.4$ V

When these ILs are solely consisting of $[dema]^+$ and $[HHTMG]^+$ cations and $NTf_2^–$ anions, i.e. in the absolute absence of excess dema or HHTMG, the only proton acceptor is $NTf_2^–$ and similarly in the absolute absence of NTf_2, the only proton donors are $[dema]^+$ and $[HHTMG]^+$ respectively.
In fuel cells the hydrogen oxidation at the anode needs a proton acceptor to carry the produced protons away. It has always been assumed that the base functions as the proton acceptor and the anode half-reactions are hence:

a) $H_2 + 2\ dema \rightarrow 2\ [dema]^+ + 2e^-$

b) $H_2 + 2\ HHTMG \rightarrow 2\ [HHTMG]^+ + 2e^-$

And then the $[dema]^+$ and $[HHTMG]^+$ as the proton carriers travel through the PIL electrolytes and deliver the protons to the cathode for the oxygen reduction reaction:

a) $½O_2 + 2\ [dema]^+ + 2e^– \rightarrow 2\ dema + H_2O$
b) $½O_2 + 2\ [HHTMG]^+ + 2e^– \rightarrow 2\ HHTMG^+ H_2O$

Thus the overall reactions are therefore simply like:

$½O_2 + H_2 \rightarrow H_2O$

This, however, can never be the case because there is no molecular dema and HHTMG in the pure PILs. At the anode the only proton acceptor is $[NTf_2]–$, not the bases. The anode half-reaction should therefore be:

$H_2 + 2\ [NTf_2]^– \rightarrow 2\ NTf_2 + 2e^-$

And the formed NTf_2, if possible at all, is not the charge carrier that is transporting proton through the electrolyte from the anode to the cathode. At the cathode the only proton donor, which is involved in the oxygen reduction reaction, is the protonated $[dema]^+$ or $[HHTMG]^+$, respectively. This means that the only possible cathode half-reactions are:

a) $½O_2 + 2\ [DEMA]^+ + 2e^- \rightarrow 2\ DEMA + H_2O$
b) $½O_2 + 2\ [HHTMG]^+ + 2e^- \rightarrow 2\ HHTMG + H_2O$

As a result the overall reactions will be
a) $H_2 + ½O_2 + 2\ [NTf_2]^- + 2\ [DEMA]^+ \rightarrow 2\ DEMA + 2\ NTf_2 + H_2O$
b) $H_2 + ½O_2 + 2\ [NTf_2]^- + 2\ [HHTMG]^+ \rightarrow 2\ HHTMG + 2\ NTf_2 + H_2O$

This is the sum of the two reactions:

a)
$½O_2 + H_2 \rightarrow H_2O$
$2\ [NTf_2]^- + 2\ [DEMA]^+ \rightarrow 2\ [DEMA] + 2\ [NTf_2]$

b)
$½O_2 + H_2 \rightarrow H_2O$
$2\ [NTf_2]^- + 2\ [HHTMG]^+ \rightarrow 2\ [HHTMG] + 2\ [NTf_2]$

This phenomenon supports the idea of a synergy effect of protic ILs and PA post-doping proposed in this work. Since ILs are not absorbed well by PBI, the conduction mechanism of the PA doped PBI matrix should be similar to that of homogenous PA doped PBI membranes, and has been well investigated by others [65,117]. However, the mechanism in the mixed system is not evident and requires some advanced theoretical studies.

Conductivities of the doped QSILMs were compared to those of pure ILs which were immobilized into PBI network and pristine PBI doped with PA (Table 9).

Table 9 - Conductivities of the neat ionic liquids and PA-doped PBI

Compound	Conductivity	Temperature	Relative humidity	Reference
$[dema][NTf_2]$	86	200	0	Figure 20
$[HHTMG][NTf_2]$	70	200	0	Figure 20
PBI - 5.6 PA	68	200	5	[28]
PBI - 6.6 PA	80	180	8	[118]
PBI - 11PA	150	180	0	[119]

The conductivities of our dry protic ionic liquids used in this work correspond approximately to the conductivities of PBI with ADL values of 6–7 and RH values around 5%. The neat conductivity of the protic ILs extrapolated to 200 °C is higher or comparable to other ILs investigated in the literature, although there are only few investigations for ILs at such elevated temperatures, which is due to limitations of the conductivity setups. To give a short comparison, the specific conductivity of 1H-1,2,4-triazolium methanesulfonate at 200 °C is reported to be about 60 mS cm^{-1} [120] thus lower than the values obtained here. The protic ionic liquid [dema][TfO], that was also investigated for fuel cell applications, is reported to have a conductivity of 55 mS cm^{-1} at 150 °C which is comparable to the results for the ILs investigated here [96]. The conductivity of [dema][NTf2] was extrapolated to be 59 mS cm^{-1} at 150 °C and for [HHTMG][NTf_2] to be 44 mS cm^{-1} at the same temperature. The values of some aprotic ILs were also reported to be in the same range than for the PILs investigated here. For instance, the conductivity of 1-butyl-3-methylimidazolium hexafluorophosphate [BMIM][PF6] was reported to be 76.9 mS cm^{-1} at 195 °C and the conductivity of the IL [BMIM][OTf] to be 75.0 mS cm^{-1} at 195 °C [121].The temperature dependence of the specific conductivity was also fitted with the VFT-equation, similar to our protocol.

TGA in air was performed in order to evaluate the thermal stability of pristine and doped QSILMs at real operating conditions of HT-PEMFCs and the influence of acid post-doping. Figure 58 shows the TGA curves of QSILMs at operating temperatures of HT-PEM-FC. Pristine membranes lose water (1-4wt%) which is associated with PA while heated up till 100 °C. Doped membranes exhibit higher loss of water (5-7wt%) which indicates they are more hydroscopic than pristine membranes due to PA content. The second weight loss for doped membranes appears at 150 °C when thermal decomposition of PA takes place and reaches 4-5 wt% loss at 200 °C, 6-9wt% at 220 °C and 8-13wt% at 240 °C.

In case of both ILs, the membranes containing less amount of IL exhibit 0-4wt% less weight loss within 100-250 °C. The difference becomes more pronounced in the temperature range of 250-450 °C which is related to IL decomposition and associated with thermal decomposition of ILs confined in the membranes (Figure 58b). It can be observed that the higher content of IL immobilized in the matrix, the higher is the weight loss within this temperature range. That confirms the difference in the loading of ILs.

The most noticeable difference in thermal behavior between pristine and doped membranes occurs above 450 °C when the decomposition of polymer backbone starts. We could observe that at 650 °C 40-60wt% of doped membranes still remained when pristine QSILMs are already completely decomposed which may indicate the formation of different decomposition products. The results of analysis suggest that both pristine and doped QSILMs can be operated in HT-PEMFCs up till 250 °C.

The decomposition of PA at 150-250 ºC can occur because of complete water loss. In HT-PEMFCs water is constantly produced on a cathode side. Hence, some portion of it may diffuse into the membrane and reduce the effect of thermal decomposition. We believe that doped QSILMs can be operated at chosen operated temperatures of 200-220 ºC.

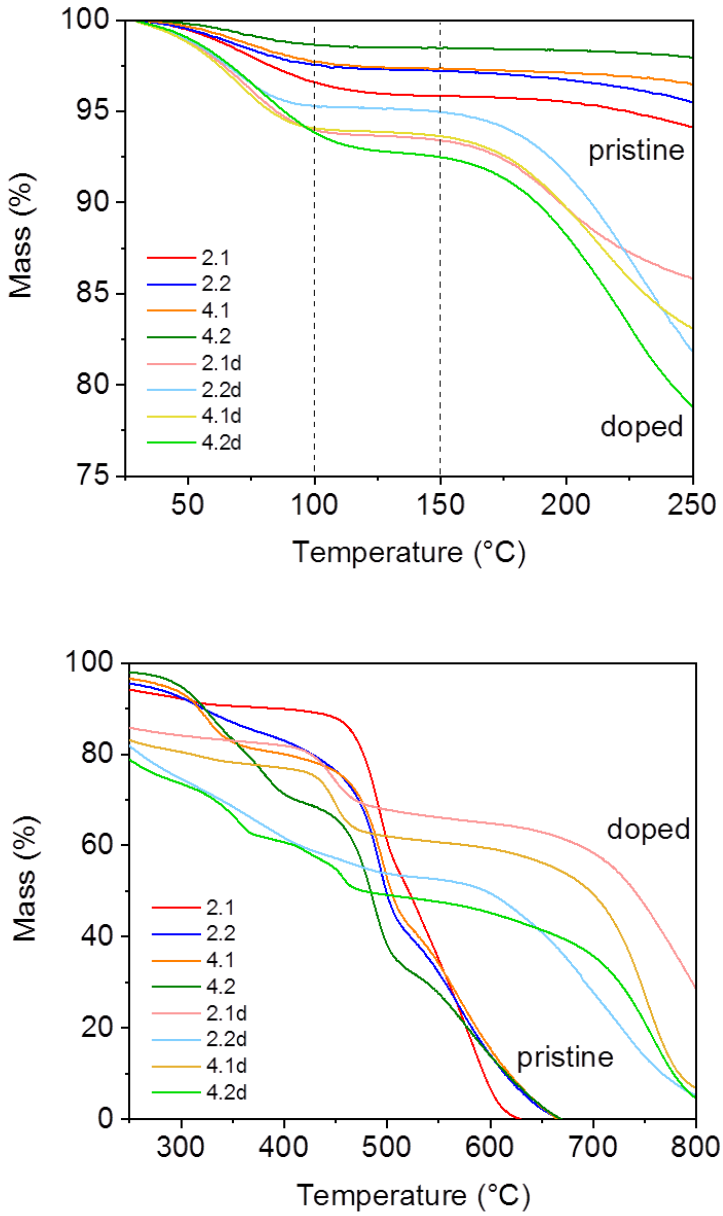

Figure 58 - Comparative TGA curves of pristine QSILMs and QSILMs doped with phosphoric acid measured in air with 10 mL min^{-1} rate (top) below 250 ºC (HT-PEMFC operating temperatures) and (bottom) above 250 ºC

3.2.2. Catalyst layer treatment and MEA fabrication

A MEA consists of a membrane sandwiched between two GDEs. A MEA can be mounted by layer by layer fixation of the GDEs and membrane between the flow fields. Typically, a few metal or ceramic rods are used to correctly position the layers on order to ensure the precise overlap of the electrodes. When the fuel cell is closed by metal end plates, certain pressure is applied to the torch wrench to provide a good contact between the membrane and GDEs and ensure three-phase boundary.

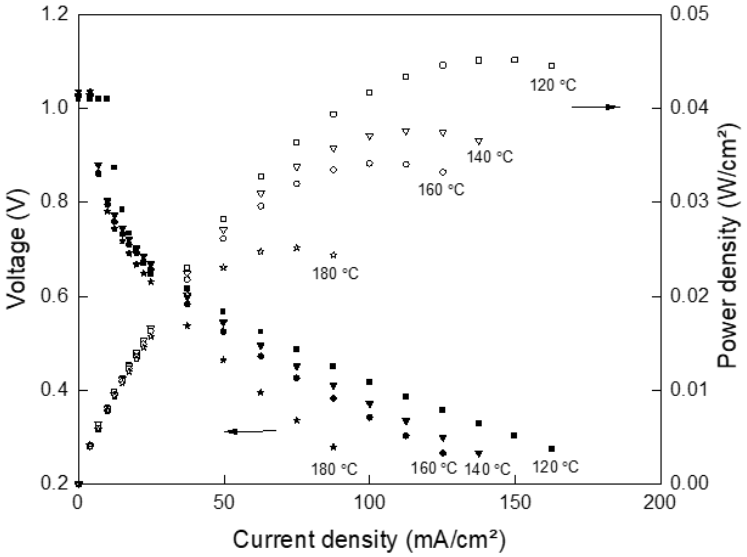

(a)

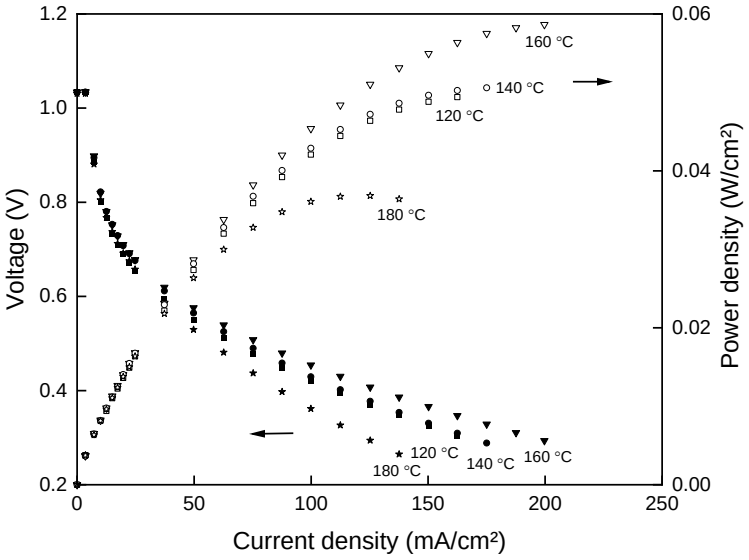

(b)

Figure 59 - Polarization curves for MEAs fabricated (a) without preliminary hot pressing and (b) by means of hot press. Membrane: PA doped QSILM (3.1d), gas-diffusion electrode: DPS. Torch applied to close the cell: 2 N m^{-1}. H_2/air fueled.

Another approach to fabricate MEA is to press the layers together at elevated temperatures. Application of such a technique for the studied QSILMs showed the improved electrochemical characteristic of the cell (Figure 59). When the temperature approaches T_g of the membrane, it becomes more flexible and therefore, easier to "glue" to the electrode surface.

Doped QSILMs were found to not "sweat", which indicates that they do not lose free PA from the matrix compared to PA doped PBI membranes. This causes poor adhesion between the membrane and GDE during MEA preparation. Therefore, the GDE were doped with 1.7mg·cm^{-2} of PA in order to improve three-phase boundary (Figure 60).

The doping of GDE with PA causes improved performance of the cell. This can be possibly explained by the hypothesis that PA dopes the polymer binder which holds the catalyst particles together on the GDL surface. When the conductivity of the binder is improved, then the three-phase boundary has a better contact for proton and electron transport. It is typical that in LT-PEMFC PFSA (e.g., Nafion) is used as a binder and exhibits good conductive properties at operating temperature and humidity level [122]. In case of HT-PEMFC PBI or PTFE are more suitable ionomers should be used as a binder since its T_g is significantly higher than those of PFSA. However, doping of these ionomers with PA is required. Moreover, commercial GDE fabricated with no ionomer in the catalytic layer are available and were used in this work. Therefore, there is no doping of the binder happening, instead PA acts as a binder itself connecting the catalyst particles.

When the MEA for a HT-PEMFC is fabricated, PA is anticipated to leak from the doped PBI membrane into the catalyst layer either during hot pressing or during fuel cell operation. Therefore, PA migrates from the membrane to the GDEs and is known in some cases to cause corrosion of the flow fields (which are often made of carbon) if doping level is pronouncedly high or when GDL has mechanical defects. A decrease in performance was observed when a significantly higher amount of PA was applied onto the GDE by pipetting (10 mg cm^{-2}) (Figure 60c).

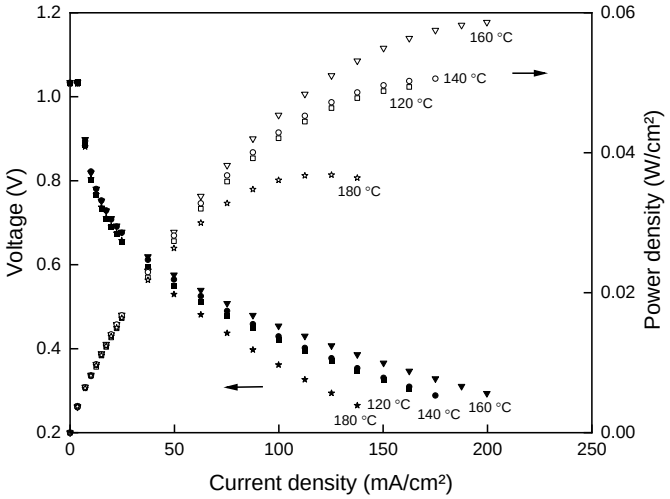

(a)

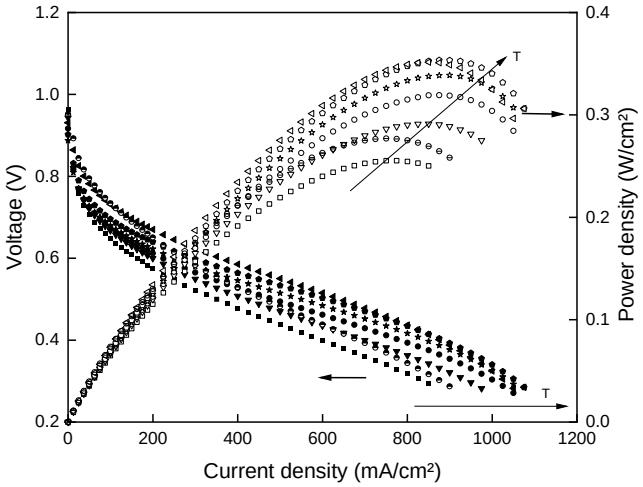

(b)

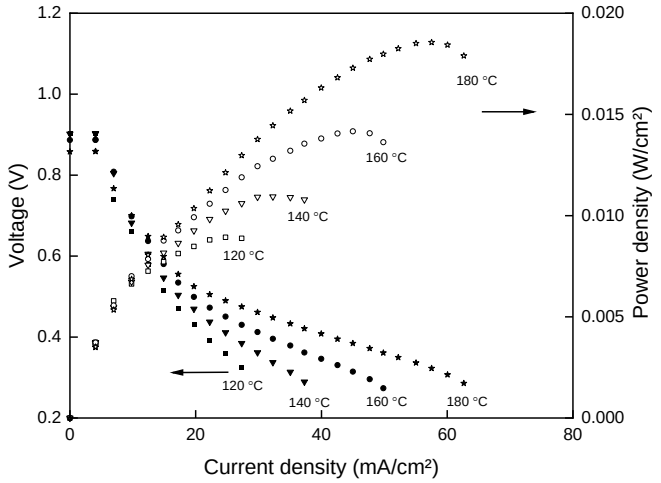

(c)

Figure 60 - Polarization curves for MEAs fabricated with: (a) pristine GDE (DPS), (b) GDE (DPS)doping with PA using "membrane-contact technique" and (c) GDE (DPS) doped with PA using "pipetting technique". Hot pressed. Membrane: PA doped QSILM (3.1d). Torch applied to close the cell: 2 N m^{-1}. H_2/air fueled.

As stated above, fabricated QSILMs do not exhibit visible PA loss, which, however, could happen during hot pressing or fuel cell operation to the certain degree. Doping of the GDE by the technique reproduces natural PA migration from the membrane to the catalyst layer. That allows to distribute the desired amount of PA all over the GDE surface homogeneously. That is anticipated to prevent catalyst flooding with PA when distributed improperly and leads to carbon support corrosion and hydrogen starvation followed damage of the catalyst [123,124]. Oh et al. communicated that it is critically important to remove the water content in the feed gases to reduce electrochemical carbon corrosion [125]. Therefore, the developed technique allows to prevent GDE flooding with water which would happen if PA were applied by pipetting from the aqueous solution. Additionally, the doping level can be controlled to a certain extend by varying the contact time, some deviations were excepted and indicated in this work since the proof-of-the-concept was the target. This technique of commercial GDEs treatment with PA were further used to test fabricated QSILMs in a single fuel cell test.

In order to have a reference performance, a commercial PBI membrane was fully doped in concentrated PA solution at RT and hot pressed between two identical commercial GDE with 1.3 mg_{Pt} cm^{-2} catalyst loading. Polarization curves were recorded in a single H_2/air fuel cell (Figure 61).

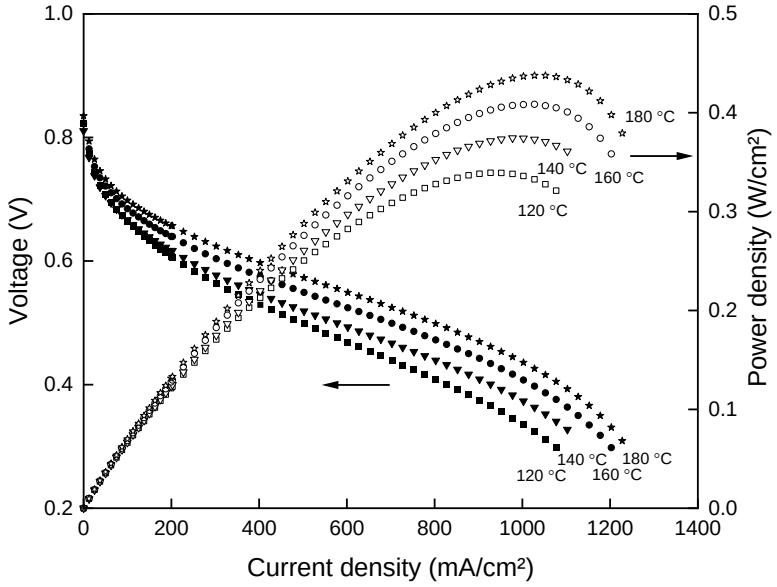

Figure 61 - Polarization curves for a fabricated MEA: PA-doped PBI (reference) membrane and DPS gas-diffusion electrodes with 1.3 mg_{Pt} cm^{-2} catalyst loading. Hot pressed. Torch applied to close the cell: 1 N m^{-1}. H_2/air fueled.

After obtaining the reference data, GDE with different catalyst loadings on the anode and cathode were fabricated. The MEAs produced with and without hot pressing were closed with different torch and tested in a single H_2/air fuel cell (Figure 62). The very

pronounced positive impact of hot pressing and increased torch was observed. However, the possible contribution of the PBI thickness should not be overseen.

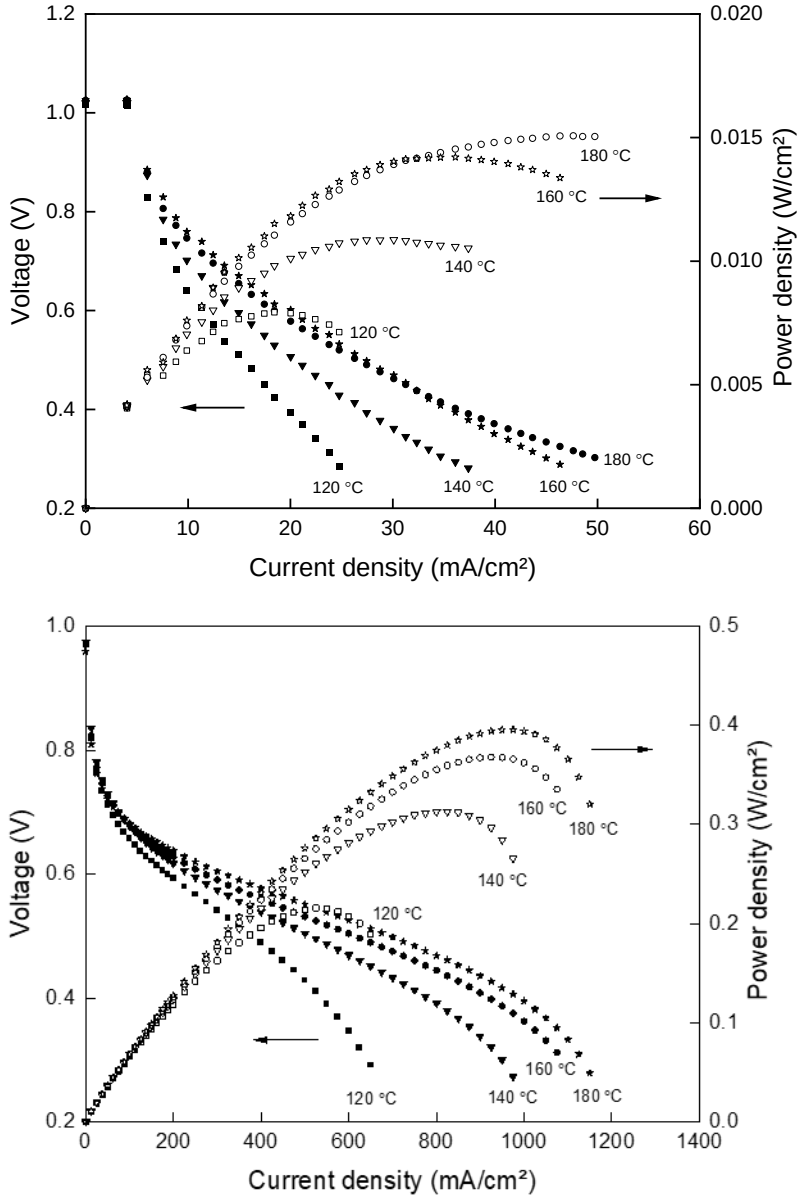

Figure 62 - Polarization curves for a fabricated MEA obtained from operating the H_2/air fuel cell. Anode 0.4 mg_{Pt} cm^{-2}, cathode 0.6 mg_{Pt} cm^{-2}, no binder. (a) PA-doped PBI (self-made), no hot press used, torch applied to close the cell - 1 N m^{-1}; (b) PBI (reference), hot pressed, torch applied to close the cell - 2 N m^{-1}

3.2.3. Single fuel cell test

As a few reference data on a single fuel cell performance of a lab scale, the following works can be mentioned. Erik et al. used commercial ELAT® GDE (BASF) with catalyst loading of 5.0 mg_{Pt} cm^{-2}, which is ca. 4 times higher than what was used in this work. They reported an OCV of 0.6 V. The maximum current density and the maximum power density they achieved at 150C° are 150 mA cm^{-2} and 40 mW cm^{-2} , respectively [88].

Kongstein et al. fabricated an anode with 0.4 mg_{Pt} cm^{-2} and a cathode with 0.6 mg_{Pt} cm^{-2} of catalyst loading. That can be explained by the fact that ORR is more complicated than HOR, and requires more catalyst for activation [126]. They noted that deposition of Pt/C catalyst containing higher concentration of Pt resulted into the thinner catalyst layer and vice versa. Authors used PBI as a binder with the optimal loading of 0.2-0.4 mg_{PBI} cm^{-2}. Fabricated GDE were used to make MEAs and their performance characteristics were tested. OCV was measured at 0.8 V, while maximum current density and power density were reported at 175ºC of 2500 mA cm^{-2} and 800 mW cm^{-2} respectively.

It is important to note that in both works pure oxygen was fed at the cathode side, which is proven to exhibit significantly higher fuel cell performance compared to air as a fuel. It was decided in this work to operate a fuel cell with air due to its practical and relatively safe envisioned application of such feed compared to pure oxygen.

It is known that the operating temperature has a significate impact on the performance of a fuel cell. A temperature increase improves the electrochemical reaction kinetics and hence, fuel cell performance to the point when thermal or chemical stability limits of the material are reached. Therefore, polarization curves were recorded for the fabricated MEA in the temperature range of 120-220ºC (Figure 63,Figure 64).

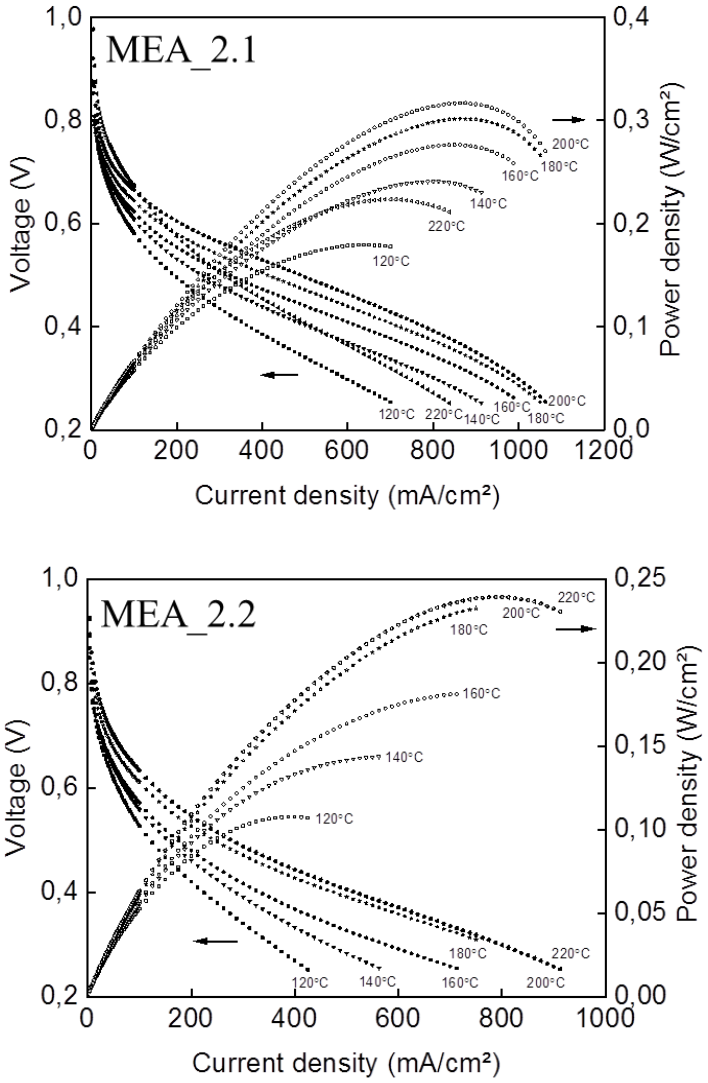

Figure 63 - Polarization curves of doped QSILMs based on IL2 (2.1d and 2.2d) in dependence of operating temperature

In case of all MEAs the performance increases gradually with the temperature increase and reaches maximum at 200-220 ºC. The highest power density of 0.32 W·cm^{-2} was achieved for membrane 2.1d while operated at 200 ºC and 900 mA·cm^{-2}. At this current density the flows were the following: λ_{H2}=2.2 , λ_{Air}=2.8.

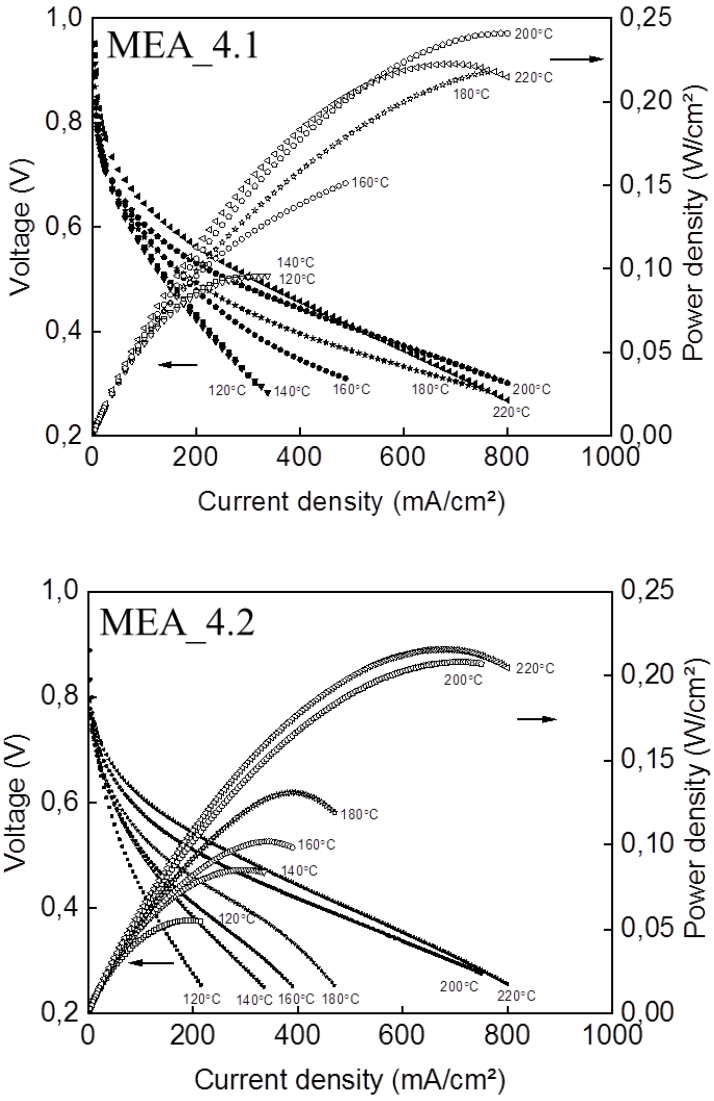

Figure 64 - Polarization curves of doped QSILMs based on IL4 (4.1d and 4.2d) in dependence of the operating temperature

The MEAs containing membranes 4.1 and 4.2 exhibit lower performances than those with 2.1 and 2.2 respectively despite having higher conductivities. Similar effect Rewar et al. experienced in their work when conductivity values did not correlate with the performances [121]. Maximum performance was obtained for the composite PBI membrane containing 25wt% of P[DADMA][TfO] and 107.3wt% PA uptake and reached 0.5 W cm^{-2} at 160 °C in H_2/O_2 fuel cell. No data on the tests under higher temperatures and air flow on the cathode side were provided. Authors reported the utilization of Nafion solution during the catalyst ink preparation. In our work we used ionomer-free GDE since Nafion does not work as electrolyte at high temperatures under nonhumidified conditions [127].

3.3.Ionic liquids immobilized onto the catalyst

3.3.1. Solid catalysts with ionic liquid layer (SCILL)

Figure 65 shows how SCILL ink gets distributed on the glassy carbon surface prior to CV measurements. It is clear that the GC surface is not covered homogeneously. It happens due to the fact that IL2 gives Pt/C hydrophobic properties. That leads to segregation of the particles while drying, since the GC surface is hydrophilic.

To prove such a theory both inks were left for 30 min after sonication. Figure 66 shows the state of the ink for both pristine catalyst and SCILL. It is clearly observed that SCILL particles have majorly precipitated from the hydrophilic solution, even though Nafion was used as a binder.

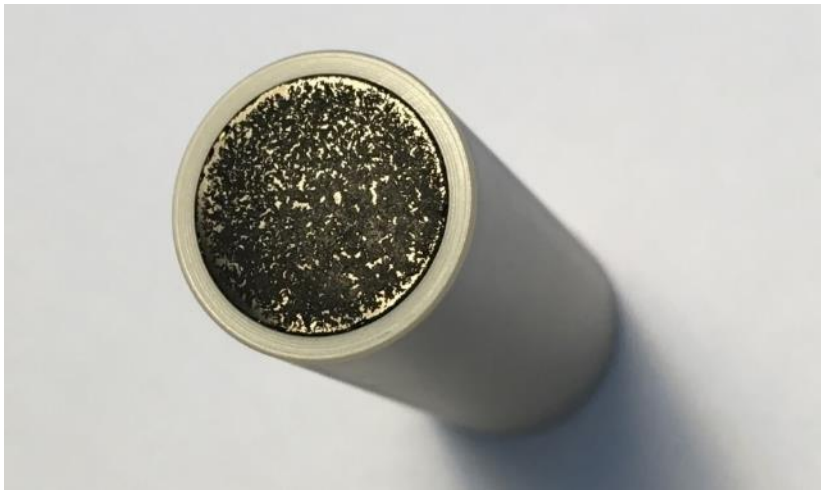

Figure 65 - SCILL deposited on glassy carbon by evaporation of a droplet

Figure 66 - Catalyst ink 30 min after the end of sonication: left - pristine 10%wtPt/C; right - SCILL (10%wtPt/C+IL2)

Figure 67 shows CV curves for pristine 10%wtPt/C catalyst and the same catalyst impregnated with [dema][NTf_2] (IL2) named as SCILL. At the left-hand side, there are peaks corresponding to 1) hydrogen adsorption on platinum surface and evolution (negative *I* values) and 2) hydrogen desorption from the platinum surface (positive *I* values). At the right-hand side, there is a peak of Pt-OH formation followed by Pt-O formation which is later reduced during the reverse scanning (negative *I* values).

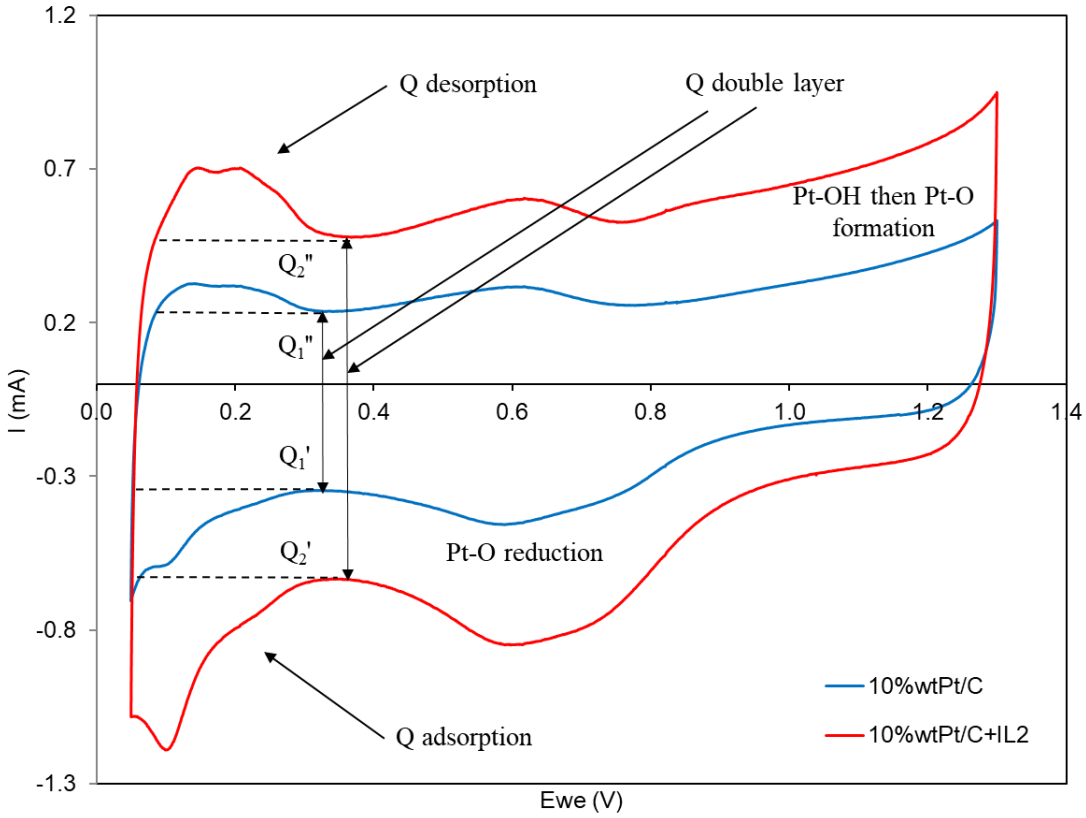

Figure 67 - Cyclic voltammograms for pristine catalyst 10%wtPt/C and SCILL based on 10%wtPt/C impregnated with [dema][NTf_2]

The peaks corresponding to hydrogen adsorption and desorption were integrated and the mean value was calculated. Table 10 shows the calculated EAS for both samples. It is clear that EAS for SCILL is higher than the pristine catalyst by 78%. However, double layer measure for SCILL is also much higher giving an indication about a higher capacitance and therefore, less transport of charge. That probably explains the poor performance of previously reported SILM based on pPIL2. As discussed in Section 3.1.3, during the fuel cell operation, the IL becomes less viscose and leaks out of the pores covering the catalyst particles on the cathode side. This increases the capacitance, and the proton transport stops. ILs have been previously studied and proven by Lewandowski et al. for application in double-layer electrochemical capacitors [128].

This theory will be supported in the next Section 3.3.2 when the performance of the two GDEs impregnated with PA and ILs is compared.

Table 10 - Electrochemically active surface area for the sample with the following constants: scan rate v = 10 mV/s; platinum loading L = 20.4 $\mu g_{Pt}/cm^2$; GC electrode surface S_{el} = 1.77 cm^2

Sample	Coulombic charge of hydrogen adsorption	Coulombic charge of hydrogen desorption	Mean value of the coulombic charge	Electrochemicaly active surface
	Qads (mC)	Qdes (mC)	Q_H (mC)	EASA (m^2/g_{Pt})
10%wtPt/C	1.595	1.500	1.548	20.408
10%wtPt/C+IL2	2.888	2.582	2.735	36.069

3.3.2. Gas diffusion electrode treatment with ionic liquids

Since PA loses water and undergoes thermal decomposition at temperatures above 150 °C, PA in the catalytic layer was replaced by a corresponding IL in order to improve durability of the membranes. Membrane 4.1 was chosen for this experiment due to its lowest doping level. The GDE was prepared by means of spraying catalytic ink containing 1.3 mg_{Pt} cm^{-2} and 0.4 mg_{IL4} cm^{-2}. The MEA was prepared with the same procedure as previously described.

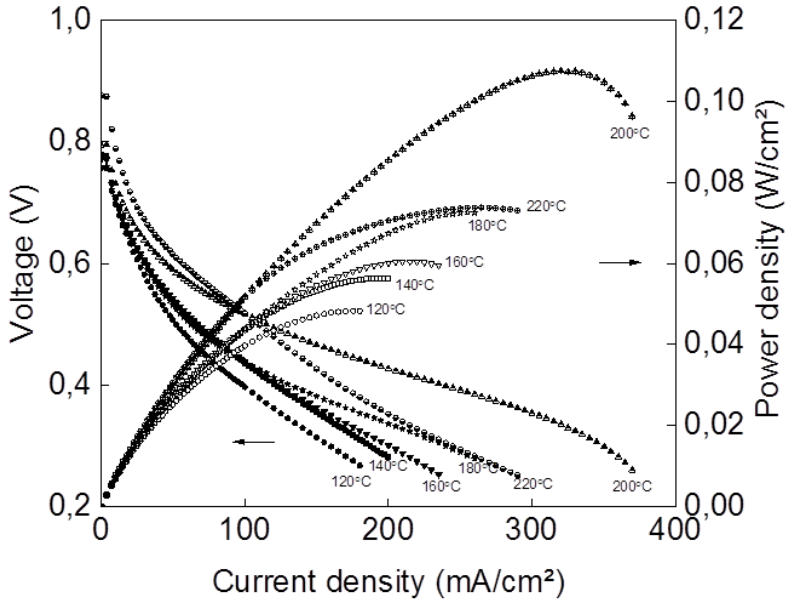

(b)

Figure 68 shows the comparison of the performances of MEAs with membrane 4.1 as electrolyte and GDEs doped IL4 and PA respectively. MEA carrying IL in the catalytic layer exhibits performance twice lower than the one with PA in GDE. Further increase of the IL loading in the catalyst layer to 1.0 mg_{IL} cm^{-2} reduced the performance ca. 5 times, whereas the increase in PA loading yields an higher single fuel cell performance. That

fact supports the hypothesis stated in the previous Section 3.3.1 and proposes that the catalyst is sensitive to the amount of impregnated IL.

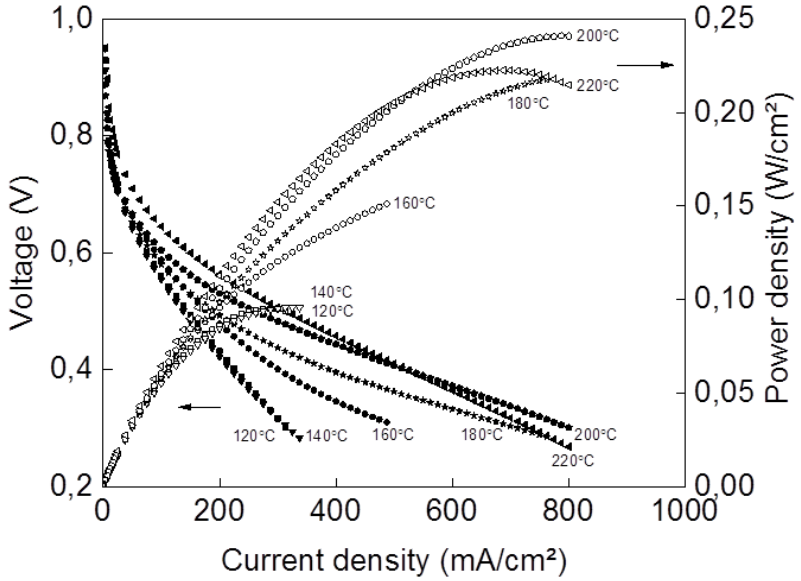

(a)

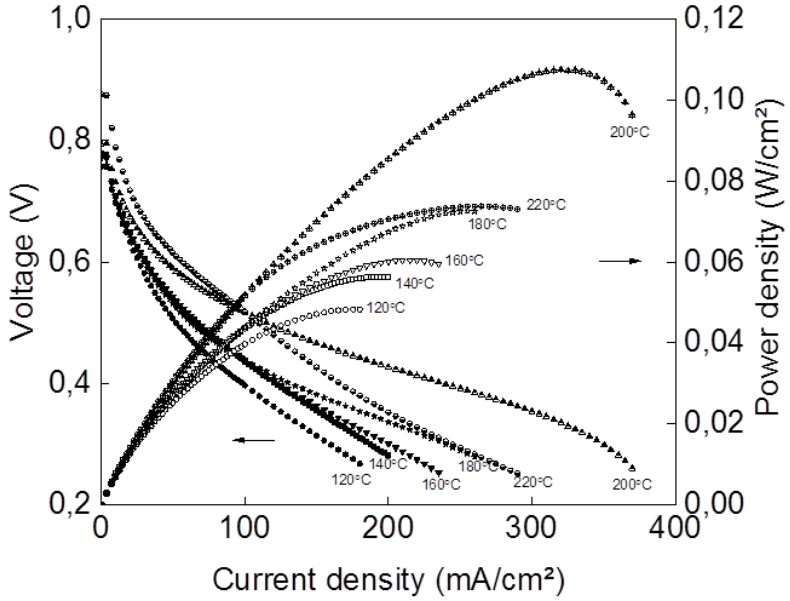

(b)

Figure 68 - Polarization curves of MEA_4.1 with the following GDL doping: (a) PA; (b) – [HHTMG][NTf₂]

3.3.3. Durability test

In order to estimate the long-term stability, durability tests were performed at 200 °C for both MEAs. Figure 69 shows the voltage response at a constant current density of 0.2 mA cm^{-2} within 100 h of operation.

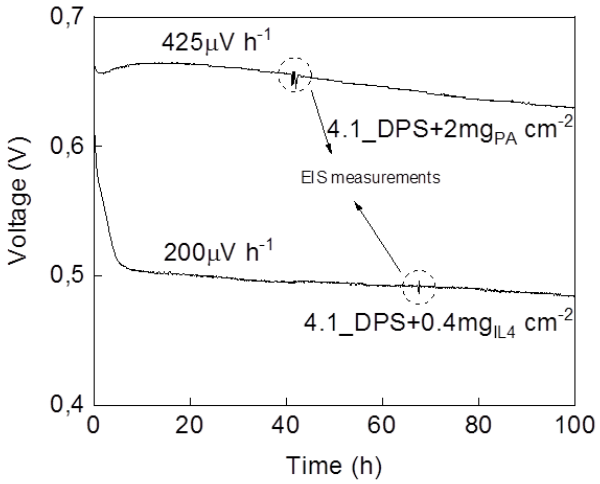

Figure 69 - Comparative durability tests of QSILMs containing 50wt% IL4 and electrodes treated with phosphoric acid (above) and IL4 (below)

The voltage difference after 20 h of operation is 0.164 V and after 100 h is 0.145 V. From the slopes it can be seen that the thermal degradation of the MEA containing IL in GDEs is twice slower than the one containing PA in GDEs. Hence, usage of IL in catalytic layer can be beneficial for the long-term stability. We believe that the content of IL in GDE has to be optimized in order to reach higher absolute performance. Further electrochemical experiments on the influence of the IL content on the catalytic activity of Pt will be performed in our laboratory in the future.

4. Conclusions

In this work two different ways of immobilization of ILs inside PBI matrices were studied. Several PILs containing bis(trifluoromethanesulfonyl) imide as anion were explored as promising electrolytes for HT-PEMFC including a newly designed and synthesized [HHTMG][NTf_2].

Firstly, supported ionic liquid structures were investigated. Porous PBI support were fabricated via phase-inversion method with a further loading with PILs. It was found out that PILs with a melting point below room temperature such as [dema][NTf_2] and [C_2Im][NTf_2] act as plasticizers, providing the necessary flexibility to the PBI backbone. Moreover, SILM containing [dema][NTf_2] exhibited the highest in-plane conductivity among the samples which reached up to 20.74 mS cm^{-1} at 180 ºC in anhydrous conditions. All examined SILMs are thermally stable till 280 ºC which ensures their possible operation in desired temperature range of 160-200 ºC.

However, further single fuel cell test of the MEA based of SILM containing [dema][NTf_2] exhibited a rapid loss in the performance. The OCV could be recovered after the restart of the experiment. Hydrogen pump and EMF experiments revealed that the selected SILM structure cannot be exploited in HT-PEMFC in the current state of development. It is assumed, that despite their good conductive properties, the proton transport across the membranes is supported by vehicle mechanism, when the ions of ILs shuttle protons from anode to cathode side and lose their transport activity afterwards. The proposed transport has been further described.

Additionally, cross-section SEM analysis coupled with EDX revealed a leakage of the IL from the membrane to the gas-diffusion electrode. That leakage covers a solid Pt/C catalyst forming so called SCILL structure. An increased capacitance was measured for such a structure compared to the pristine catalyst, presumably blocking the proton transport.

Secondly, quasi-solidified ionic liquids membranes containing different content of the PILs have been fabricated by blending and co-casting technique. The formation of the porous structure was detected by cross-section SEM analysis, and the presence of ILs inside the pores was confirmed by FT-IR spectroscopy. Membranes with IL/PBI ratios of 1 and 2 exhibited satisfying mechanical stability similar to that of PBI membranes doped with phosphoric acid. Elongation at break increases with an increase in IL content, confirming their plasticizing effect. However, the conductive properties of the studied QSILMs were significantly low.

For the first time fluorescence microscopy was used for investigation of the structure of PBI based composite membranes. It was possible to see that QSILMs exhibit phase separation with segregated globules of ILs dispersed inside the PBI matrix due to

fluorescence on the interface. The segregation effect stands for closed-pore structures and explains the lack of proton transport across the membrane. Therefore, in order to provide the continuous proton transport between the globules, PBI was post-doped with PA via different techniques. Doped membranes exhibited high ion conductivities and good mechanical properties. The performances of MEAs fabricated with PA doped QSILMs and PA doped GDEs showed performances comparable to state-of-the-art PA doped PBI membranes operated in H_2/air HT-PEMFC. The maximum power density was obtained for MEA_2.1d at 200 ºC and reached 0.32 $W \cdot cm^{-2}$ at 900 $mA \cdot cm^{-2}$. It was found that the performance depends on several factors besides conductivity such as MEA elaboration, membrane thickness and catalyst treatment and cannot be always predicted.

For the first time IL was used as electrolyte within the catalytic layer of GDE. Short-term durability test at 200 ºC and 0.2 A cm^{-2} revealed better thermal stability of MEA containing IL in GDE than the GDE containing PA. Hence we assume that utilization of ILs as a doping agent for the catalytic layer can prolong the lifetime of MEA at temperatures over 160 ºC. This can be beneficial for HT-PEMFCs coupled with a reforming unit for a better heat management. Optimization of the IL content and long-term durability tests will be done in our group in order to prove the advantage of IL as alternative electrolytes at 200 ºC and reach the highest performance.

5. Outlook

To summarize, ILs are excellent electrolytes which can be immobilized in both membranes and GDEs operated in HT-PEMFCs providing good thermal stability and durability at temperatures over 180ºC. However, the conductive mechanism needs to be further studied in acid-base systems. Since PBI was additionally doped with PA in this work, some of the PA stayed in free form affecting the durability of the HT-PEMFC. Next to a membrane post-treatment with acid, another approach to provide the backbone with conductive properties is a chemical grafting of functional groups prior to mixing with IL. The anticipated advantages of such an approach are 1) better control over the doping level; 2) ensuring the fixation of the functional groups to the backbone; 3) while avoiding the potential reaction with ILs before grafting. Therefore, as a future research, grafting acidic functional groups such as sulfogroups directly to the backbone of PBI might help avoid PA doping and potentially improve the performance of the fabricated QSIMs based on such a polymer.

As a part of the outlook a few samples of sulfonated PBI polymers with different degrees of sulfonation were fabricated. The polymer is expected to have the structure shown in Figure 70.

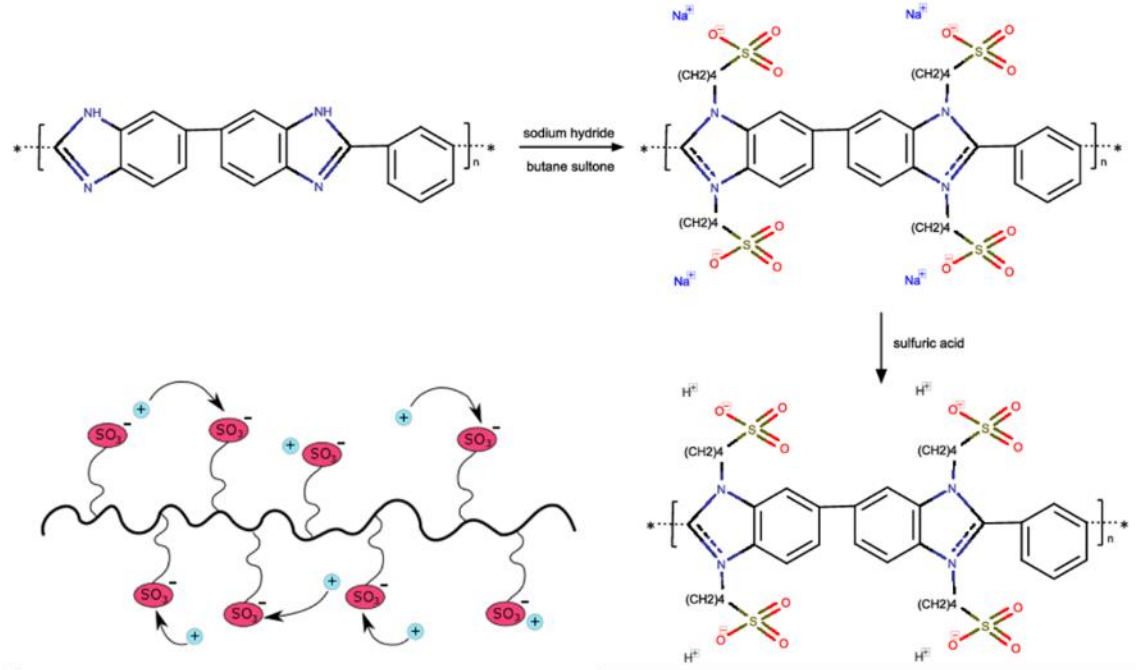

Figure 70 – Expected mechanism of proton hopping for -SO_3H-graphted PBI polymer

The samples expressed high level of hydrophilicity, explaining the formation of a polyanion structure with sulfur groups carrying a negative charge (Figure 71). Unfortunately, the DMAc solutions based on such the polymers were immiscible with the

studied ILs and showed immediate and irreversible phase separation. Therefore, it would be important to conduct more extensive studies in this direction.

Figure 71 - Modified PBI: left – dry; right – after water uptake

Additionally, the influence of the membrane thickness can be studied as well as application of the catalyst directly onto the membrane in order to improve three-phase boundary connection. Sulfonated PBI could be also studied as a binder within the catalytic layer.

Another direction of the future research could be studies of the gas solubility and electrochemical activity of IL-covered catalyst in order to investigate the influence of impregnated or leached PILs on interface process and catalytic activity.

Bibliography

[1] The Paris Agreement, (n.d.). https://unfccc.int/process-and-meetings/the-paris-agreement/the-paris-agreement.

[2] EU role in the Paris Agreement, (n.d.). https://ec.europa.eu/clima/policies/international/negotiations/paris_en.

[3] Global Emissions, (n.d.). https://www.c2es.org/content/international-emissions/.

[4] E. Michelides, Green Energy and Technology, Springer Netherlands, 2012. https://doi.org/10.1007/978-3-642-20951-2.

[5] P. Parthasarathy, S.K. Narayanan, Effect of Hydrothermal Carbonization Reaction Parameters on, Environ. Prog. Sustain. Energy. 33 (2014) 676–680. https://doi.org/10.1002/ep.

[6] I. EG&G Technical Services, Fuel Cell Handbook (Seventh Edition), National Technical Information Service, U.S. Department of Commerce, 2004. https://doi.org/10.1016/s0031-9422(00)82398-5.

[7] R. O'Hayre, Chapter 1: Fuel Cell Principles, in: 2016.

[8] R. O'Hayre, S.-W. Cha, W. Colella, F.B. Prinz, Chapter 8: Overview of Fuel Cell Types, Fuel Cell Fundam. (2016) 269–302. https://doi.org/10.1002/9781119191766.ch8.

[9] J. Marcinkoski, J. Spendelow, A. Wilson, D. Papageorgopoulos, DOE Hydrogen and Fuel Cells Program Record - Fuel Cell System Cost - 2017, J. Mech. Robot. 9 (2017) 1–9. http://mechanismsrobotics.asmedigitalcollection.asme.org/article.aspx?doi=10.1115/1.4036738.

[10] J. Zhang, Z. Xie, J. Zhang, Y. Tang, C. Song, T. Navessin, Z. Shi, D. Song, H. Wang, D.P. Wilkinson, Z.S. Liu, S. Holdcroft, High temperature PEM fuel cells, J. Power Sources. 160 (2006) 872–891. https://doi.org/10.1016/j.jpowsour.2006.05.034.

[11] M.G. Waller, M.R. Walluk, T.A. Trabold, Performance of high temperature PEM fuel cell materials. Part 1: Effects of temperature, pressure and anode dilution, Int. J. Hydrogen Energy. 41 (2016) 2944–2954. https://doi.org/10.1016/j.ijhydene.2015.12.069.

[12] G.G. Scherer, Fuel Cells I, 2008. https://doi.org/10.1007/978-3-540-69757-2.

[13] X. Gang, L. Qingfeng, H.A. Hjuler, N.J. Bjerrum, Hydrogen Oxidation on Gas Diffusion Electrodes for Phosphoric Acid Fuel Cells in the Presence of Carbon Monoxide and Oxygen, J. Electrochem. Soc. 142 (1995) 2890–2893. https://doi.org/10.1149/1.2048660.

[14] H.P. Dhar, A.K. Kush, D.N. Patel, L.G. Christner, Modeling for Co Poisoning of a Fuel Cell Anode., Proc. - Electrochem. Soc. 86–12 (1986) 284–297.

[15] Q. Li, R. He, J.-A. Gao, J.O. Jensen, N.J. Bjerrum, The CO Poisoning Effect in PEMFCs Operational at Temperatures up to 200°C, J. Electrochem. Soc. 150 (2003) A1599. https://doi.org/10.1149/1.1619984.

[16] W. Vogel, L. Lundquist, P. Ross, P. Stonehart, Reaction pathways and poisons-II. The rate controlling step for electrochemical oxidation of hydrogen on Pt in acid and poisoning of the reaction by CO, Electrochim. Acta. 20 (1975) 79–93. https://doi.org/10.1016/0013-4686(75)85048-1.

[17] B. Lakshmanan, W. Huang, D. Olmeijer, J.W. Weidner, Polyetheretherketohe Membranes for Elevated Temperature PEMFCs, Electrochem. Solid-State Lett. 6 (2003) 282–285. https://doi.org/10.1149/1.1619647.

[18] J.T. Wang, R.F. Savinell, J. Wainright, M. Litt, H. Yu, A H2/O2 fuel cell using acid doped polybenzimidazole as polymer electrolyte, Electrochim. Acta. 41 (1996) 193–197. https://doi.org/10.1016/0013-4686(95)00313-4.

[19] S. Malhotra, R. Datta, Membrane-Supported Nonvolatile Acidic Electrolytes Allow Higher Temperature Operation of Proton-Exchange Membrane Fuel Cells, J. Electrochem. Soc. 144 (1997) L23–L26. https://doi.org/10.1149/1.1837420.

[20] Q. Li, R. He, J.O. Jensen, N.J. Bjerrum, Approaches and Recent Development of Polymer Electrolyte Membranes for Fuel Cells Operating above 100 °C, Chem. Mater. 15 (2003) 4896–4915. https://doi.org/10.1021/cm0310519.

[21] DuPont, https://www.fuelcellsetc.com/store/N117, (n.d.). https://www.fuelcellsetc.com/store/N117.

[22] AGC Chemicals Companyhttps://www.agc-chemicals.com/cn/en/fluorine/products/detail/index.html?pCode=CN-EN-F020, https://www.agc-chemicals.com/cn/en/fluorine/products/detail/index.html?pCode=CN-EN-F020, (n.d.). https://www.agc-chemicals.com/cn/en/fluorine/products/detail/index.html?pCode=CN-EN-F020.

[23] GORE Fuel Cell Technologies, GORE, (n.d.). https://www.gore.com/fuelcells.

[24] SOLVAY, https://www.solvay.com/en/brands/aquivion-ion-conducting-polymers, (n.d.). https://www.solvay.com/en/brands/aquivion-ion-conducting-polymers.

[25] 3M, https://multimedia.3m.com/mws/media/1895877O/3m-ionomers-725ew-ionomer-800ew-ionomer-tds-experimental.pdf, (n.d.). https://multimedia.3m.com/mws/media/1895877O/3m-ionomers-725ew-ionomer-800ew-ionomer-tds-experimental.pdf.

[26] W.Y. Hsu, T.D. Gierke, Ion transport and clustering in nafion perfluorinated membranes, J. Memb. Sci. 13 (1983) 307–326. https://doi.org/10.1016/S0376-7388(00)81563-X.

[27] Q. Li, R. He, J.O. Jensen, N.J. Bjerrum, Approaches and Recent Development of Polymer Electrolyte Membranes for Fuel Cells Operating above 100 °C, Chem. Mater. 15 (2003) 4896–4915. https://doi.org/10.1021/cm0310519.

[28] Q. Li, R. He, J.O. Jensen, N.J. Bjerrum, PBI-based polymer membranes for high temperature fuel cells - Preparation, characterization and fuel cell demonstration, Fuel Cells. 4 (2004) 147–159. https://doi.org/10.1002/fuce.200400020.

[29] V. Di Noto, M. Piga, G.A. Giffin, S. Lavina, E.S. Smotkin, J.Y. Sanchez, C. Iojoiu, Influence of anions on proton-conducting membranes based on

neutralized Nafion 117, triethylammonium methanesulfonate, and triethylammonium perfluorobutanesulfonate. 1. synthesis and properties, J. Phys. Chem. C. 116 (2012) 1361–1369. https://doi.org/10.1021/jp204241y.

[30] J. Maiti, N. Kakati, S.P. Woo, Y.S. Yoon, Nafion®based hybrid composite membrane containing GO and dihydrogen phosphate functionalized ionic liquid for high temperature polymer electrolyte membrane fuel cell, Compos. Sci. Technol. 155 (2018) 189–196. https://doi.org/10.1016/j.compscitech.2017.11.030.

[31] P. Staiti, A.S. Aricò, V. Baglio, F. Lufrano, E. Passalacqua, V. Antonucci, Hybrid Nafion-silica membranes doped with heteropolyacids for application in direct methanol fuel cells, Solid State Ionics. 145 (2001) 101–107. https://doi.org/10.1016/S0167-2738(01)00919-5.

[32] C. Yang, S. Srinivasan, A.B. Bocarsly, S. Tulyani, J.B. Benziger, A comparison of physical properties and fuel cell performance of Nafion and zirconium phosphate/Nafion composite membranes, J. Memb. Sci. 237 (2004) 145–161. https://doi.org/10.1016/j.memsci.2004.03.009.

[33] P. Bébin, M. Caravanier, H. Galiano, Nafion®/clay-SO3H membrane for proton exchange membrane fuel cell application, J. Memb. Sci. 278 (2006) 35–42. https://doi.org/10.1016/j.memsci.2005.10.042.

[34] Y.F. Lin, C.Y. Yen, C.C.M. Ma, S.H. Liao, C.H. Lee, Y.H. Hsiao, H.P. Lin, High proton-conducting Nafion®/-SO3H functionalized mesoporous silica composite membranes, J. Power Sources. 171 (2007) 388–395. https://doi.org/10.1016/j.jpowsour.2007.06.049.

[35] D.C. Lee, H.N. Yang, S.H. Park, W.J. Kim, Nafion/graphene oxide composite membranes for low humidifying polymer electrolyte membrane fuel cell, J. Memb. Sci. 452 (2014) 20–28. https://doi.org/10.1016/j.memsci.2013.10.018.

[36] A.K. Mishra, T. Kuila, D.-Y. Kim, N.H. Kim, J.H. Lee, Protic ionic liquid-functionalized mesoporous silica-based hybrid membranes for proton exchange membrane fuel cells, J. Mater. Chem. 22 (2012) 24366. https://doi.org/10.1039/c2jm33288d.

[37] A.K. Mishra, N.H. Kim, J.H. Lee, Effects of ionic liquid-functionalized mesoporous silica on the proton conductivity of acid-doped poly(2,5-benzimidazole) composite membranes for high-temperature fuel cells, J. Memb. Sci. 449 (2013) 136–145. https://doi.org/10.1016/j.memsci.2013.08.023.

[38] D. Aili, M.K. Hansen, C. Pan, Q. Li, E. Christensen, J.O. Jensen, N.J. Bjerrum, Phosphoric acid doped membranes based on Nafion®, PBI and their blends - Membrane preparation, characterization and steam electrolysis testing, Int. J. Hydrogen Energy. 36 (2011) 6985–6993. https://doi.org/10.1016/j.ijhydene.2011.03.058.

[39] M. Díaz, A. Ortiz, M. Isik, D. Mecerreyes, I. Ortiz, Highly conductive electrolytes based on poly([HSO3-BVIm][TfO])/[HSO3-BMIm][TfO] mixtures for fuel cell applications, Int. J. Hydrogen Energy. 40 (2014) 11294–11302. https://doi.org/10.1016/j.ijhydene.2015.03.109.

[40] C. Jia, Y. Cheng, X. Ling, G. Wei, J. Liu, C. Yan, Sulfonated poly(Ether Ether Ketone)/functionalized carbon nanotube composite membrane for vanadium redox flow battery applications, Electrochim. Acta. 153 (2015) 44–48. https://doi.org/10.1016/j.electacta.2014.11.123.

[41] W. Dai, Y. Shen, Z. Li, L. Yu, J. Xi, X. Qiu, SPEEK/Graphene oxide nanocomposite membranes with superior cyclability for highly efficient vanadium redox flow battery, J. Mater. Chem. A. 2 (2014) 12423–12432. https://doi.org/10.1039/c4ta02124j.

[42] R.S. Malik, P. Verma, V. Choudhary, A study of new anhydrous, conducting membranes based on composites of aprotic ionic liquid and cross-linked SPEEK for fuel cell application, Electrochim. Acta. 152 (2015) 352–359. https://doi.org/10.1016/j.electacta.2014.11.167.

[43] S. Gahlot, V. Kulshrestha, Dramatic improvement in water retention and proton conductivity in electrically aligned functionalized CNT/SPEEK nanohybrid PEM, ACS Appl. Mater. Interfaces. 7 (2015) 264–272. https://doi.org/10.1021/am506033c.

[44] X. Wang, M. Jin, Y. Li, L. Zhao, The influence of various ionic liquids on the properties of SPEEK membrane doped with mesoporous silica, Electrochim. Acta. 257 (2017) 290–300. https://doi.org/10.1016/j.electacta.2017.10.098.

[45] P. Xing, G.P. Robertson, M.D. Guiver, S.D. Mikhailenko, K. Wang, S. Kaliaguine, Synthesis and characterization of sulfonated poly(ether ether ketone) for proton exchange membranes, J. Memb. Sci. 229 (2004) 95–106. https://doi.org/10.1016/j.memsci.2003.09.019.

[46] P.R. Jothi, S. Dharmalingam, An efficient proton conducting electrolyte membrane for high temperature fuel cell in aqueous-free medium, J. Memb. Sci. 450 (2014) 389–396. https://doi.org/10.1016/j.memsci.2013.09.034.

[47] H. Zhang, C. Ma, J. Wang, X. Wang, H. Bai, J. Liu, Enhancement of proton conductivity of polymer electrolyte membrane enabled by sulfonated nanotubes, Int. J. Hydrogen Energy. 39 (2014) 974–986. https://doi.org/10.1016/j.ijhydene.2013.10.145.

[48] B. Singh, N.M.H. Duong, D. Henkensmeier, J.H. Jang, H.J. Kim, J. Han, S.W. Nam, Influence of Different Side-groups and Cross-links on Phosphoric Acid Doped Radel-based Polysulfone Membranes for High Temperature Polymer Electrolyte Fuel Cells, Electrochim. Acta. 224 (2017) 306–313. https://doi.org/10.1016/j.electacta.2016.12.088.

[49] N.Y. Abu-Thabit, S.A. Ali, S.M. Javaid Zaidi, New highly phosphonated polysulfone membranes for PEM fuel cells, J. Memb. Sci. 360 (2010) 26–33. https://doi.org/10.1016/j.memsci.2010.04.041.

[50] J. Yang, Q. Li, J.O. Jensen, C. Pan, L.N. Cleemann, N.J. Bjerrum, R. He, Phosphoric acid doped imidazolium polysulfone membranes for high temperature proton exchange membrane fuel cells, J. Power Sources. 205 (2012) 114–121. https://doi.org/10.1016/j.jpowsour.2012.01.038.

[51] K. Rambabu, G. Bharath, A.F. Arangadi, S. Velu, F. Banat, P.L. Show, ZrO2

incorporated polysulfone anion exchange membranes for fuel cell applications, Int. J. Hydrogen Energy. 45 (2020) 29668–29680. https://doi.org/10.1016/j.ijhydene.2020.08.175.

[52] J. Liu, R. Qu, P. Peng, W. Liu, D. Chen, H. Zhang, X. Liu, Covalently functionalized graphene oxide and quaternized polysulfone nanocomposite membranes for fuel cells, RSC Adv. 6 (2016) 71305–71310. https://doi.org/10.1039/c6ra12822j.

[53] J. Li, H. Wu, L. Cao, X. He, B. Shi, Y. Li, M. Xu, Z. Jiang, Enhanced Proton Conductivity of Sulfonated Polysulfone Membranes under Low Humidity via the Incorporation of Multifunctional Graphene Oxide, ACS Appl. Nano Mater. 2 (2019) 4734–4743. https://doi.org/10.1021/acsanm.9b00446.

[54] T. Yasuda, M. Watanabe, Supported Protic Ionic Liquids in Polymer Membranes for Electrolytes of Nonhumidified Fuel Cells, Support. Ion. Liq. Fundam. Appl. (2014) 407–418. https://doi.org/10.1002/9783527654789.ch20.

[55] S.-Y. Lee, A. Ogawa, M. Kanno, H. Nakamoto, T. Yasuda, M. Watanabe, Nonhumidified intermediate temperature fuel cells using protic ionic liquids., J. Am. Chem. Soc. 132 (2010) 9764–9773. https://doi.org/10.1021/ja102367x.

[56] T. Yasuda, S. Nakamura, Y. Honda, K. Kinugawa, S.-Y. Lee, M. Watanabe, Effects of Polymer Structure on Properties of Sulfonated Polyimide/Protic Ionic Liquid Composite Membranes for Nonhumidified Fuel Cell Applications, ACS Appl. Mater. Interfaces. 4 (2012) 1783–1790. https://doi.org/10.1021/am300031k.

[57] S.Y. Lee, T. Yasuda, M. Watanabe, Fabrication of protic ionic liquid/sulfonated polyimide composite membranes for non-humidified fuel cells, J. Power Sources. 195 (2010) 5909–5914. https://doi.org/10.1016/j.jpowsour.2009.11.045.

[58] S. Galbiati, A. Baricci, A. Casalegno, R. Marchesi, Experimental study of water transport in a polybenzimidazole-based high temperature PEMFC, Int. J. Hydrogen Energy. 37 (2012) 2462–2469. https://doi.org/10.1016/j.ijhydene.2011.09.159.

[59] J. Zhang, Y. Tang, C. Song, J. Zhang, Polybenzimidazole-membrane-based PEM fuel cell in the temperature range of 120-200 °C, J. Power Sources. 172 (2007) 163–171. https://doi.org/10.1016/j.jpowsour.2007.07.047.

[60] Q. Li, J.O. Jensen, R.F. Savinell, N.J. Bjerrum, High temperature proton exchange membranes based on polybenzimidazoles for fuel cells, Prog. Polym. Sci. 34 (2009) 449–477. https://doi.org/10.1016/j.progpolymsci.2008.12.003.

[61] Q. Li, R. He, J.O. Jensen, N.J. Bjerrum, PBI-based polymer membranes for high temperature fuel cells - Preparation, characterization and fuel cell demonstration, Fuel Cells. (2004). https://doi.org/10.1002/fuce.200400020.

[62] Y. Oono, A. Sounai, M. Hori, Long-term cell degradation mechanism in high-temperature proton exchange membrane fuel cells, J. Power Sources. 210 (2012) 366–373. https://doi.org/10.1016/j.jpowsour.2012.02.098.

[63] J. Lobato, P. Cañizares, M.A. Rodrigo, J.J. Linares, G. Manjavacas, Synthesis and characterisation of poly[2,2-(m-phenylene)-5,5-bibenzimidazole] as polymer

electrolyte membrane for high temperature PEMFCs, J. Memb. Sci. 280 (2006) 351–362. https://doi.org/10.1016/j.memsci.2006.01.049.

[64] D. Mecerreyes, H. Grande, O. Miguel, E. Ochoteco, R. Marcilla, I. Cantero, Porous Polybenzimidazole Membranes Doped with Phosphoric Acid: Highly Proton-Conducting Solid Electrolytes, Chem. Mater. 16 (2004) 604–607. https://doi.org/10.1021/cm034398k.

[65] J.P. Melchior, G. Majer, K.D. Kreuer, Why do proton conducting polybenzimidazole phosphoric acid membranes perform well in high-temperature PEM fuel cells?, Phys. Chem. Chem. Phys. 19 (2017) 601–612. https://doi.org/10.1039/c6cp05331a.

[66] H. Nakamoto, M. Watanabe, Brønsted acid-base ionic liquids for fuel cell electrolytes, Chem. Commun. (2007) 2539–2541. https://doi.org/10.1039/b618953a.

[67] A.S. Rewar, H.D. Chaudhari, R. Illathvalappil, K. Sreekumar, U.K. Kharul, New approach of blending polymeric ionic liquid with polybenzimidazole (PBI) for enhancing physical and electrochemical properties, J. Mater. Chem. A. 2 (2014) 14449–14458. https://doi.org/10.1039/c4ta02184c.

[68] S. Liu, L. Zhou, P. Wang, F. Zhang, S. Yu, Z. Shao, B. Yi, Ionic-Liquid-Based Proton Conducting Membranes for Anhydrous H2/Cl2 Fuel-Cell Applications, ACS Appl. Mater. Interfaces. 6 (2014) 3195–3200. https://doi.org/10.1021/am404645c.

[69] J. Lemus, J. Palomar, M.A. Gilarranz, J.J. Rodriguez, Characterization of Supported Ionic Liquid Phase (SILP) materials prepared from different supports, Adsorption. 17 (2011) 561–571. https://doi.org/10.1007/s10450-011-9327-5.

[70] C. Iojoiu, M. Hana, Y. Molmeret, M. Martinez, L. Cointeaux, N. El Kissi, J. Teles, J.C. Leprêtre, P. Judeinstein, J.Y. Sanchez, Ionic liquids and their hosting by polymers for HT-PEMFC Membranes, Fuel Cells. 10 (2010) 778–789. https://doi.org/10.1002/fuce.201000026.

[71] T.L. Greaves, C.J. Drummond, Protic ionic liquids: Properties and applications, Chem. Rev. 108 (2008) 206–237. https://doi.org/10.1021/cr068040u.

[72] M. Anouti, J. Jacquemin, D. Lemordant, Transport properties of protic ionic liquids, pure and in aqueous solutions: Effects of the anion and cation structure, Fluid Phase Equilib. 297 (2010) 13–22. https://doi.org/10.1016/j.fluid.2010.05.019.

[73] T.L. Greaves, C.J. Drummond, Protic Ionic Liquids: Evolving Structure-Property Relationships and Expanding Applications, Chem. Rev. 115 (2015) 11379–11448. https://doi.org/10.1021/acs.chemrev.5b00158.

[74] T. Yasuda, A. Ogawa, M. Kanno, K. Mori, K. Sakakibara, M. Watanabe, Hydrophobic Protic Ionic Liquid for Nonhumidified Intermediate-temperature Fuel Cells, Chem. Lett. 38 (2009) 692–693. https://doi.org/10.1246/cl.2009.692.

[75] M. Díaz, A. Ortiz, I. Ortiz, Progress in the use of ionic liquids as electrolyte membranes in fuel cells, J. Memb. Sci. 469 (2014) 379–396. https://doi.org/10.1016/j.memsci.2014.06.033.

[76] T. Yasuda, M. Watanabe, Protic ionic liquids: Fuel cell applications, MRS Bull. 38 (2013) 560–566. https://doi.org/10.1557/mrs.2013.153.

[77] S. Zhang, J. Zhang, Y. Zhang, Y. Deng, Nanoconfined Ionic Liquids, Chem. Rev. 117 (2017) 6755–6833. https://doi.org/10.1021/acs.chemrev.6b00509.

[78] J. Yuan, D. Mecerreyes, M. Antonietti, Poly(ionic liquid)s: An update, Prog. Polym. Sci. 38 (2013) 1009–1036. https://doi.org/10.1016/j.progpolymsci.2013.04.002.

[79] F. Yan, S. Yu, X. Zhang, L. Qiu, F. Chu, J. You, J. Lu, Enhanced proton conduction in polymer electrolyte membranes as synthesized by polymerization of protic ionic liquid-based microemulsions, Chem. Mater. 21 (2009) 1480–1484. https://doi.org/10.1021/cm900098r.

[80] M.D.V.M. De Yuso, M.T. Cuberes, V. Romero, L. Neves, I. Coelhoso, J.G. Crespo, E. Rodríguez-Castellón, J. Benavente, Modification of a Nafion membrane by n-dodecyltrimethylammonium cation inclusion for potential application in DMFC, Int. J. Hydrogen Energy. 39 (2014) 4023–4029. https://doi.org/10.1016/j.ijhydene.2013.05.046.

[81] M. Díaz, A. Ortiz, M. Vilas, E. Tojo, I. Ortiz, Performance of PEMFC with new polyvinyl-ionic liquids based membranes as electrolytes, Int. J. Hydrogen Energy. 39 (2014) 3970–3977. https://doi.org/10.1016/j.ijhydene.2013.04.155.

[82] V. Di Noto, M. Piga, G.A. Giffin, S. Lavina, E.S. Smotkin, J.Y. Sanchez, C. Jojoiu, Influence of Anions on Proton-Conducting Membranes Based on Neutralized Nafion 117, Triethylammonium Methanesulfonate, and Triethylammonium Perfluorobutanesulfonate. 2. Electrical Properties, J. Phys. Chem. C. 116 (2012) 1370–1379. https://doi.org/10.1021/jp204242q.

[83] C.W. Liew, S. Ramesh, A.K. Arof, A novel approach on ionic liquid-based poly(vinyl alcohol) proton conductive polymer electrolytes for fuel cell applications, Int. J. Hydrogen Energy. 39 (2014) 2917–2928. https://doi.org/10.1016/j.ijhydene.2013.07.092.

[84] A. Eguizábal, J. Lemus, M.P. Pina, On the incorporation of protic ionic liquids imbibed in large pore zeolites to polybenzimidazole membranes for high temperature proton exchange membrane fuel cells, J. Power Sources. 222 (2013) 483–492. https://doi.org/10.1016/j.jpowsour.2012.07.094.

[85] J. Wang, J. Luo, S. Feng, H. Li, Y. Wan, X. Zhang, Recent development of ionic liquid membranes, Green Energy Environ. 1 (2016) 43–61. https://doi.org/10.1016/j.gee.2016.05.002.

[86] H. Nakajima, H. Ohno, Preparation of thermally stable polymer electrolytes from imidazolium-type ionic liquid derivatives, Polymer (Guildf). 46 (2005) 11499–11504. https://doi.org/10.1016/j.polymer.2005.10.005.

[87] H. Ye, J. Huang, J.J. Xu, N.K.A.C. Kodiweera, J.R.P. Jayakody, S.G. Greenbaum, New membranes based on ionic liquids for PEM fuel cells at elevated temperatures, J. Power Sources. 178 (2008) 651–660. https://doi.org/10.1016/j.jpowsour.2007.07.074.

[88] E. Van De Ven, A. Chairuna, G. Merle, S.P. Benito, Z. Borneman, K. Nijmeijer,

Ionic liquid doped polybenzimidazole membranes for high temperature Proton Exchange Membrane fuel cell applications, J. Power Sources. 222 (2013) 202–209. https://doi.org/10.1016/jjpowsour.2012.07.112.

[89] D. Langevin, Q.T. Nguyen, S. Marais, S. Karademir, J.Y. Sanchez, C. Iojoiu, M. Martinez, R. Mercier, P. Judeinstein, C. Chappey, High-temperature ionic-conducting material: Advanced structure and improved performance, J. Phys. Chem. C. 117 (2013) 15552–15561. https://doi.org/10.1021/jp312575m.

[90] F. Tian, R. Jinnouchi, A.B. Anderson, How potentials of zero charge and potentials for water oxidation to OH(ads) on Pt(111) electrodes vary with coverage, J. Phys. Chem. C. 113 (2009) 17484–17492. https://doi.org/10.1021/jp905377d.

[91] G.R. Zhang, M. Munoz, B.J.M. Etzold, Accelerating oxygen-reduction catalysts through preventing poisoning with non-reactive species by using hydrophobic ionic liquids, Angew. Chemie - Int. Ed. 55 (2016) 2257–2261. https://doi.org/10.1002/anie.201508338.

[92] U. Kernchen, B. Etzold, W. Korth, A. Jess, Solid catalyst ionic liquid layer (SCILL) - A new concept to improve selectivity illustrated by hydrogenation of cyclooctadiene, Chem. Eng. Technol. 30 (2007) 985–994. https://doi.org/10.1002/ceat.200700050.

[93] J. Gao, Y. Guo, B. Wu, L. Qi, B. Li, J. Liu, Z. Wang, W. Liu, J. Gu, Z. Zou, Impact of cation selection on proton exchange membrane fuel cell performance with trimethylethyl amide, ethylpyridinium and ethylmethyl imidazolium ionic liquid carried by poly(vinylidene fluoride) membrane as electrolyte, J. Power Sources. 251 (2014) 432–438. https://doi.org/10.1016/j.jpowsour.2013.11.038.

[94] IoLiTec Catalog, 1-Ethyl-3-methylimidazolium bis(trifluoromethylsulfonyl)imide, 99%, (n.d.). https://iolitec.de/products/ionic_liquids/catalogue/imidazolium-based/il-0023-hp.

[95] M.S. Miran, T. Yasuda, M.A.B.H. Susan, K. Dokko, M. Watanabe, Binary protic ionic liquid mixtures as a proton conductor: High fuel cell reaction activity and facile proton transport, J. Phys. Chem. C. 118 (2014) 27631–27639. https://doi.org/10.1021/jp506957y.

[96] M.S. Miran, T. Yasuda, M.A.B.H. Susan, K. Dokko, M. Watanabe, (Keynote) Protic Ionic Liquids Based on a Super-Strong Acid: Bulk and Electrochemical Properties, ECS Trans. 50 (2013) 285–291. https://doi.org/10.1149/05011.0285ecst.

[97] M.S. Miran, H. Kinoshita, T. Yasuda, M.A.B.H. Susan, M. Watanabe, Physicochemical properties determined by ΔpK a for protic ionic liquids based on an organic super-strong base with various Brønsted acids, Phys. Chem. Chem. Phys. 14 (2012) 5178–5186. https://doi.org/10.1039/c2cp00007e.

[98] B.A. Caine, C. Dardonville, P.L.A. Popelier, Prediction of Aqueous p K a Values for Guanidine-Containing Compounds Using Ab Initio Gas-Phase Equilibrium Bond Lengths, ACS Omega. 3 (2018) 3835–3850. https://doi.org/10.1021/acsomega.8b00142.

[99] G. Skorikova, D. Rauber, D. Aili, S. Martin, Q. Li, D. Henkensmeier, R. Hempelmann, Protic ionic liquids immobilized in phosphoric acid-doped polybenzimidazole matrix enable polymer electrolyte fuel cell operation at 200 °C, J. Memb. Sci. 608 (2020). https://doi.org/10.1016/j.memsci.2020.118188.

[100] S. Bulut, P. Eiden, W. Beichel, J.M. Slattery, T.F. Beyersdorff, T.J.S. Schubert, I. Krossing, Temperature dependence of the viscosity and conductivity of mildly functionalized and non-functionalized [Tf2N]- ionic liquids, ChemPhysChem. 12 (2011) 2296–2310. https://doi.org/10.1002/cphc.201100214.

[101] J. Vila, P. Ginés, J.M. Pico, C. Franjo, E. Jiménez, L.M. Varela, O. Cabeza, Temperature dependence of the electrical conductivity in EMIM-based ionic liquids: Evidence of Vogel-Tamman-Fulcher behavior, Fluid Phase Equilib. 242 (2006) 141–146. https://doi.org/10.1016/j.fluid.2006.01.022.

[102] Y. Yip, A.J. McHugh, Modeling and simulation of nonsolvent vapor-induced phase separation, J. Memb. Sci. 271 (2006) 163–176. https://doi.org/10.1016/j.memsci.2005.06.063.

[103] J. Li, X. Li, S. Yu, J. Hao, W. Lu, Z. Shao, B. Yi, Porous polybenzimidazole membranes doped with phosphoric acid: Preparation and application in high-temperature proton-exchange-membrane fuel cells, Energy Convers. Manag. 85 (2014) 323–327. https://doi.org/10.1016/j.enconman.2014.05.052.

[104] T. Luo, O. David, Y. Gendel, M. Wessling, Porous poly(benzimidazole) membrane for all vanadium redox flow battery, J. Power Sources. 312 (2016) 45–54. https://doi.org/10.1016/j.jpowsour.2016.02.042.

[105] Z. Yuan, Y. Duan, H. Zhang, X. Li, H. Zhang, I. Vankelecom, Advanced porous membranes with ultra-high selectivity and stability for vanadium flow batteries, Energy Environ. Sci. 9 (2016) 441–447. https://doi.org/10.1039/c5ee02896e.

[106] Scribbner, In Situ PEM FC Electrochemical Surface Area, (n.d.) 1–4. https://www.scribner.com/faq/1-in-situ-pem-fc-electrochemical-surface-area-and-catalyst-utilization-measurement/ (accessed June 20, 2021).

[107] Y.A. Gandomi, D.S. Aaron, J.R. Houser, M.C. Daugherty, J.T. Clement, A.M. Pezeshki, T.Y. Ertugrul, D.P. Moseley, M.M. Mench, Critical Review—Experimental Diagnostics and Material Characterization Techniques Used on Redox Flow Batteries, J. Electrochem. Soc. 165 (2018) A970–A1010. https://doi.org/10.1149/2.0601805jes.

[108] D.E. Smith, D.A. Walsh, The Nature of Proton Shuttling in Protic Ionic Liquid Fuel Cells, Adv. Energy Mater. 1900744 (2019) 1–6. https://doi.org/10.1002/aenm.201900744.

[109] S.E. Goodwin, D.E. Smith, J.S. Gibson, R.G. Jones, D.A. Walsh, Electroanalysis of Neutral Precursors in Protic Ionic Liquids and Synthesis of High-Ionicity Ionic Liquids, Langmuir. 33 (2017) 8436–8446. https://doi.org/10.1021/acs.langmuir.7b02294.

[110] G.L. Burrell, I.M. Burgar, F. Separovic, N.F. Dunlop, Preparation of protic ionic liquids with minimal water content and 15N NMR study of proton transfer, Phys. Chem. Chem. Phys. 12 (2010) 1571–1577. https://doi.org/10.1039/b921432a.

[111] L. Johnson, A. Ejigu, P. Licence, D.A. Walsh, Hydrogen oxidation and oxygen reduction at platinum in protic ionic liquids, J. Phys. Chem. C. 116 (2012) 18048–18056. https://doi.org/10.1021/jp303749k.

[112] A. Konovalova, H. Kim, S. Kim, A. Lim, H.S. Park, M.R. Kraglund, D. Aili, J.H. Jang, H.J. Kim, D. Henkensmeier, Blend membranes of polybenzimidazole and an anion exchange ionomer (FAA3) for alkaline water electrolysis: Improved alkaline stability and conductivity, J. Memb. Sci. 564 (2018) 653–662. https://doi.org/10.1016/j.memsci.2018.07.074.

[113] D. Aili, L.N. Cleemann, Q. Li, J.O. Jensen, E. Christensen, N.J. Bjerrum, Thermal curing of PBI membranes for high temperature PEM fuel cells, J. Mater. Chem. 22 (2012) 5444–5453. https://doi.org/10.1039/c2jm14774b.

[114] A. Sannigrahi, D. Arunbabu, R. Murali Sankar, T. Jana, Aggregation behavior of polybenzimidazole in aprotic polar, Macromolecules. 40 (2007) 2844–2851. https://doi.org/10.1021/ma070049q.

[115] T. Kojima, Studies of Molecular Aggregation of a Polybenzimidazole in Solution By Fluorescence Spectroscopy., J. Polym. Sci. Part A-2, Polym. Phys. 18 (1980) 1685–1695. https://doi.org/10.1002/pol.1980.180180802.

[116] B. Lin, G. Qiao, F. Chu, S. Zhang, N. Yuan, J. Ding, Phosphoric acid doped hydrophobic ionic liquid-based composite membranes for anhydrous proton exchange membrane application, RSC Adv. 7 (2017) 1056–1061. https://doi.org/10.1039/c6ra25460h.

[117] Y.-L. Ma, J.S. Wainright, M.H. Litt, R.F. Savinell, Conductivity of PBI Membranes for High-Temperature Polymer Electrolyte Fuel Cells, J. Electrochem. Soc. 151 (2004) A8. https://doi.org/10.1149/1.1630037.

[118] R. He, Q. Li, A. Bach, J.O. Jensen, N.J. Bjerrum, Physicochemical properties of phosphoric acid doped polybenzimidazole membranes for fuel cells, J. Memb. Sci. 277 (2006) 38–45. https://doi.org/10.1016/j.memsci.2005.10.005.

[119] J.S. Yang, L.N. Cleemann, T. Steenberg, C. Terkelsen, Q.F. Li, J.O. Jensen, H.A. Hjuler, N.J. Bjerrum, R.H. He, High molecular weight polybenzimidazole membranes for high temperature PEMFC, Fuel Cells. 14 (2014) 7–15. https://doi.org/10.1002/fuce.201300070.

[120] J. Luo, J. Hu, W. Saak, R. Beckhaus, G. Wittstock, I.F.J. Vankelecom, C. Agert, O. Conrad, Protic ionic liquid and ionic melts prepared from methanesulfonic acid and 1H-1,2,4-triazole as high temperature PEMFC electrolytes, J. Mater. Chem. 21 (2011) 10426–10436. https://doi.org/10.1039/c0jm04306k.

[121] A. Stoppa, O. Zech, W. Kunz, R. Buchner, The conductivity of imidazolium-based ionic liquids from (-35 to 195) °c. A. variation of cations alkyl chain, J. Chem. Eng. Data. 55 (2010) 1768–1773. https://doi.org/10.1021/je900789j.

[122] A. El Kaddouri, L. Flandin, C. Bas, Chemical degradation of PFSA ionomer binder in PEMFC's catalyst layer, Int. J. Hydrogen Energy. 43 (2018) 15386–15397. https://doi.org/10.1016/j.ijhydene.2018.06.049.

[123] R.E. Rosli, A.B. Sulong, W.R.W. Daud, M.A. Zulkifley, T. Husaini, M.I. Rosli, E.H. Majlan, M.A. Haque, A review of high-temperature proton exchange

membrane fuel cell (HT-PEMFC) system, Int. J. Hydrogen Energy. 42 (2017) 9293–9314. https://doi.org/10.1016/j.ijhydene.2016.06.211.

[124] V. Bandlamudi, P. Bujlo, C. Sita, S. Pasupathi, Study on electrode carbon corrosion of high temperature proton exchange membrane fuel cell, Mater. Today Proc. 5 (2018) 10602–10610. https://doi.org/10.1016/j.matpr.2017.12.393.

[125] H.S. Oh, J.H. Lee, H. Kim, Electrochemical carbon corrosion in high temperature proton exchange membrane fuel cells, Int. J. Hydrogen Energy. 37 (2012) 10844–10849. https://doi.org/10.1016/j.ijhydene.2012.04.095.

[126] O.E. Kongstein, T. Berning, B. Børresen, F. Seland, R. Tunold, Polymer electrolyte fuel cells based on phosphoric acid doped polybenzimidazole (PBI) membranes, Energy. 32 (2007) 418–422. https://doi.org/10.1016/j.energy.2006.07.009.

[127] B. Lin, S. Cheng, L. Qiu, F. Yan, S. Shang, J. Lu, Protic ionic liquid-based hybrid proton-conducting membranes for anhydrous proton exchange membrane application, Chem. Mater. 22 (2010) 1807–1813. https://doi.org/10.1021/cm9033758.

[128] A. Lewandowski, M. Galiński, Carbon-ionic liquid double-layer capacitors, J. Phys. Chem. Solids. 65 (2004) 281–286. https://doi.org/10.1016/j.jpcs.2003.09.009.

DECLARATION

I hereby declare that this dissertation is my own original work except where otherwise indicated. All data or concepts drawn directly or indirectly from other sources have been correctly acknowledged. This dissertation has not been submitted in its present or similar form to any other academic institution either in Germany or abroad for the award of any other degree.

Saarbrücken, 2021

_____

Galina Skorikova